National Library of Canada
Acquisitions and Bibliographic Services Branch
395 Wellington Street
Ottawa Ontario
K1A 0N4

Bibliothèque nationale du Canada
Direction des acquisitions et des services bibliographiques
395, rue Wellington
Ottawa (Ontario)
K1A 0N4

Your file Votre référence

Our file Notre référence

NOTICE

The quality of this microform is heavily dependent upon the quality of the original thesis submitted for microfilming. Every effort has been made to ensure the highest quality of reproduction possible.

If pages are missing, contact the university which granted the degree.

Some pages may have indistinct print especially if the original pages were typed with a poor typewriter ribbon or if the university sent us an inferior photocopy.

Reproduction in full or in part of this microform is governed by the Canadian Copyright Act, R.S.C. 1970, c. C-30, and subsequent amendments.

AVIS

La qualité de cette microforme dépend grandement de la qualité de la thèse soumise au microfilmage. Nous avons tout fait pour assurer une qualité supérieure de reproduction.

S'il manque des pages, veuillez communiquer avec l'université qui a conféré le grade.

La qualité d'impression de certaines pages peut laisser à désirer, surtout si les pages originales ont été dactylographiées à l'aide d'un ruban usé ou si l'université nous a fait parvenir une photocopie de qualité inférieure.

La reproduction, même partielle, de cette microforme est soumise à la Loi canadienne sur le droit d'auteur, SRC 1970, c. C-30, et ses amendements subséquents.

Canada

Electron Transport in $Al_{70-x}Pd_{15}Mn_{15}B_x$ Quasicrystals

by

Mammo H. Yewondwossen

Submitted in partial fulfillment of the requirements
for the degree of Doctor of Philosophy

at

Dalhousie University
Halifax, Nova Scotia, Canada
August, 1995

ISBN 0-612-08822-7

Name MAMMO H YEWONDWOSSEN

Dissertation Abstracts International is arranged by broad, general subject categories. Please select the one subject which most nearly describes the content of your dissertation. Enter the corresponding four digit code in the spaces provided.

PHYSICS

SUBJECT TERM

0523

SUBJECT CODE

U·M·I

Subject Categories

THE HUMANITIES AND SOCIAL SCIENCES

COMMUNICATIONS AND THE ARTS

Architecture	0729
Art History	0377
Cinema	0900
Dance	0378
Fine Arts	0357
Information Science	0723
	0391
	0399
	0708
Music	0413
Speech Communication	0459
Theater	0465

EDUCATION

General	0515
Administration	0514
Adult and Continuing	0516
Agricultural	0517
Art	0273
Bilingual and Multicultural	0282
Business	0688
Community	
	0518
	0524
Finance	0277
Guidance and Counseling	0519
Health	0680
Higher	0745
History of	0520
Home Economics	0278
Industrial	0521
Language and Literature	0279
Mathematics	0280
Music	0522
Philosophy of	0998
Physical	0523
Psychology	0525
Reading	0535
Religious	0527
Sciences	0714
Secondary	0533
Social Sciences	0534
Sociology of	0340
Special	0529
Teacher Training	0530
Technology	0710
Tests and Measurements	0288
Vocational	0747

LANGUAGE, LITERATURE AND LINGUISTICS

Language	
General	0679
Ancient	0289
Linguistics	0290
Modern	0291
Literature	
General	0401
Classical	0294
Comparative	0295
Medieval	0297
Modern	0298
African	0316
American	0591
Asian	0305
Canadian (English)	0352
Canadian (French)	0355
English	0593
Germanic	0311
Latin American	0312
Middle Eastern	0315
Romance	0313
Slavic and East European	0314

PHILOSOPHY, RELIGION AND THEOLOGY

Philosophy	0422
Religion	
General	0318
Biblical Studies	0321
Clergy	0319
History of	0320
Philosophy of	0322
Theology	0469

SOCIAL SCIENCES

American Studies	0323
Anthropology	
Archaeology	0324
Cultural	0326
Physical	0327
Business Administration	
General	0310
Accounting	0272
Banking	0770
Management	0454
Marketing	0338
Canadian Studies	0385
Economics	
General	0501
Agricultural	0503
Commerce Business	0505
Finance	0508
History	0509
Labor	0510
Theory	0511
Folklore	0358
Geography	0366
Gerontology	0351
History	
General	0578
Ancient	0579
Medieval	0581
Modern	0582
Black	0328
African	0331
Asia, Australia and Oceania	0332
Canadian	0334
European	0335
Latin American	0336
Middle Eastern	0333
United States	0337
History of Science	0585
Law	0398
Political Science	
General	0615
International Law and Relations	0616
Public Administration	0617
Recreation	0814
Social Work	0452
Sociology	
General	0626
Criminology and Penology	0627
Demography	0938
Ethnic and Racial Studies	0631
Individual and Family Studies	0628
Industrial and Labor Relations	0629
Public and Social Welfare	0630
Social Structure and Development	0700
Theory and Methods	0344
Transportation	0709
Urban and Regional Planning	0999
Women's Studies	0453

THE SCIENCES AND ENGINEERING

BIOLOGICAL SCIENCES

Agriculture	
General	0473
Agronomy	0285
Animal Culture and Nutrition	0475
Animal Pathology	0476
Food Science and Technology	0359
Forestry and Wildlife	0478
Plant Culture	0479
Plant Pathology	0480
Plant Physiology	0817
Range Management	0777
Wood Technology	0746
Biology	
General	0306
Anatomy	0287
Biostatistics	0308
Botany	0309
Cell	0379
Ecology	0329
Entomology	0353
Genetics	0369
Limnology	0793
Microbiology	0410
Molecular	0307
Neuroscience	0317
Oceanography	0416
Physiology	0433
Radiation	0821
Veterinary Science	0778
Zoology	0472
Biophysics	
General	0786
Medical	0760

EARTH SCIENCES

Biogeochemistry	0425
Geochemistry	0996
Geodesy	0370
Geology	0372
Geophysics	0373
Hydrology	0388
Mineralogy	0411
Paleobotany	0345
Paleoecology	0426
Paleontology	0418
Paleozoology	0985
Palynology	0427
Physical Geography	0368
Physical Oceanography	0415

HEALTH AND ENVIRONMENTAL SCIENCES

Environmental Sciences	0768
Health Sciences	
General	0566
Audiology	0300
Chemotherapy	0992
Dentistry	0567
Education	0350
Hospital Management	0769
Human Development	0758
Immunology	0982
Medicine and Surgery	0564
Mental Health	0347
Nursing	0569
Nutrition	0570
Obstetrics and Gynecology	0380
Occupational Health and Therapy	0354
Ophthalmology	0381
Pathology	0571
Pharmacology	0419
Pharmacy	0572
Physical Therapy	0382
Public Health	0573
Radiology	0574
Recreation	0575
Speech Pathology	0460
Toxicology	0383
Home Economics	0386

PHYSICAL SCIENCES

Pure Sciences

Chemistry	
General	0485
Agricultural	0749
Analytical	0486
Biochemistry	0487
Inorganic	0488
Nuclear	0738
Organic	0490
Pharmaceutical	0491
Physical	0494
Polymer	0495
Radiation	0754
Mathematics	0405
Physics	
General	0605
Acoustics	0986
Astronomy and Astrophysics	0606
Atmospheric Science	0608
Atomic	0748
Electronics and Electricity	0607
Elementary Particles and High Energy	0798
Fluid and Plasma	0759
Molecular	0609
Nuclear	0610
Optics	0752
Radiation	0756
Solid State	0611
Statistics	0463

Applied Sciences

Applied Mechanics	0346
Computer Science	0984
Engineering	
General	0537
Aerospace	0538
Agricultural	0539
Automotive	0540
Biomedical	0541
Chemical	0542
Civil	0543
Electronics and Electrical	0544
Heat and Thermodynamics	0348
Hydraulic	0545
Industrial	0546
Marine	0547
Materials Science	0794
Mechanical	0548
Metallurgy	0743
Mining	0551
Nuclear	0552
Packaging	0549
Petroleum	0765
Sanitary and Municipal	0554
System Science	0790
Geotechnology	0428
Operations Research	0796
Plastics Technology	0795
Textile Technology	0994

PSYCHOLOGY

General	0621
Behavioral	0384
Clinical	0622
Developmental	0620
Experimental	0623
Industrial	0624
Personality	0625
Physiological	0989
Psychobiology	0349
Psychometrics	0632
Social	0451

"To the only wise God be glory forever ..." Rm 16:27.

To

Tsedale, Hannah and Abel

CONTENTS

List of Figures

List of Tables

Abstract

A systematic and quantitative study of the electronic properties of the magnetically ordered $Al_{70-x}Pd_{15}Mn_{15}B_x$ (x=0, 2, 4, 6, 8, 10) icosahedral quasicrystalline alloys under the combined influences of externally applied electric and magnetic fields and the internal quasiperiodic potential due to ionic quasilattice is the subject of this thesis.

Results from the measurement of the temperature dependence of the magnetic susceptibility indicates re-entrant magnetic behaviour. The temperature dependence of the resistivity has been measured between 4 and 300K. At low temperature, T < 30 K, the resistivity showed a rapid decrease with increasing temperature. Weak localization and magnetic scattering effects describe the temperature dependence of the resistivity in this temperature range. At higher temperatures the resistivity is adequately described by the temperature dependence of the structural and magnetic contributions to the resistivity.

The transverse magnetoresistance is measured in fields up to *5.5 T* at different temperatures between *4.2* and *28 K*. The magnetoresistance consists of a superposition of the weak localization contribution and a negative classical spin disorder scattering at local magnetic moments. The results showed a systematic change as a function of boron concentration. The magnetoresistance for x < 6 showed a negative field dependence which became weak with increasing x. The samples with x = 8, 10 showed a positive magnetoresistance. The analysis of the results has been based on the theory of three-dimensional weak localization.

The present Hall resistivity measurement ρ_H show that ρ_H is the result of two contributions; the normal and anomalous. The normal Hall coefficient is independent of temperature in all the alloys and it passes from negative to positive with increasing Boron concentration. This is explained by the effects of s-d hybridization. The anomalous Hall coefficient (R_s) is also found to be temperature independent. The compositional dependence of R_s showed a systematic change with increasing x and this change is correlated with that of the spin-orbit scattering rate obtained from the magnetoresistance measurement and this suggests that the anomalous Hall effect is spin-orbit interaction induced.

List of Symbols

B - magnetic induction
B_x - ($x = i$: inelastic, so: spin-orbit, and s: magnetic spin-flip) characteristic field
χ - magnetic susceptibility
$\chi'(T)$, $\chi''(T)$ - real and imaginary part of the complex *ac* susceptibility
CGR - carbon glass thermometer
D - diffusion constant/local anisotropy
DAC - digital-to-analog converter
DMM - digital multimeter
DOS - density of states
$\Delta\rho(B)$ - magnetoresistance
$\Delta\rho_{CL}$ - classical magnetoresistance
$\Delta\rho_{WL}$ - magnetoresistance due to weak localization
DSC - differential scanning calorimetry
EEI - Electron-Electron Interactions
e - electron charge.
E_F - Fermi energy
e/a - electrons per atom
$f_3(x)$ - Kawabata function
FS-JZB - Fermi-surface-Jones-zone boundary
g^* - Lande factor
h - Plaanck's constant/2π
$_2(E_F)$ - the d-wave phase shift
i - icosahedral
J - exchange energy
k_B - Boltzmann constant
k_F - Fermi wave vector
μ - magnetic moment
μ_B - Bohr magneton
M - magnetization
M_s. - spontaneous magnetization
n^* - effective number of electrons per unit volume
NMR - Nuclear magnetic resonance
OHE - ordinary Hall effect
QC's - quasicrystals
QIE - Quantum interference effects
θ_s - spontaneous Hall angle
ρ - resistivity
ρ_{Kondo} - Kondo type magnetic scattering contribution to the resistivity
ρ_H - Hall resistivity
ρ_m - the magnetic contribution to the resistivity
ρ_s - the structural contributions to the resistivity

R_H - Hall coefficient
RKKY - Rudermann-Kittel-Kasuya-Yoshida interaction
R_o - ordinary Hall coefficient
R_s - extraordinary or spontaneous Hall coefficient
RSG - re-entrant spin-glass
S - Fermi surface
$S_T(k)$ - the structure factor
SD - silicon diode sensor
SHE - extraordinary or spontaneous Hall effect
T- temperature
τ - electron relaxation time
TCR - temperature coefficient of resistivity
τ_i, - the inelastic relaxation time
T_{max} - resistivity maximum temperature
T_{mm} - resistivity minimum temperature
τ_s. - spin-flip relaxation time
τ_{so}, - spin-orbit relaxation time
v_g - group velocity
V_H - Hall voltage
Ω - atomic volume
W - probability amplitude
WL - weak localization
x - Boron concentration
Ψ - electron wave function

Acknowledgments

I wish to express my gratitude to Professor R.A. Dunlap, my thesis supervisor, for the invaluable guidance and support throughout this work. The great confidence he showed in me throughout this work and his constant interest and incessant drive have made it an enjoyable Ph. D. experience. In addition, I would like to thank the former members of our group-S.P. Ritcey , Z. J. Yang, D.W. Lawther and Z. Wang-for their friendship, help and many useful discussions. I would like to express my appreciation to Professors A. Simpson and W. Geldart for useful discussions and suggestions.

I would also like to express my gratitude to the staff and faculty of the physics department who made my stay here as a graduate student enjoyable. I am especially thankful to A.. Feargrieve and R. Deveau for technical assistance and advice.

Finally, my greatest appre iation goes to my wife, Tsedale, and children, Hannah and Abel, who bore the burden imposed on them by my work with great understanding.

I am grateful for financial support by the Faculty of Graduate Studies, Dalhousie University.

1. Introduction

Condensed matter exhibits a rich variety of order with the crystalline and amorphous states being the two extremes. The crystalline state exhibits long range translational and orientational order whereas both are absent in the amorphous state. The discovery of icosahedral (*i*) symmetry in rapidly solidified AlMn alloys [1] in 1985 introduced a new field of condensed matter research, quasicrystals (QC's). QC's possess long-range orientational order (evident from sharp diffraction peaks) yet lack transiational order (due to the non-crystallographic symmetries present). Since the discovery of the *i*-phase, quasicrystals with other long-range orientational symmetries have also been found. These new phases show two dimensional quasicrystalline order with eight, ten, and 12-fold rotational symmetries and are known as octagonal [2], decagonal [3], and dodecagonal [4] phases, respectively. The icosahedral quasicrystals, so-called because their diffraction patterns possess the rotational point group symmetries of the icosahedron (see Figure 1.1), are the most studied group to date.

The peculiar structure of QC's can be pictured as the three dimensional real-space projection of a six dimensional periodic structure (for an extensive review see [6]). The six dimensional nature is best illustrated by the problem of indexing the diffraction patterns of these materials [7]. According to the six dimensional picture, the diffraction peaks from the icosahedral structure are indexed by sets of six Miller indices ($n_1n_2n_3n_4n_5n_6$). Models which describe icosahedral crystals in terms of the stacking of structural units, or tilings, in

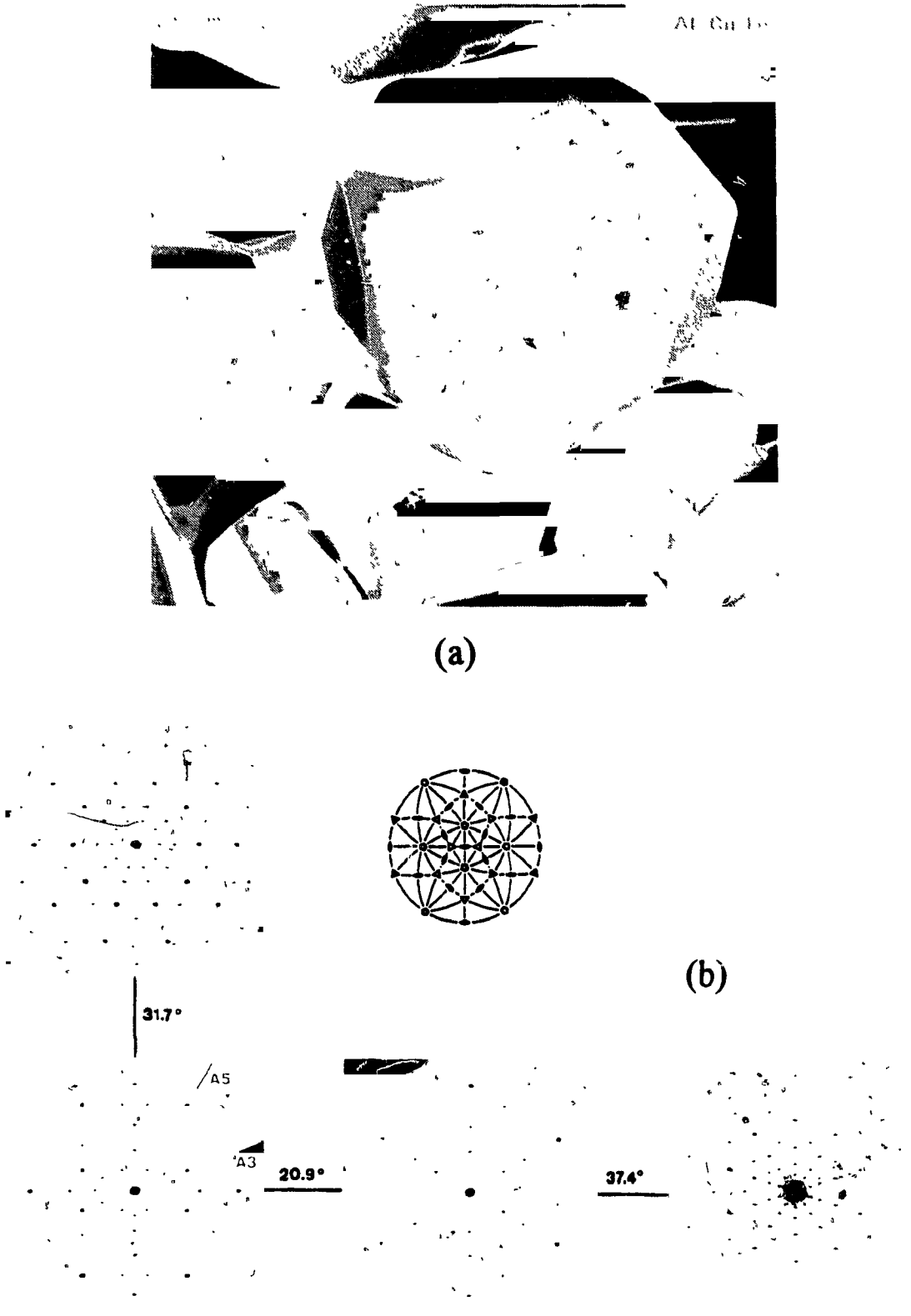

Figure 1.1: (a) The dodecahedral shape observed in initially rapidly quenched and then annealed Al-Cu-Fe alloy and (b) the diffraction pattern of an icosahedral quasicrystal. The relative orientations of various symmetry axes is also shown. (Adapted from Figure 7 of [5] and Figure 2.16 of [6], respectively)

three dimensions have also been proposed [8] and based on the extension of two dimensional Penrose tilings [9, 10] to three dimensions.

Most experimental and theoretical work on QC's has focused on the understanding of the unique structural features of these new phases. Fewer publications have been concerned about the physical properties of QC's and it is only in recent years that important progress has been made in this area (for extensive reviews see e.g. [11, 12, 13]) The atomic structure in condensed matter determines the potential felt by an electron and has a fundamental influence on the electronic properties of the system The existence of a quasiperiodic atomic structure thus raises many questions concerning the electronic properties of QC's. One such question dealt with whether the long range order in QC's as revealed by the electron diffraction leads to specific properties or not. In other words, to what extent electronic behaviour and derived physical properties are sensitive to the long range order rather than to local structural environments.

Electronic properties of QC's have been studied experimentally as well as theoretically [11, 12]. Systems which have been investigated include alloys of simple metals (*sp* quasicrystals) and those that contain transition metals (*sp-d* quasicrystals) Classification of QC alloys and representative examples of each class are given in Table 1.1. Some of the i-QC phases are thermally stable while others are metastable and the degree of structural order varies within each stability class.

Experimental investigations have revealed that the electronic properties of QC's, and in particular their transport and magnetic properties, depend very much on their structural quality (for extensive reviews see e.g. [6, 11, 14]). The first discovered

thermally metastable QC's (AlMn, PdUSi or AlMgZn) are, in general, highly resistive, with low temperature resistivity ρ~100-500 $\mu\Omega cm$ and ρ which decreases slightly (by a few percent) with increasing temperature up to ~300 K. These QC's contain many structural defects. The 1986 discovery of the first stable icosahedral phase in Al-Li-Cu was an important step in the study of the electronic properties of QC's, since single grains could then be grown. Later, high structural quality i-phases were discovered in the Al-Cu-Fe and Al-Pd-Mn systems. The electronic properties of these thermodynamically stable phases are remarkable, in particular with very large ρ values for alloys made of metallic elements. These ρ values are similar to those measured in highly doped semiconductors. Recent studies of the electrical resistivity on high-quality samples have revealed various interesting features; (1) resistivity as high *as* 10^3 - 10^4 $\mu\Omega cm$ with a pronounced negative temperature coefficient ($\rho_{4.2K}/\rho_{300K} \cong 1.5$ to 4). Both these effects are enhanced as the structural quality increases [15, 16]; (2) a low density of states at the Fermi energy as indicated by specific heat [11, 17], soft x-ray emission and photoabsorption [18] measurements and (3) QC phase occurrence and stability which are very sensitive to stoichiometry and well correlated with the specific number of conduction electrons per atom, e/a [19].

Table 1.1. Classification of QC alloys studied so far and representative system.

	sp quasicrystals	*sp-d* quasicrystals
Metastable	AlMg (Ag, Cu, Zn)	AlMn
Stable	AlCuLi	AlCuFe, AlPdMn, AlCuRu

At the theoretical level, the electronic properties of QC's are still far from being fully understood. Two approaches have been taken. The first approach is based on the similarity between QC materials and the well known Hume-Rothery crystalline alloys. This gives a coherent description of some, but not all, of the experimental results. In particular the nature of the metal-insulator transition and the mechanism of electronic conduction are not known in real three dimensional QC's. The second approach, the electronic band approach, consists of the study of the very particular electronic states existing in a quasiperiodic tiling. This was used successfully to interpret the transport data for the highly resistive *i*-phases. The high resistivity of QC's has been attributed to the existence of a pseudogap at the Fermi level and a tendency for localization of the electrons in the pseudogap states (see e.g. 11, 14, 20]), this tendency has been explained by detailed theoretical calculations [21]. The existence of the pseudogap at the Fermi level in stable QC's has been experimentally shown by specific heat measurements [11] and has been indicated by photoelectron emission spectroscopy [22, 23, 24]. Theoretical calculations of the electron density of states for quasicrystalline lattices and also for crystalline approximants have shown that the density of states is extremely spiky, exhibiting densely distributed gaps (see e g. [20]) It is thus considered that in real QC's the density of states near the bottom of the pseudogap fluctuates with small changes of energy. Such a spiky density of states is thought to be the origin of the sensitivity of the resistivity behavior to composition. It is established that the Fermi-surface-Jones-zone boundary (FS-JZB) interaction is a viable mechanism for describing the stability, electronic structure, and

electron transport in *i*-phases and their approximant phases The FS-JZB interaction causes the opening of pseudogaps in the electron density of states (see e g [11])

In most thermodynamically stable QC's diamagnetic or very weakly paramagnetic behavior has been observed. It is also found that the more diamagnetic samples are also the more resistive ones (see e.g [14]). Experiments show that magnetic moments and magnetic ordering are also exhibited in some QC alloys (for an extensive review see e.g.[25]) Unexpected magnetic moments are observed in *i*-AlMn phases since neither Al-Mn solid solutions, nor the crystalline compounds of similar compositions (o-Al_6Mn, α-$Al_9Mn_2Si_2$, β-Al_9Mn_3Si) possess moments. Nuclear magnetic resonance (NMR) experiments indicate that the magnetism is not uniform and that only a few percent of the Mn atoms are magnetic [26] Magnetic moments are also present in thermodynamically stable Al-Pd-Mn *i*-phases of very high structural quality [27] Not only melt-spun polycrystalline samples, but also single grains are shown to possess moments [28] The QC magnetic phases exhibit magnetic order (weakly ferromagnetic or anti-ferromagnetic) as well as disorder (spin-glass) and sometimes a regime of co-existing behaviour (ferromagnetic-spin-glass or antiferromagnetic-spin-glass) [25].

Recently, Yokoyama et al [29] reported the synthesis and structural and magnetic characterization of $Al_{70-x}Pd_{15}Mn_{15}B_x$ icosahedral alloys These icosahedral alloys are reported to be ferromagnetic (FM) below the Curie temperature [30] and the origin of ferromagnetism was believed to be primarily from Mn-B bonding. The room temperature magnetization was found to increase with increasing B content up to 10 at % B and showed a maximum of

$2.1\times10^{-7} H\cdot m^2\cdot kg^{-1}$ (mass susceptibility) at 10 at % B The magnetization is observed only in the metastable quasicrystalline phase and is not present in the equilibrium crystalline phase.

Magnetic properties of magnetic systems are sensitive to the atomic structure The quasicrystalline structure is expected to influence the magnetism. The influence of the QC structure on magnetism as well as the influence of magnetism on the transport properties of QC's is not yet known. The lack of reasonable quality samples (size and quality of ribbon) with systematically varying magnetization for transport measurements has contributed towards this lack of understanding. The $Al_{70-x}Pd_{15}Mn_{15}B_x$ icosahedral alloys overcome this shortcoming The description of the motion of an electron (electron transport properties) under the combined influences of externally applied electric and magnetic fields and the internal quasiperiodic potential due to the ionic quasilattice of $Al_{70-x}Pd_{15}Mn_{15}B_x$ alloys is the subject of this thesis

The reminder of the thesis is organized as follows Chapter 2 describes in detail the experimental techniques used in this work In Chapter 3 an introduction to the magnetic properties of QC's and the results of the current investigations of the magnetic properties of $Al_{70-x}Pd_{15}Mn_{15}B_x$ are given. Experiments show that the resistivity of QC's is very high and indicate the proximity of metal insulator transition Quantum interference effects (QIE), which are well known for disordered metals, are also observed in QC's These and other results lead many authors to compare QC's to disordered systems like amorphous metals or doped semiconductors [11, 14] In Chapter 4 the zero field electrical resistivity measurements from 4 K to 300 K are analyzed in light of QIE and theories developed for amorphous metals. The field dependence of the resistivity (transverse magnetoresistance)

was analyzed using QIE theories (weak localization) in Chapter 5. Chapter 6 presents the field and temperature dependence of the measured Hall coefficient. A brief review of various theories of electronic properties relevant to the understanding of the transport properties in question in each chapter is discussed at the beginning of the chapter. Conclusions of this work are given in Chapter 7.

2. Experimental Techniques

In this chapter the most relevant details of sample preparation and characterization, along with cryostat design and measurement techniques used in this work are discussed

2.1. Sample Preparation and Characterization

$Al_{70-x}Pd_{15}Mn_{15}B_x$ alloy master ingots, of about 2 *g*, of the appropriate compositions (x=0, 2, 4, 6, 8, 10) were prepared from high purity elements by arc melting under flowing argon. The purity of the starting elements was: Al; 99 9%, Pd, 99 99%, Mn, 99 8%, B, 99%. Homogeneity of the ingots was ensured by arc melting about four times, where each melting was held for about one minute. The resulting compositions of the ingots were assumed to be identical with the initial ones since the typical overall weight loss during preparation was ~ 1%.

The as-cast alloys were found to contain both the icosahedral phase and a crystalline phase. To obtain a pure icosahedral phase the ingot was melt spun using a single copper roller The procedures for melt spinning are as follows. About 1 *g* of the ingot was placed in an 8 *mm* inside diameter quartz tube with a circular orifice of 0 7 to 0 8 *mm* in diameter. The quartz tube was positioned about 0 5 *mm* above a Cu wheel (~ 15 *cm* diameter) inside a copper *rf* induction heating coil. The rotation of the copper wheel was then stabilized to a surface speed of about 60 $m \cdot s^{-1}$ and power was applied to the induction coil to melt the ingot within the quartz tube. The molten alloy was then

ejected through the orifice by applying about 120 *kPa* Ar gas pressure The stream of molten alloy solidified in the form of ribbons Resulting ribbons had cross-sections of ~ 25 *μm* thick by ~ 1 5 *mm* wide

The single phase quasicrystalline nature of the powdered ribbons was confirmed by room temperature X-ray diffraction using Cu-K_α radiation on a Siemens D500 scanning diffractometer No traces of contaminant phases were observed in the X-ray diffraction patterns of the ribbons

2.2. Cryostat Design

Measurements were performed from liquid helium temperature to room temperature in a modified Oxford Instruments L1091 Mossbauer cryostat This cryostat was originally designed for low temperature Mössbauer effect measurements. The system is shown schematically in Figure 2 1 Construction of the cryostat is principally of stainless steel and aluminum with copper in critical heat conducting regions Superinsulation is employed to aid long hold times The cryostat is equipped with a 6 *T* superconducting magnet. The helium and nitrogen working volumes are 10 and 11 5 *liters*, respectively.

The procedure for cooling the cryostat is as follows The outer vacuum can was first evacuated using a rotary pump. Residual moisture that may have collected in the liquid helium chamber is removed by rough pumping to about 1 *Torr* and flushing with dry helium gas at 1 *atm* pressure The probe (as described in the next section), loaded with the

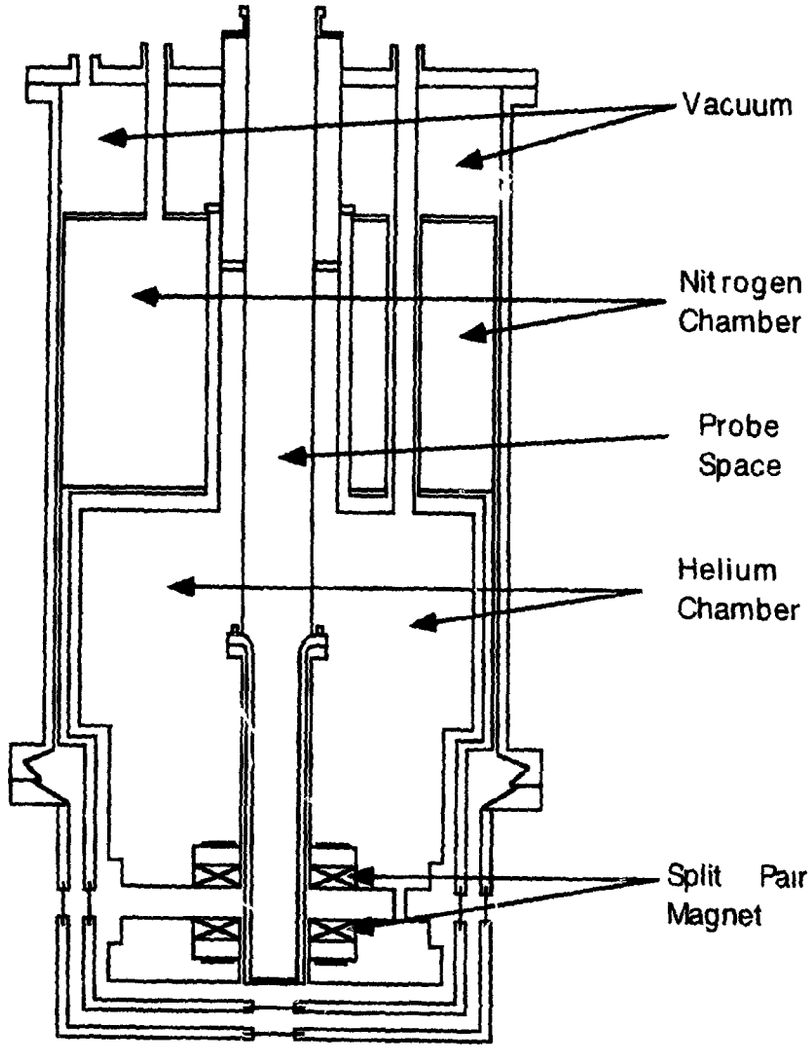

Figure 2 1 Schematic of the L 1091 Mossbauer cryostat

sample is then placed in the sample space and this space is evacuated to about 1 *Torr* then filled with 1 *atm* dry helium gas

The liquid nitrogen chamber is then filled with liquid nitrogen and kept filled for at least five days prior to filling the cryostat with liquid helium This procedure ensured that the magnet and liquid helium chamber temperature were at less than 100 *K* and this helped to achieve an efficient liquid helium transfer

The superconducting magnet is energized by an Oxford Instruments 60 *A* MK3 power supply The power supply can be operated in two different modes In constant voltage mode the magnet will be charged to the set current value, at a rate which is determined by the value set on the positive output voltage control and the magnet inductance In constant current operation with over voltage trip mode utilizes an external voltage ramp to program the output current of the power supply A voltage ramp of 0 to -5 *V* corresponds to an output current of 0 to 60 *A* In this work the magnet was operated in constant current mode A computer controlled digital-to-analog converter (DAC) was used to generate 0 to -4 3 *V* The DAC was constructed on a standard 8-bit PC bus card. The circuit diagram is illustrated in Figure 2 2 The magnitude of the magnetic field was monitored by a Keithley 197 DMM which measured the voltage at the current monitoring terminals on the power supply (0 to 120 *mV* corresponding to 0 to 6 *T*). The computer controlled magnetic field was increased in steps of 0 04 *T* in low field region ($\leq$ 1 *T*) and in steps of 0 1 *T* in the higher field region (between 1 and 5 5 *T*) At each step the current is allowed to commute in the magnet coil and is held until measurements are taken The magnetic field fluctuation was less than 0 0002 *T* which is determined by the stability of

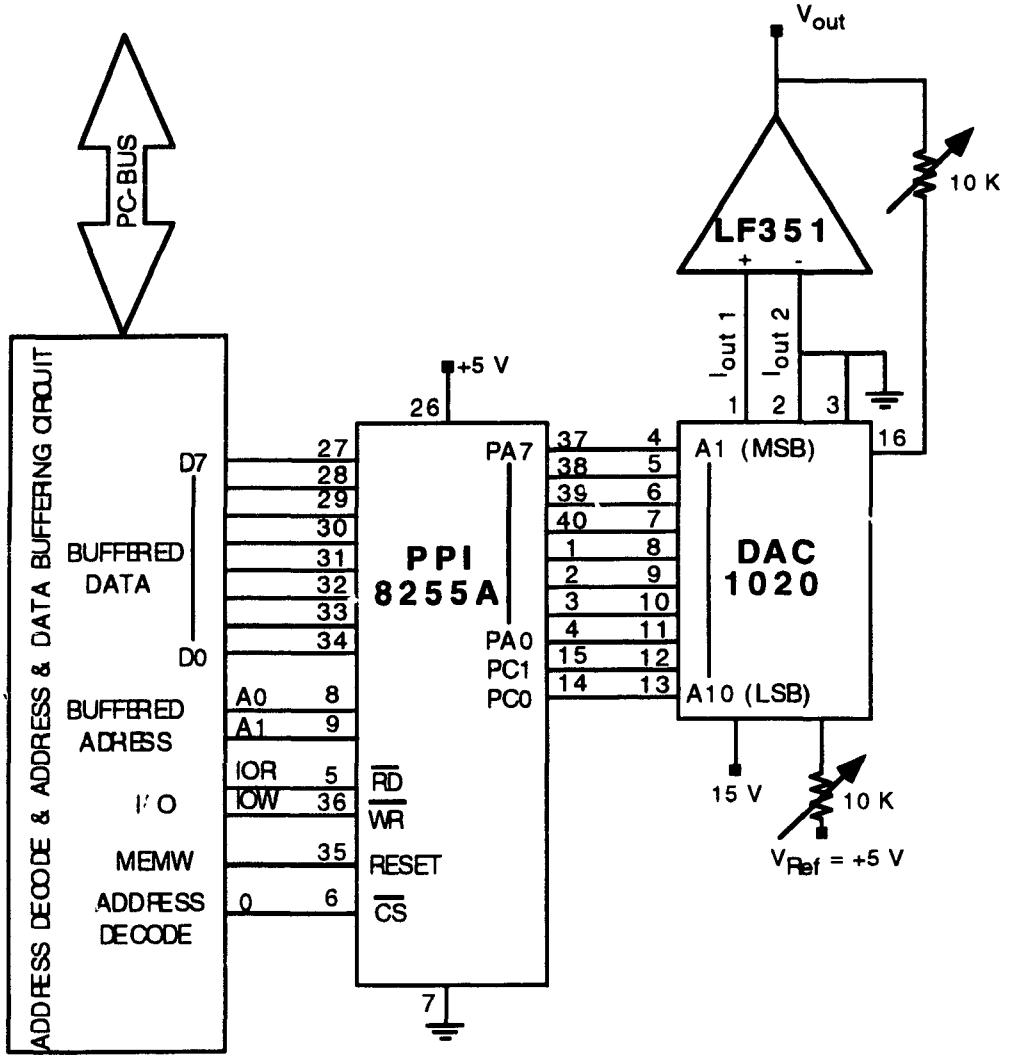

Figure 2 2 Block diagram of PC controlled digital-to-analog converter (DAC) PPI 8255A Intel general purpose programmable peripheral interface I/O device, DAC 1020 10-bit digital-to-analog converter, LF351 operational amplifier

the voltage output of the DAC which in turn determines the stability of the output current of the magnet power supply.

2.3. ac *Susceptibility Measurements*

The *ac* susceptibility of the powdered samples was measured by a standard mutual inductance technique. The measurements were made using Stanford Research systems SR530 two phase lock-in amplifier at a frequency of 127 *Hz* with an *ac* primary magnetic field of about 80 *A/m*. The current through the heater was turned on, the sample was allowed to reach an equilibrium temperature and the sample temperature was measured using a Lakeshore CGR-1-2000 carbon glass thermometer. The susceptometer circuit diagram is shown in Figure 2.3. A primary coil, P, is wound on the outside of two secondary coils S_1 and S_2 and is driven by a Hewlett-Packard (HP) 33312 oscillator. The secondary coils are wound in series opposition. The outputs of the two secondary coils are input into the lock-in amplifier which is used in differential mode. At each temperature two lock-in amplifier output voltage readings were taken: in the absence of the sample and after the sample was placed in one of the secondary coils. The difference of these two readings is proportional to the susceptibility of the sample. The two lock-in amplifier output voltages, corresponding to in-phase and out-of-phase susceptibility, were measured using two Keithley 195A digital voltmeters. The temperature dependent susceptibility measurements were carried out during warming runs from 10 to 300 *K*. A detailed description of the ac susceptibility probe is given by Koszegi et al [31].

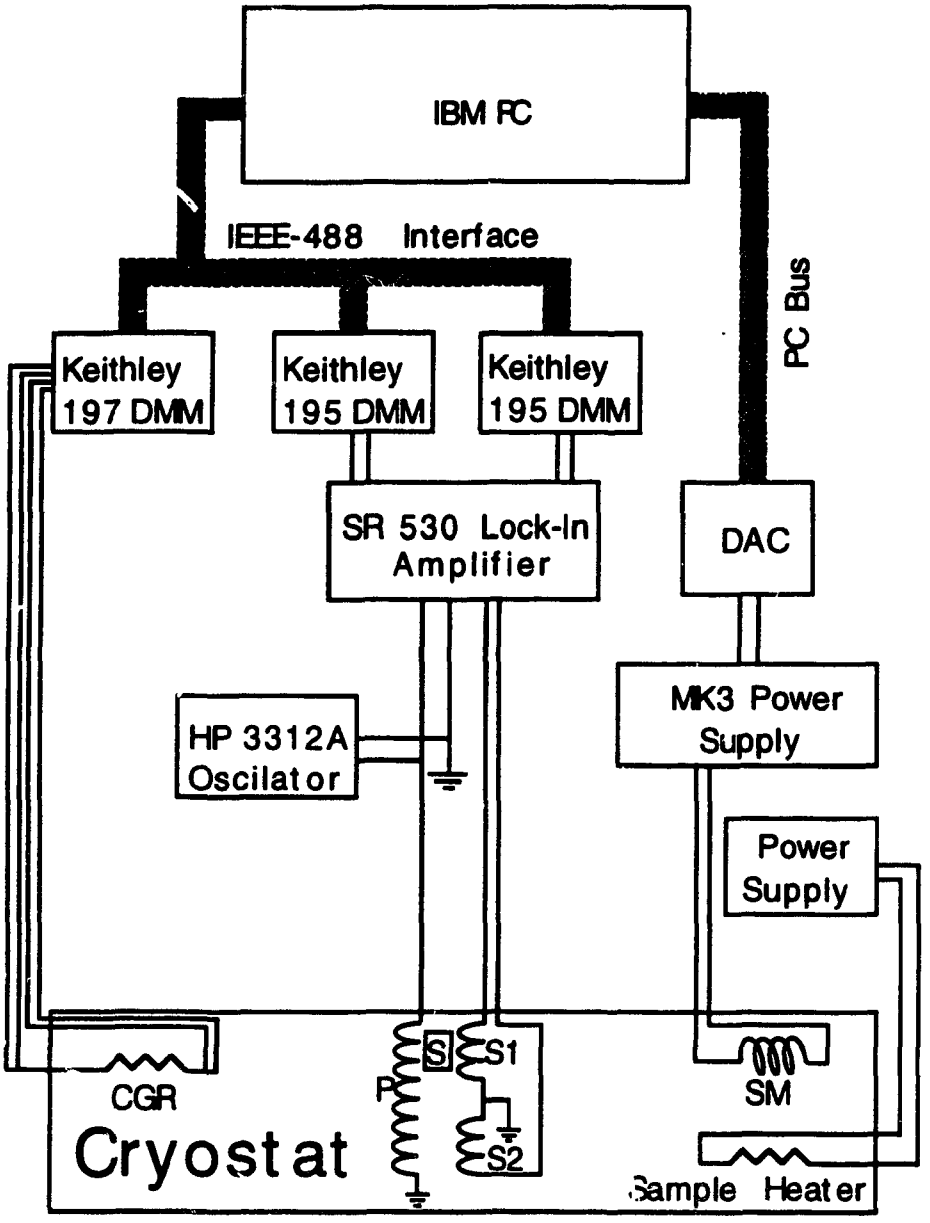

Figure 2 3 Schematic diagram of the *ac* susceptibility instrumentation; CGR = carbon glass thermometer; S = sample, P = primary winding; S_1, S_2 = secondary windings; SM = superconducting magnet.

The calibration of the susceptometer is performed by comparing the voltage output of the lock-in to the known magnetic susceptibility of the paramagnetic salt Gd_2O_3. The magnetic susceptibility of this material follows the Curie-Weiss law,

$$\chi = \frac{C}{T-\theta}, \tag{2.1}$$

with C = 0.221 *(emu·K)/(g·Oe)* and θ = 20 *K*. The data were fitted to the Curie-Weiss law as shown in Figure 2.4 with C=0.25 *(emu·K)/(g·Oe)* and θ = 24 *K*. The agreement of the experimental results with the literature values indicates reasonable accuracy of the method and the lack of excessive thermal gradients.

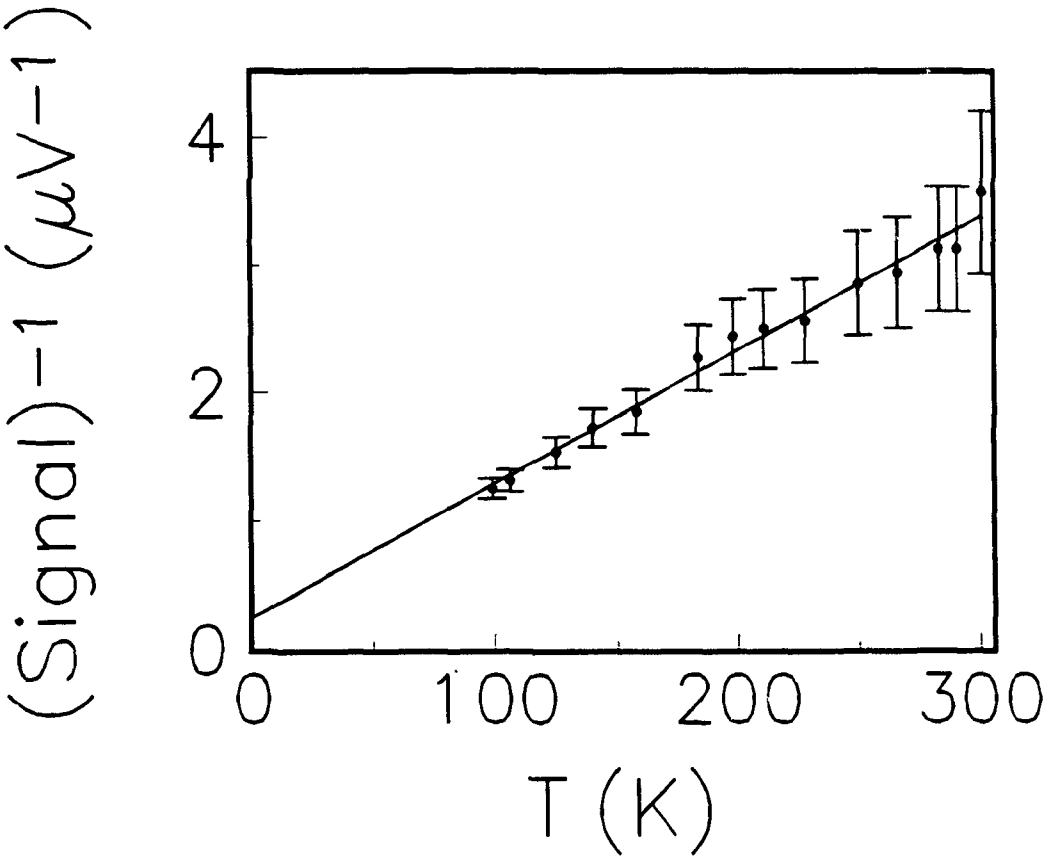

Figure 2.4 Inverse susceptibility of Gd_2O_3 as fitted with the Curie-Weiss law.

2.4. Electrical Transport Measurements

The resistivity, magnetoresistivity and Hall effect measurements were performed using a conventional six-point *dc* technique, see Figure 2.5 Contacts for the transport measurements were made by evaporating gold pads on the surface of the ribbons and attaching 25 μm gold wires using silver loaded epoxy The sample to be measured was glued (using GE varnish #7031) onto a copper platform and electrically insulated from the copper using cigarette paper Two samples could be mounted on the copper block at the same time This increased the efficiency of the measurements by reducing cool-down time The gold electrical leads were soldered to a fibreglass circuit board glued to the copper block To achieve magnetic isolation a twisted pair of 0 16 *mm* diameter copper wires was used from the circuit board to the vacuum feedthrough at the top of the probe Magnetic coupling was avoided by passing the pick-up wires (resistance voltage and Hall leads) through one stainless steel tube and the current leads through another The tubes were grounded to ensure shielding The probe used for resistivity, magnetoresistivity and Hall effect measurements is schematically shown in Figure 2 6

The measuring setup was connected by an IEEE-488 interface to an IBM PC computer which is used to control the experiment and collect the data The sample temperature in the presence of a magnetic field was monitored using a Lakeshore CGR-1-2000 carbon glass sensor (which minimizes magnetic field-dependent temperature error) while in the absence of field a Lakeshore DT-470-LR-12 silicon diode sensor (which has low magnetic field dependence up to 5 T above 60 K and is not recommended for use in magnetic field application below 60 K) was used These sensors were excited by a 0 1 *mA*

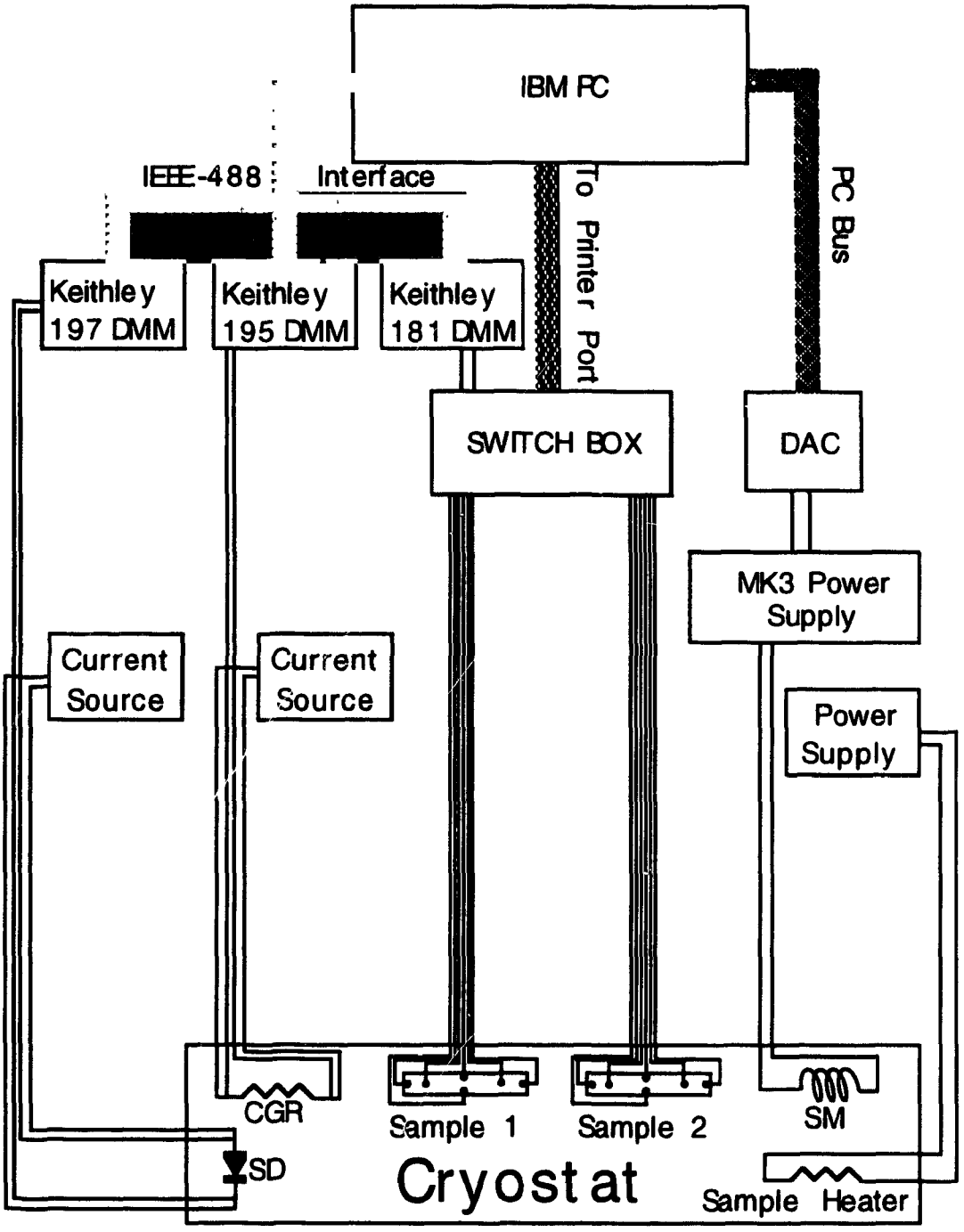

Figure 2.5. Schematic diagram of the apparatus used to measure electronic transport properties: CGR = carbon glass thermometer, SD = silicon diode, SM = superconducting magnet.

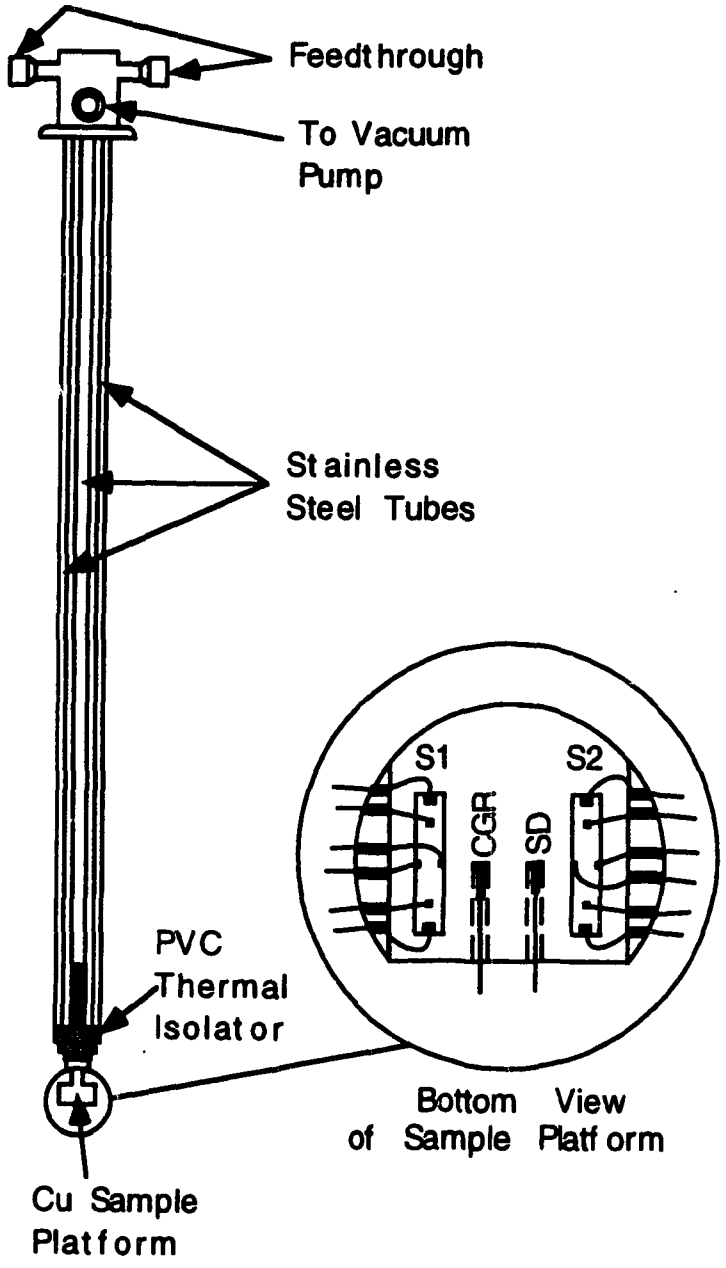

Figure 2.6 Schematic diagram the probe used for resistivity, magnetoresistivity and Hall effect measurements.

current and the output voltage was read by the computer via a Keithley 197 DMM (digital multimeter). The temperature was evaluated using a Chebychev series obtained from a fit to the calibration data supplied by the manufacturer.

The temperature dependence of the resistance was measured in the temperature range 4 to 300 K during slow cooling and warming run (at a typical rate of ~ 2 K/min) A 1 mA constant current provided by a Lakeshore C1396 constant current source was passed through the sample and the voltage developed across the voltage leads was measured using a Keithley 181 nanovoltmeter. During measurements, voltages for both directions of current were taken and averaged to correct for any thermal *emf* present The resistivity for a uniform ribbon is defined as

$$\rho = \frac{AR}{l} = \frac{AV}{Il} \tag{2 2}$$

where A is the cross-sectional area, V is the voltage, I is the sample current, l is the distance between the voltage leads, and R is the resistance. Direct measurements of A (width and thickness of the sample) and l were used to calculate the resistivity. The accuracy of the resistance measurement was better than 0.1%. Measurements of the width and thickness of the ribbons gave a systematic error in A of ~ 12 %. The largest error in the resistivity arises from this uncertainty in A

The steps involved in resistance measurements of the two samples are the following: During slow cooling or warming, the computer switches the current to one of the samples and takes 10 readings from the Keithley 181 nanovoltmeter, reverses the polarity of the current and takes another 10 readings. The mean of the 20 readings was

then recorded. The computer then switches the current to the second sample and again takes the average of 10 readings for each of the two current directions. The circuit diagram of the computer controlled switch used for reversing the current polarity and for connecting the current leads to one sample at a time and the voltage leads (resistance or Hall) to the nanovoltmeter is shown in Figure 2.7.

The field dependence of the magnetoresistance was measured in the bore of the superconducting solenoid. The steps used in measuring the transverse magnetoresistance were as follows: The current through the heater was turned on and the sample was allowed to reach an equilibrium temperature (fluctuation less than 0.1 *K*). The computer controlled magnetic field was increased in steps and at each step the resistance of the samples was measured as described above.

The Hall effect was also measured in the bore of the superconducting solenoid using a Keithley 181 nanovoltmeter to measure the Hall voltage as illustrated in Figure 2.5. The actual voltage measured is not the true Hall voltage since the true Hall voltage is obscured by additional *emf's* due to magnetoresistance, thermal effects, and misalignment of the Hall leads. The Hall voltage can be determined by measuring the voltage across the sample for all four possible combinations of magnetic field and current direction. The Hall voltage, V_H, which is an odd function of both field and current direction, can then be found by

$$V_H = \frac{1}{4}\left[V(I_+,H_+) - V(I_-,H_+) - V(I_+,H_-) + V(I_-,H_-)\right]. \tag{2.3}$$

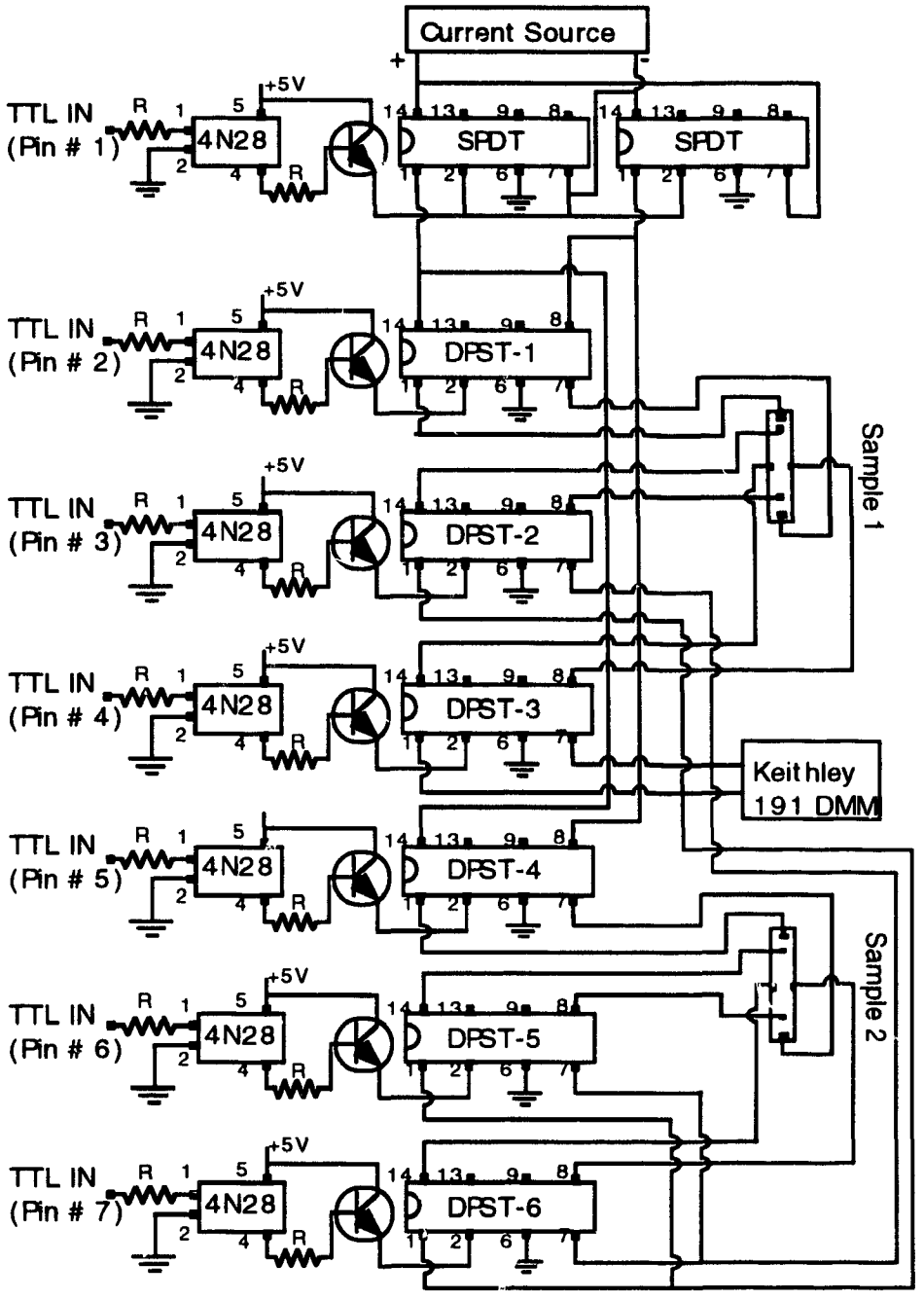

Figure 2.7 Circuit diagram of the computer controlled switch box. 4N28: 300-4N28 Opto Isolator, SPDT: 344-JWD-172-5 single pole double throw relay, DPST: 344-JWD-171-25 double pole single throw relay, R= 100 Ω.

The Hall coefficient, R_H, at a field H was determined from the expression

$$R_H = \frac{V_H t}{IH}, \tag{2.4}$$

where I and t are the current and sample thickness.

The output of the nanovoltmeter was coupled to the IBM PC as described above and the Hall voltage was measured by sweeping the field from -5.5 T to +5.5 T at a constant temperature in two stages (0 to +5.5 T and 0 to -5 5 T). The computer controlled magnetic field was increased in steps and the Hall voltage was measured for the two current polarities at each step. Spurious magnetoresistance contributions (of even parity in H) due to slight misalignment of the Hall voltage leads were eliminated by a 180° magnetic field reversal achieved by interchanging the current output terminals. The measuring current was 3 mA. The largest error in the Hall coefficient arises from the uncertainty in sample thickness and amounts to ~ 7 %.

3. Structure and Magnetic Properties of $Al_{70-x}Pd_{15}Mn_{15}B_x$

A detailed knowledge of the magnetic properties of $Al_{70-x}Pd_{15}Mn_{15}B_x$ is a prerequisite to a full understanding of their electronic transport properties. The aim of this chapter is to present: (a) an introductory literature survey of the magnetic properties of QC's and more specifically $Al_{70-x}Pd_{15}Mn_{15}B_x$ alloys and (b) the current investigation of the magnetic properties of $Al_{70-x}Pd_{15}Mn_{15}B_x$; since the magnetic properties of these alloys are not at the core of the thesis, only the most important features of the data are given.

3.1. Magnetism and Quasicrystals: Literature Review

As is well known, QC's exhibit the local icosahedral symmetry absent in conventional periodic solids. A basic concern is the effect of this symmetry on the magnetic properties Magnetic properties of QC's should, in principle, be sensitive to local atomic environments (relative to the existence of moments) as well as to long range order (through the interaction between moments) Experimental investigations show that a variety of Al-based QC's exhibit magnetic behavior that ranges from diamagnetic to ferromagnetic [25] Most quasicrystalline materials, however, have been reported to be either diamagnetic or paramagnetic, while a few have exhibited spin glass-like behaviour [25]. Weak ferromagnetism has been found in Al-Ce-Fe [32], Al-Mn-Ge [33] and Al-Mn-Si [34,35]. Al-Mn based icosahedral alloys have been

particularly fascinating by virtue of a large variation in magnetic properties [33, 36-39] Experimental investigations of QC's support the following features·

1 Unexpected magnetic moments Experimental evidence [25] for the existence of magnetic moments in QC phases came from susceptibility, magnetization and specific heat measurements, and in a less direct way from NMR and transport properties QC's possess unexpected magnetic moments, for example, Al-Mn-Si QC's have magnetic moments which are not observed in either Al-Mn solid solutions or in the related crystalline Al-Mn-Si compounds [40] For a host, such as Al, the possibility of local moment formation on an impurity ion is a maximum for impurities near the centre of the 3*d* transition metal series For Mn in Al, a weak coupling between the *s* and *p* electrons results in a marginal case for moment formation [41, 42] Therefore, with small variations in composition or the method of synthesis, large variations in moment formation capabilities have been reported for Al-Mn based systems

2 Only a fraction of Mn atoms possess a moment Experimental evidence indicates that a large fraction of Mn sites are magnetically similar to those in related crystalline materials and carry no moments The magnetism is provided by a subset of sites having moments substantially larger than the average value Berger and Prejean [43] estimated the number of magnetic sites and the value of the magnetic moment, μ, in $Al_{73}Mn_{21}Si_6$ *i*-QC by the measurement of the nonlinear terms of the magnetization in the zero field limit A low fraction of magnetic entities was found (1 3% of the number of Mn) carrying an unexpectedly high moment value ($\mu = 7\ 5\mu_B$) compared to the $5\mu_B$ value generally found for dilute Mn alloys It has also been confirmed that there are magnetic and nonmagnetic Mn atoms in quasicrystalline Al-Mn alloys (by means of NMR [26]) and in Al-Mn(Fe) and Al-Mn-(Fe)-Si alloys (by

Mossbauer effect [44]) For example, a combination of Curie-like behavior and Pauli paramagnetism has been reported in some systems indicating two kinds of Mn sites, the former being representative of localized behavior, while the later is representative of collective electron behavior [39, 45] The presence of two kinds of sites in such icosahedral alloys has been corroborated through several studies on the structural and electronic properties [36, 46, 44]

3 The overall magnetization increases drastically with the nominal Mn concentration in the sample It is found that the Al-Mn QC alloys with Mn concentration less than 5 % are nonmagnetic and as the Mn concentration is increased beyond 5 %, the alloys become magnetic and the effective moment on Mn sites increases as the square of the Mn concentration [47] These results show that Mn-Mn interactions probably play an important role in stabilizing the Mn moment

4 Evidence for magnetic ordering (ferromagnetism, ferrimagnetism, spin glass, etc) in icosahedral QC's has been reported in several systems such as Al-Mn-Si [48], Al-Cu-Mn-Ge [33] and Al-Mn-Pd-B [29] These systems are metastable and are typically produced by rapid solidification methods They generally possess small magnetic moments but show large coercivities and high Curie temperatures

The overall magnetic properties of QC's seem to be dominated by electronic structure effects due to the atomic species present (for instance in terms of hybridization of Mn 3*d* states with the Al *sp* conduction band) The presence of magnetic moments in QC's is surprising, since dilute Mn in Al does not show a magnetic moment and Mn exhibits no moment in the related crystalline compounds which have compositions similar to the QC phase and are thought to have similar local environments.

The theoretical study of the electronic structure of quasicrystals has, to a certain extent, been limited by an inadequate knowledge of the structure at an atomic level. Further, the absence of traditional Bloch periodicity in these materials rules out the use of some of the most powerful theoretical techniques in elucidating solid-state electronic structure. While a comprehensive characterization of the electronic structure of a three-dimensional quasicrystal comparable to state-of-the-art band structure calculations is not yet feasible, inroads have, nevertheless, been made by considering features in the electronic structure resulting directly from local icosahederal symmetry. Among the more common methods used to address the influence of icosahederal symmetry on the electronic structure has been cluster calculations using a variety of techniques for solving the Hamilitonian.

To understand the experimental findings, theoretical calculations modeling quasicrystals by small finite clusters have been carried out. McHenry et al. [49] used a multiple-scattering X-α (MS-X-α) technique to study a $MnAl_{32}$ icosahederal cluster and $MnAl_{18}$ cuboctahederal cluster. The former is motivated by the symmetry exhibited by Al-Mn quasicrystals while the latter corresponds to the symmetry group possessed by bulk Al. These cluster calculations showed that the icosahedral configuration (Mn being at the center of the Al cluster) is not energetically favorable, and enhances the local density of electronic states in relation with the energy level degeneracy induced by the icosahedral environment. Following the Stoner criterion, such a density of states (DOS) enhancement would favor moment formation. These peculiar icosahedral sites might be occupied only when all other sites are filled, and this agrees with the increase of the magnetic moment in the icosahedral phases with increasing Mn concentration. Bagayoko at al. [50] also carried out density-functional calculations on a

$MnAl_{18}$ cluster It was found that while the Mn atoms did not carry moments in a cuboctahedral cluster, they did have a moments of 3 6 μ_B in sites with icosahedral symmetry This has been taken to imply that the icosahederal symmetry is responsible for the formation of magnetic Mn sites in Al-Mn QC's A review of this work can be found in O'Handley et al [25]

Along somewhat different lines, de Coulon et al [51] recently investigated the effect of icosahedral symmetry on the magnetic moment at Mn sites in $Al_{1-x}Mn_x$ quasicrystals by modeling the quasicrystals as clusters This study was based on self-consistent density-functional calculations on clusters having a central Mn surrounded by Al_n ($n \leq 54$) atoms in cuboctahedral and icosahedral arrangements and showed that the Mn atoms do carry a magnetic moment for small cluster sizes The moment is, however, quenched as the cluster size is increased irrespective of the geometry This quenching is shown to be a direct consequence of the mixing between the Mn *d* states and the Al *sp* states in these geometries The extent of the mixing depends on the interatomic distances and on the cluster size For small clusters, the mixing is small and the Mn sites carry a finite moment In view of these results the authors suggested two possibilities for the origin of magnetic Mn sites in QC's First, those geometries which do not lead to Al *p* orbitals which can mix with Mn *d* orbitals may stabilize the Mn moment The second situation is that the Mn-Mn interactions are responsible for stabilizing magnetic sites These authors [51] have also argued that the above theoretical picture of McHenry et al. [49], which is based on calculations on smaller clusters and predicts that the magnetic Mn sites in Al-Mn quasicrystals are a result of icosahedral symmetry, is incorrect

Magnetism in solids basically arises from the lifting of the degeneracy of *d* and *f* atomic states by the crystal field symmetry The icosahedral symmetry in quasicrystals is 'more

spherical' than the other crystallographic symmetries present in cubic, tetragonal, , etc. crystals This point is clearly illustrated in Figure 3 1 the *d* orbital degeneracy is not lifted by icosahederal symmetry (but possibly lifted by the spin-orbit interaction) Several concepts are of specific importance to a consideration of the magnetic properties of icosahederal quasicrystals

1 Reduced crystal field splitting may leave the *d* and *f* levels more closely spaced in energy, and hence give rise to sharper peaks and deeper valleys in the density of states

2 As a consequence of (1), *d* and *f* levels would be more spatially localized than in conventional crystalline materials

3 Magnetic anisotropy should be affected

4 Owing to the sharp features in the density of states, the density of states at the Fermi level will be a sensitive function of the chemical composition of alloy

5 The interaction between atomic moments and the crystalline anisotropy is governed by the relative importance of the local anisotropy, D, and the exchange energy, J [52,53] In the case where $D/J > 1$, as may be the case for $4f$ moments (if $L \neq 0$), the local anisotropy dominates and dispersed moment structures are possible [54] as the local anisotropy is randomly oriented [55,56] On the other hand, if $D/J < 1$, as is the case for $3d$ moments, then the effect of long-range exchange interactions dominates, the magnetization direction is uniform over larger distances, and it is the long range anisotropy (or symmetry) which is more important than the local anisotropy (or symmetry) Since, in known quasicrystalline materials, it is $3d$ magnetic moments, predominantly on Mn, that determine the magnetic behavior, then it is the long-range symmetry of the system that is of relevance. These effects of long-range

icosahedral symmetry are, therefore, limited to icosahedral QC's and will not be observed in crystalline materials with local icosahedral coordination, unlike the consequences of local icosahedral symmetry, which may be seen in both crystalline and quasicrystalline materials

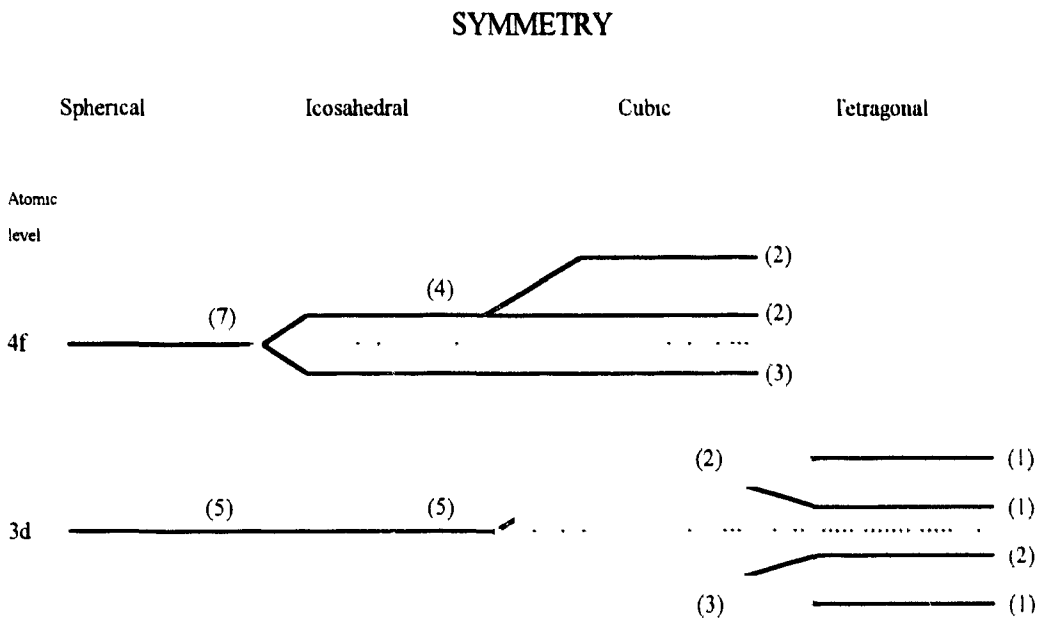

Figure 3 1 Effect of lowering symmetry from spherical to icosahedral, cubic, and tetragonal, on 5-fold degenerate *d* states and 7-fold degenerate *f* states State degeneracies are given in curved brackets

3.1.1. Magnetism in Quasicrystalline $Al_{70-x}Pd_{15}Mn_{15}B_x$

Recently, Yokoyama et al [29] reported the synthesis, structural and magnetic characterization of $Al_{70-x}Pd_{15}Mn_{15}B_x$ icosahedral alloys The room temperature magnetization was found to increase with increasing B content up to 10 at % B and showed a maximum of $2.1\times10^{-7}\ H\cdot m^2\cdot kg^{-1}$ at 10 at % B The magnetization is observed only in the metastable quasicrystalline phase and is not present in the equilibrium crystalline phase The quasilattice

parameter, a_o, was found to decrease as the B content was increased. The Curie temperatures have been reported to be around 470 ~ 500 *K*. These alloys exhibit magnetic moments up to 18 *emu/g* which disappear after crystallization at around 1000 *K*. These icosahedral alloys were first reported to be ferrimagnetic below the Curie temperature. Later NMR studies [30] of Al-Pd-Mn-B QC's showed that these alloys are ferromagnetic rather than ferrimagnetic and the origin of ferromagnetism was indicated to be primarily from Mn-B bonding. The NMR studies also showed the coexistence of magnetic and paramagnetic Mn sites in Al-Pd-Mn-B alloys [30].

Recently, Bahadur et al [57], using ferromagnetic resonance (FMR) techniques, investigated the magnetic interactions, number of magnetic sites and magnetic anisotropy in the icosahedral $Al_{70-x}Pd_{15}Mn_{15}B_x$ alloys. These samples are from the same batch used in the study of transport properties reported in the present work. Bahadur et al [57] also carried out differential scanning calorimetry (DSC) measurements on these samples. Generally, three thermal features were observed in the DSC scan of each sample: (a) a very weak transition varying between 330 and 630 *K* as *x* is varied between 1 and 10, (b) a very broad and large exothermic transition with the maximum temperature varying between 650 and 700 *K* as a function of *x* and (c) a large sharp exothermic transition occurring at yet higher temperatures which increased with x. The first and the third transitions were identified with the magnetic transition temperature and the crystallization transition of the icosahedral phase corresponding to the quasicrystalline to crystalline transformation, respectively. The origin of the second broad transition is not clear. However, this can most likely be attributed to structural relaxation of disorder and phason strains introduced in the system during the quenching process.

The room temperature magnetization measurements of Bahadur et al [57] showed that when $x = 0$ no indication of magnetic ordering was observed. With 1 at % boron introduced into the system, a spontaneous magnetic moment is observed which increases with increasing boron concentration. The magnetization increased with x up to at least $x = 10$. A similar observation has been made by Yokoyama et al [29].

The FMR study of Bahadur et al [57] showed that

(a) for $x = 0$, a single resonance was observed at a field of 3240 *Oe* for temperatures above 77 *K*.

(b) for $x \geq 1$, however, two resonances were observed below a critical temperature, T_c. Above T_c, only a single resonance was observed at a field of about 3220 *Oe* This corresponds to a free *g*-factor value of 2 and is essentially temperature and composition independent and is characteristic of the paramagnetic Mn ions.

(c) The low field resonance, which was broader and more intense, occurred between 200 *Oe* and 2500 *Oe*. It was strongly temperature and composition dependent and identified with the existence of magnetic interactions in the system. As the temperature approached T_c, the intensity decreased drastically and the resonance was undetectable above this characteristic transition temperature. Above this temperature only a single high field (3220 *Oe*) resonance was observed.

From the above observations Bahadur et al [57] confirmed the duality of Mn sites in $Al_{70-x}Pd_{15}Mn_{15}B_x$. The low field resonance was identified with coupled spins while the high field resonance in the $x = 0$ (nonmagnetic) sample and in the magnetic samples above T_c was due to paramagnetic Mn ions.

3.2. Structure

Figure 3 2 shows the room temperature X-ray diffraction patterns of the melt spun $Al_{70-x}Pd_{15}Mn_{15}B_x$ (x = 0 - 10) icosahedral alloys. The diffraction patterns show the samples to be essentially single phase icosahedral QC alloys. The peaks in the diffraction patterns were indexed with the indexing scheme of Elser [7]. The quasilattice constant evaluated from the wave vector of the (211111) reflection showed a decrease from 4 587 Å for x = 0 to 4 572 Å for x = 10 with increasing x. A similar observation has been reported by Yokoyama et al [29] although the change reported in this work is nearly twice as large. The full-width at half maximum for the (211111) diffraction line increased from 0 140° to 0 274° with increasing in x This peak broadening can be related to increasing disorder or can be the result of differences in grain size of the quasicrystallites.

3.3. ac *Susceptibility Measurement Results*

Figure 3 3 shows the room temperature *ac* susceptibility of $Al_{70-x}Pd_{15}Mn_{15}B_x$ (x = 0 - 10) The magnetic susceptibility shows an almost linear increase with increasing Boron concentration This result is consistent with the FMR result reported by Bahadur et al [57] and with magnetization results reported by Yokoyama et al [29].

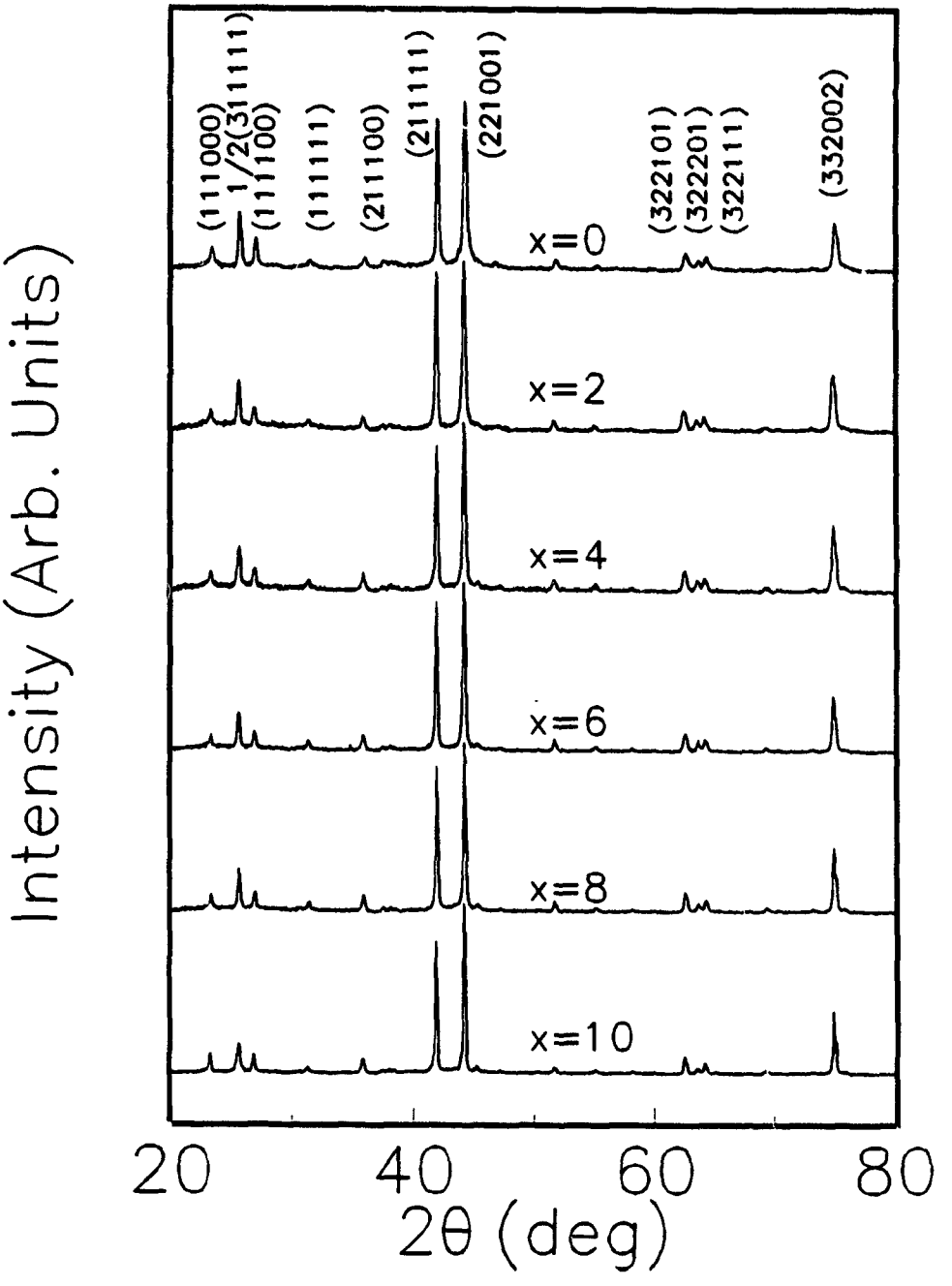

Figure 3.2 X-ray diffraction patterns for as-quenched $Al_{70-x}Pd_{15}Mn_{15}B_x$ (x = 0 - 10) alloys.

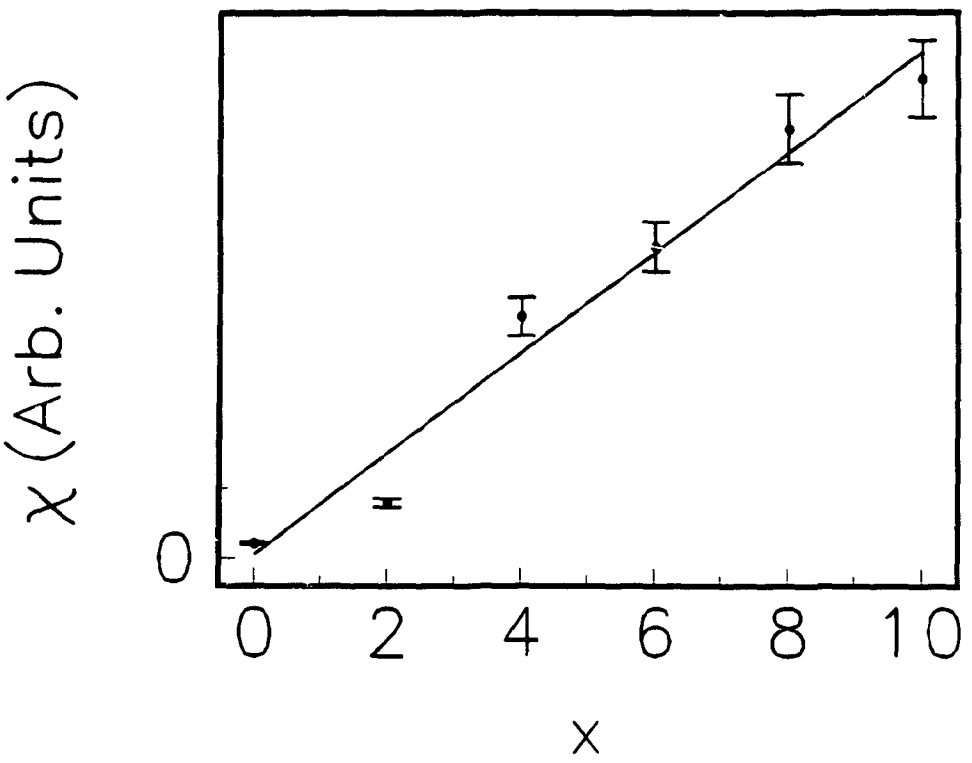

Figure 3 3 Boron concentration dependence of the *ac* susceptibility of icosahedral $Al_{70-x}Pd_{15}Mn_{15}B_x$ (x = 0 - 10) alloys at room temperature

According to the recent work of Hattori et al [58] the temperature dependence of the *ac* magnetic susceptibility of $Al_{70}Pd_{15}Mn_{15}$ followed a Curie-Weiss law over a wide temperature range except at very low temperatures where it showed a cusp at around 10 *K* From this cusp they concluded that this quasicrystalline alloy was a spin-glass Figure 3 4 shows the measured temperature dependence of the zero field cooled *ac* susceptibility of $Al_{70-x}Pd_{15}Mn_{15}B_x$ (x = 2 - 10) obtained in the present work A typical temperature dependence of the real and imaginary part of the complex *ac* susceptibility is shown in Figure 3 5 Our measurement shows a well defined knee in both $\chi'(T)$ and $\chi''(T)$ (for $6 \leq x \leq 10$); although no clear peak in $\chi''(T)$ is seen T_f determined from the first significant drop in $d\chi/dT$ is in the range 32 - 36 *K* in these alloys

No signature of re-entrant spin-glass (RSG) behaviour in alloys of low Boron concentration ($x \leq 4$) was observed.

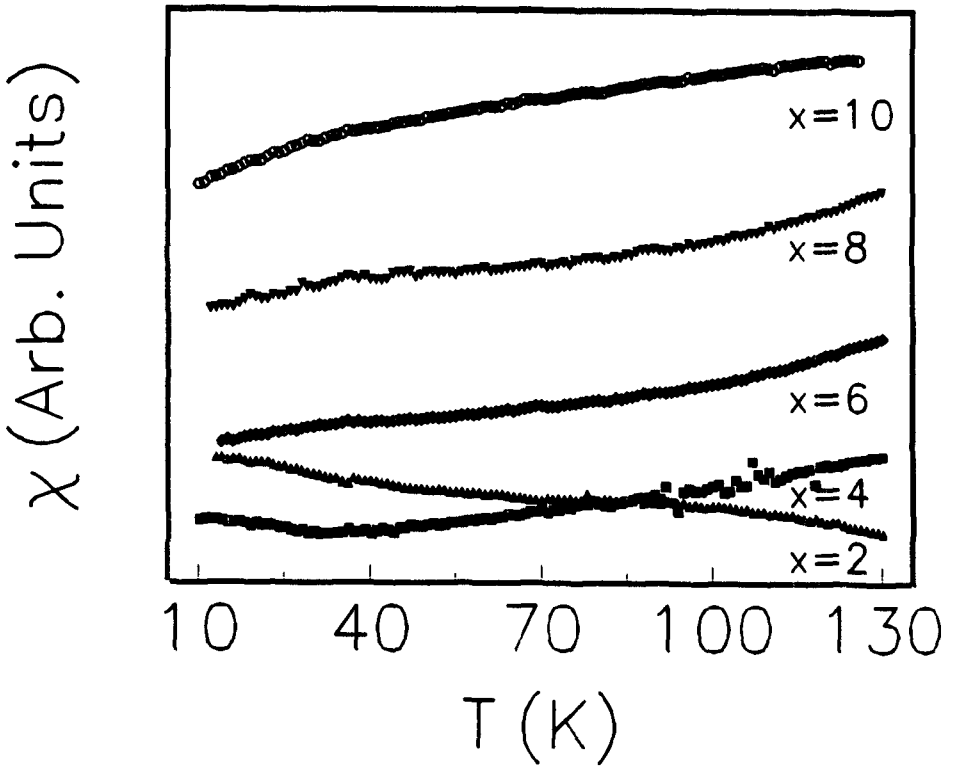

Figure 3.4 Magnetic susceptibility as function of temperature for icosahedral $Al_{70-x}Pd_{15}Mn_{15}B_x$ measured at 127 *Hz*.

The magnetic phase diagrams of systems with competing interactions exhibit order (ferromagnetic or anti-ferromagnetic), disorder (spin-glass) and often a regime of co-existing re-entrant (ferromagnetic-spin-glass or antiferromagnetic-spin-glass) states depending on alloy composition [59]. Ferromagnets with substantial exchange bond disorder, due to some form of quenched structural randomness frequently exhibit, upon cooling, first a transition from a paramagnetic state to a ferromagnetic one and then a second low temperature transition from the ferromagnetic state to a spin-glass state. However, in these systems the transitions are not

well defined [60]. Specially, the transition from ferromagnetism to spin-glass is difficult to determine.

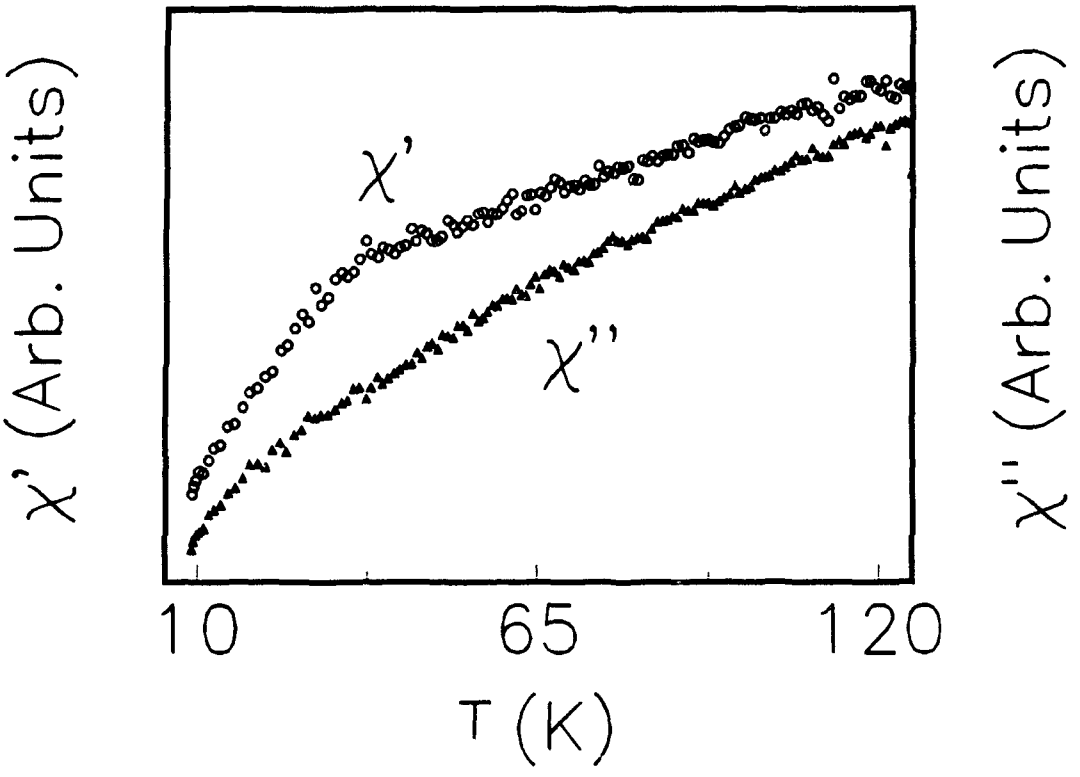

Figure 3 5 The temperature dependence of zero-field cooled real and imaginary parts of the *ac* susceptibility for $Al_{60}Pd_{15}Mn_{15}B_{10}$.

From an experimental point of view, in most cases, the transition from ferromagnetism to the re-entrant spin-glass (ReG) state is defined by the onset of deviations from the plateau in the magnetization or by a drop in the *ac* susceptibility at a well defined temperature, T_f, indicating spin freezing [60]. There are some ambiguous interpretations of the inflection or cusp observed in the temperature dependence of the *ac* susceptibility of these systems [61] Such ambiguities could arise from experimental artifacts which depend on the exciting field frequency and amplitude. Recently, Nogues and Rao [61] showed that above a certain threshold *ac*-field amplitude, system dependent coercivity and domain wall effects with the

concomitant Hopkinson peak and their field dependence mask any clear identification of the re-entrant magnetic behaviour in susceptibility measurements. These authors [61] also showed that below a threshold *ac*-field amplitude the influence of domains and domain wall motion, the well known Hopkinson peak effect, can be eliminated in the *ac* susceptibility measurement to reveal clearly the re-entrant characteristics. In this study a re-entrant freezing temperature T_f is unambiguously revealed with an evident knee in $\chi'(T)$ and a corresponding well defined peak in $\chi''(T)$. They also showed, that as the field was increased above this threshold field the Hopkinson peak broadened and shifted to lower temperatures, masking the re-entrant features.

These preliminary magnetic susceptibility measurements indicate the re-entrant magnetic behaviour in this alloys. However, due to the fact that the present temperature dependent susceptibility measurement were carried out above the threshold *ac*-field and the influence of domain and domain wall motion masked the re-entrant features, a well defined peak in $\chi''(T)$ was not observed. In order to determine precisely the nature of the low temperature phase transition encountered in these alloys a detailed study and analysis would be necessary..

The transition temperature from ferromagnetism to spin-glass behaviour for $Al_{70}Pd_{15}Mn_{15}$ was reported to be 10 *K* [58] This temperature increased to over 32 K with the addition of boron as indicated by this preliminary result.

3.4. Discussion

The RSG regime shares the characteristics of both spin-glass (SG) and ferromagnetic ordering [59, 62]. Theoretical investigations of the SG transitions which are generally used to

explain the experimental results are based particularly on the mean field model suggested by de Almida and Thouless [63] and Gabay and Toulouse [64]. Accordingly, the longitudinal ferromagnetic state is followed below some critical temperature T_g by a canted FM state, characterised by a freezing of the transverse components of spin.

The most important question to be considered is the cause of the magnetic ordering observed in these alloys with B substitution. The mechanism for the appearance of the magnetisation is assumed by Yokoyama et al [29] to originate from the RKKY interaction although they also suggest that the details of magnetic interactions are complicated. The dependence of the magnetic properties (i.e. spontaneous magnetisation and transition temperatures, both T_f and T_c) on the concentration of B suggests local moment formation as is prevalent in many Mn containing icosahederal alloys. Since the tendency for local magnetic moment formation on an impurity in an Al host is maximum for Mn the magnetic order in the present alloys presumably arises as a result of local Mn moment formation. As the magnetic behaviour is found to be strongly dependent on the boron concentration, it is likely that the boron *sp* electrons contribute to the magnetic interaction between the 3*d* electrons of neighbouring Mn atoms as suggested [57]. In view of the spin-glass behaviour observed in QC $Al_{70}Pd_{15}Mn_{15}$ [58] and the present observation of spin-glass like behaviour; the RKKY interaction is the most probable interaction responsible for the magnetic ordering. The RKKY interaction in the quasicrystalline phase seems to arise through the interaction between the icosahedral clusters [57, 29]. In a model of quasicrystalline $Al_{70}Pd_{15}Mn_{15}$, consisting of a central Mn atom surrounded by Al and Pd, the distance between Mn atoms is large and direct

overlap of $3d$ wave functions is not possible The coupling between the spins at neighbouring Mn sites is, therefore, expected to arise from an indirect exchange interaction.

4. Electrical Resistivity of $Al_{70-x}Pd_{15}Mn_{15}B_x$

Electrical resistivity provides a very sensitive probe with which to understand the various electronic scattering processes that occur in a given material. The temperature dependence of the resistivity of many magnetic and non-magnetic disordered systems below room temperature results from a number of scattering mechanisms, as well as localization and Coulomb interaction effects. The temperature dependent electron scattering mechanisms in non-periodic systems can be separated into regimes dominated by Boltzmann-type transport and transport characterized by weak localization. A large number of models for the electrical resistivity of disordered systems have been proposed (for reviews see [65, 66, 67]) over the years. Those which are most relevant for an understanding of disordered magnetic alloys are described below (section 4.1). In each case the emphasis is placed on the physics of the models and on their specific predictions. The temperature dependence of the electrical resistivity of quasicrystals is essentially the same as that observed for amorphous alloys [68, 11]. A discussion of the current experimental data in light of the existing theories originally developed for amorphous alloys and weak localization theory is given in the following sections.

4.1. Theoretical Background

Available transport data has shown that the temperature coefficient of resistivity $TCR = \rho^{-1}(\partial\rho / \partial T)$ changes from positive for small values of ρ to negative for large values of ρ for $\rho \approx 150\ \mu\Omega cm$. This correlation between ρ and TCR was first summarised in the Mooij

plot [69]. A number of models have been proposed to explain both the magnitude of the resistivity and the *TCR*-ρ correlation. Among these are mechanisms based on structural scattering in liquid and amorphous metals, phonon assisted transport, and weak localisation and interaction effects in disordered metals. Details of the models relevant to the present investigations are discussed below.

4.1.1. The Diffraction Model

Experimental evidence that electron transport properties of amorphous metals are usually similar [70] to those of the corresponding liquid metals has led various workers to the use of a theoretical formalism, originally proposed for simple liquid metals by Ziman [71], which is based on the Boltzmann equation and which treats electrons as plane waves which scatter from atomic potentials. This model was subsequently extended by Evans et al. [72] to include liquid transition metals, in order to explain a number of peculiarities observed in the transport properties of metallic glasses. This theory takes into account the scattering of conduction electrons from the potential of the disordered lattice of a transition-metal system and expresses the resistivity as [72]

$$\rho \approx \frac{30\pi^3 \mathrm{h}^3}{me^2 k_F^2 E_F \Omega} \sin^2\left[\eta_2(E_F)\right] S_T(2k_F), \tag{4.1}$$

where k_F and E_F are the Fermi wave vector and energy, respectively, Ω is the atomic volume. $\eta_2(E_F)$ is the *d*-wave phase shift describing the scattering of the conduction electrons, of energy E_F, by the ion cores which each carry a muffin-tin potential. In this expression, the temperature dependence of ρ is determined by the temperature dependence

of the structure factor $S_T(2k_F)$. Several calculations [73, 74,75, 76] of $S_T(k)$ within the framework of the diffraction model are available. Within the diffraction model the temperature dependence of the resistivity is essentially controlled by that of the structure factor $S_T(k)$, with a predicted T^2 low temperature behaviour with either positive or negative slope and a linear T dependence at high temperature.

4.1.2. Resistivity of Disordered Magnetic Alloys

In addition to a contribution due to the scattering of conduction electrons from the structural disorder, electron-magnon scattering gives a significant contribution to ρ in magnetic glasses and hence the customary approach of neglecting the magnetic contribution, $\rho_m(T)$, while analyzing the resistivity data on magnetic disordered alloys is not correct. Theoretical investigations [79, 80] that pursue this line of thinking and use the spin-wave approximation to calculate $\rho_m(T)$ for amorphous ferromagnets reveal that;

(1) $\rho_m(T)$ is composed of two positive contributions; one varying as T^2, as in crystalline ferromagnets, and the other as $T^{3/2}$, and

(2) the contribution to $\rho_m(T)$ from the $T^{3/2}$ term (which appears only in the amorphous case) is at least 2 orders of magnitude greater than the one arising from the T^2 term.

These theories, therefore, predict a $T^{3/2}$ power law for $\rho_m(T)$ at low temperatures in amorphous ferromagnets in contrast to the T^2 dependence observed experimentally in these materials.

In order to explain this discrepancy Kaul et al [81] undertook a detailed quantitative analysis of resistivity data of ferromagnetic amorphous alloys and established the existence of a magnetic contribution, ρ_m, to ρ and made a reliable estimate of ρ_m Kaul et al. [81] draw the following conclusions from their analysis:

(1) Both the electron-ion potential scattering and electron-magnon scattering contribute to the resistivity

(2) The structural contribution dominates over the magnetic contribution

(3) The competing contributions to $\rho_m(T)$ arising from the incoherent and elastic components of the electron-magnon scattering are of roughly the same magnitude Hence, the $T^{3/2}$ term which arises from this competing contribution to ρ_m is negligibly small compared to the T^2 term.

These authors also argued that the magnetic contribution to ρ goes unnoticed at low temperatures primarily because the structural contribution to ρ and $\rho_m(T)$ both follow a T^2 power law but is clearly apparent at high temperatures where the structural contribution exhibits a transition from a quadratic to linear temperature dependence while $\rho_m(T)$ continues to vary as T^2

4.1.3. The Kondo Effect

One unusual feature in the resistivity of both dilute and concentrated ferromagnet amorphous alloys is the existence of the low temperature resistance minimum The fact that low-temperature anomalies are observed in almost every amorphous alloy containing

an element capable of carrying a moment, and not in alloys that are non-magnetic, indicates that the anomalies are magnetic in origin.

The striking resistance rise at low temperatures and its sensitivity to the nature and concentration of the impurity in dilute transition metal-metalloid amorphous alloys has been associated with the Kondo effect, which has been studied extensively in crystalline materials. The Kondo effect is associated with the scattering of conduction electrons from local magnetic impurities in an otherwise non-magnetic matrix. This gives rise to a spin-dependent increase in the resistivity at low temperatures which, coupled with the usual increased scattering by phonons at higher temperatures, produces a minimum in the total resistivity of these alloys.

This spin-dependent resistivity has the form

$$\rho(T) = \rho_o - \xi \ln(T / T_K), \tag{4.2}$$

where ξ is a constant dependent on the magnetic impurity concentration and T_K is the Kondo temperature.

4.1.4. The Effects of s-d Hybridization

Several approaches to the calculation of transport coefficients consider the conducting states to be free electron-like. However, in transition metal containing alloys it is also necessary to consider the importance of the d-states, viz., whether these contribute to the conductivity and how, through hybridization, they modify the "free electron-like" states.

Transition metals are formed from atoms with an unfilled d-shell and so their band structure is considerably more complex than that of non-transition metals. As a rough

picture we can think of an *s*-band arising from the outermost *s* and *p* electrons of the free atom together with a *d*-band of electrons (or holes) formed from the *d*-states. Because the outermost *s* and *p* electron wavefunctions on one atom overlap greatly with those on a neighboring atom the s and p electrons can move more or less freely throughout the crystal and give rise to a free electron-like band. On the other hand, the *d* electron wavefunctions overlap much less and so form a band which is much narrower in energy and with a high density of states. The *s* and *p* electrons (*s* electrons for short) thus have a high velocity and the d electrons a low velocity. The s electrons carry most of the current but they can be scattered into empty *d*-states (so called *s-d* scattering) which, because of their high density, enhances the scattering and hence the resistivity. This is an oversimplification since in general there is a mixing of the character of the wavefunctions of the *s* and *d* electrons, referred to as "hybridization". Nonetheless, conceptually the electron transport properties of transition metals can be understood in terms of a conventional theory similar to that of simple metals.

4.1.5. Quantum Corrections to the Resistivity

The resistance of disordered systems shows unusual deviations from Boltzmann equation based theories, particularly at low temperature. In the weakly localized regime a number of corrections to the transport coefficients of disordered conductors have been identified [82, 83] which are broadly classified as Weak Localization (WL) and Electron-Electron Interactions (EEI) [83, 84] and are known as collectively as Quantum Corrections to the Resistivity. WL and EEI have been shown to account for the

temperature and field dependence of the resistance of disordered metallic alloys. In view of the relevance of WL and EEI in understanding the transport properties discussed in this thesis, a brief review of these effects is given below.

Weak Localization – Weak localization (WL) is a particular regime of localization of particles in disordered materials [85, 86], in which the effects of localization show themselves as small quantum perturbations of the classical behavior predicted by the Boltzmann equation. Weak localization is a unique case where the superposition principle of quantum mechanics leads to observable consequences in the properties of macroscopic systems [87].

In disordered systems particles have a diffusive motion resulting from their scattering by a random potential. At low temperature these collisions are essentially elastic and the particle wave functions retain their phase for long distances. It is, therefore, possible that two partial waves, starting from one point and experiencing scattering in a time reversed sequence with respect to each other, get back to their origin and interfere constructively (see Figure 4 1)

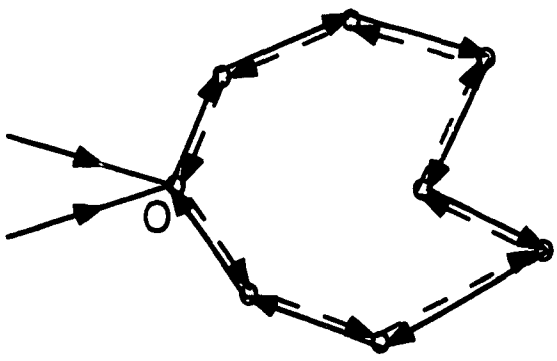

Figure 4.1 Schematic for the diffusion path of an electron in a disordered system. Backscattering of a wave packet propagating in opposite directions, $\pm k$, interfere at the origin O coherently.

Since the electrons traversing the same closed path but in opposite directions, are in the same eigenstate, the amplitudes are in phase, and the resulting coherent interference increases the resistivity If Ψ_1 is the probability amplitude of the path that involves the anticlockwise path from O and back to O, and Ψ_2 that for the corresponding clockwise path then the total probability is

$$W = \left|\sum_i \Psi_i\right|^2 = |\Psi_1|^2 + |\Psi_2|^2 + \Psi_1^*\Psi_2 + \Psi_1\Psi_2^* \qquad (4\ 3)$$

The first two terms are just the classical probabilities while the second two terms are interference terms Since Ψ_1 and Ψ_2 are coherent, they have the same phase, and the total value of W is twice the classical probability This shows that multiple scattering can enhance the probability of returning to the origin, i e the probability of backscattering and hence the probability of 'localization' The result of this is that the electrical resistivity in the presence of such scattering is higher than would be calculated from the quasi-classical approach. In the presence of inelastic scattering (e.g electron-phonon scattering), spin-flip scattering (e.g spin-orbit scattering), or a magnetic field, the phase coherence of the wave-packets is destroyed. As a result, the resistivity is reduced

The temperature dependent correction to ρ due to WL including spin-orbit and magnetic scattering is [84, 88]

$$\left(\frac{\Delta\rho}{\rho}\right)_{WL} = \frac{\rho e^2}{2\pi^2 \hbar\sqrt{D}}\left[\left(\frac{1}{4\tau_i}+\frac{1}{4\tau_s}\right)^{1/2} - 3\left(\frac{1}{\tau_s}+\frac{1}{\tau_{so}}+\frac{1}{4\tau_i}\right)^{1/2}\right] \qquad (4\ 4)$$

where τ_i, , τ_{so}, τ_s and D are the inelastic, spin-orbit and spin-flip relaxation times and diffusion constant, respectively

Electron-Electron Interaction Effects -- In addition to WL, there are effects on the transport properties of disordered metals due to electron-electron interactions, also known as Coulombic interaction effects. The interaction effects result from the modification of electron-electron interaction in disordered metals [83]. By taking into account the diffusive motion of electrons in the treatment of electron-electron interactions, a correction to the Boltzmann theory is obtained.

WL effects involve single electrons and could take place even if electrons did not interact with each other. By contrast, the Coulomb anomaly arises from the interaction of one conduction electron with another in the presence of the multiple-scattering processes that occur in a disordered system. As in the WL case, EEI depends on coherence and interference effects. But now, instead of one, we have two electrons whose wavefunctions interfere and they may have different energies so that there is here another source of dephasing between them, beyond that induced by inelastic processes or magnetic fields, that is, their difference in energy, i.e. in frequency. Only electrons near the Fermi level are involved and typically their energy difference is of order $k_B T$ with a consequent frequency difference of $k_B T / \hbar$. The resulting thermal coherence time (i.e. the time that elapses between the two waves being in phase and becoming out of phase) is $\tau_T \sim \hbar / k_B T$. If τ_0 is the mean free time between elastic scattering of an electron by ions, anomalous effects are seen only when $\tau_T >> \tau_0$ (i.e. the two electrons maintain a close phase relationship through many elastic scattering events). Since these effects depend upon coherence, electron-electron interaction effects, conspicuous at low temperatures, will ultimately disappear as

the temperature is raised. As in WL process, EEI depends upon those electrons that can achieve closed paths through elastic (and hence coherent) scattering.

The temperature dependent correction to ρ due to EEI has the form [84]

$$\left(\frac{\Delta\rho}{\rho}\right)_{EEI} = -\left(\frac{4}{3} - 2F\right)\left(\frac{13e^2}{4\pi^2\mathrm{h}}\right)\sqrt{\frac{k_B T}{2\mathrm{h}D}}, \tag{4.5}$$

where F is an integral over scattering angle of the screened Coulomb interaction and D is the diffusion constant.

4.2. Result and Discussion

Figures 4 2 shows the temperature dependence of the normalized electrical resistivity, $\rho(T)/\rho_o$ where ρ_o is the resistivity at 4.2 K, of the quasicrystalline alloys $Al_{70-x}Pd_{15}Mn_{15}B_x$ (x = 0, 2, 4, 6, 8, 10). High resistivity values are measured for all the samples (1900 - 6200 $\mu\Omega cm$ at 4 2 K) with no systematic trend. The temperature dependence of $\rho(T)$, as shown in Figure 4 2, exhibits substantial changes with increasing Boron concentration. A minimum in the resistivity which shifts to lower temperature as x increases is observed in x = 2, 4 and 6 samples as shown in Table 4 1 Above the observed resistivity maximum temperature (for x = 2, 4 and 6), the temperature coefficient of the resistivity, *TCR*, is negative. No resistivity minimum is observed for the remaining samples and the *TCR* is always negative At low temperature, the resistivity showed a rapid increase with decreasing temperature

Table 4.1. Experimentally observed values of the room temperature resistivity $\rho(300\ K)$, resistivity minimum and maximum, T_{min} and T_{max}, respectively, and the temperature coefficient of resistivity (TCR) at 300 K for icosahederal $Al_{70-x}Pd_{15}Mn_{15}B_x$.

x (*at.%*)	$\rho(300\ K)\pm12\%$ ($\mu\Omega cm$)	$TCR(300\ K)$ ($10^{-4}\ K^{-1}$)	$T_{min} \pm 1\ (K)$	$T_{max} \pm 1\ (K)$	$\rho_{4.2K}/\rho_{300K}$
0	5100	-4.48	-	-	1.23
2	1700	-3.77	49.1	120	1.11
4	3400	-4.12	46.1	88	1.11
6	3000	-5.80	31.0	76	1.13
8	4700	-6.99	-	-	1.17
10	2200	-3.958	-	-	1.08

The resistivity of the as-quenched $Al_{70-x}Pd_{15}Mn_{15}B_x$ QC alloys are observed to be 1900 - 6200 $\mu\Omega cm$ at 4.2 K. These values are about one order of magnitude higher than metastable QC's such as AlMn (a few hundred $\mu\Omega cm$) but similar to those of stable QC's. Various theories have been proposed to interpret the high values of the resistivity of QCs [89 -91]. Experimentally, the high resistivity at low temperature of QC's has generally been attributed to the following two factors: (1) small density of states at the Fermi level as a result of opening of a deep pseudogap at the Fermi level to gain electronic energy, and (2) the weakly localized nature of electrons at the Fermi level [92]. It has been shown that the electronic states in the deep pseudogap have a tendency to be localized [93]. It has also been suggested experimentally from the temperature dependence of the resistivity at high temperature that the diffusivity of electrons sharply decreases as the states move deep into the pseudogap [94]. The electronic properties of QC's, and in particular their transport and magnetic properties, depend very much on their structural quality. It was shown, for stable *i*-phase samples of AlPdMn and AlCuFe, that the resistivity increases as the structural quality improves, i.e. after defect removing by annealing [15]. The value of

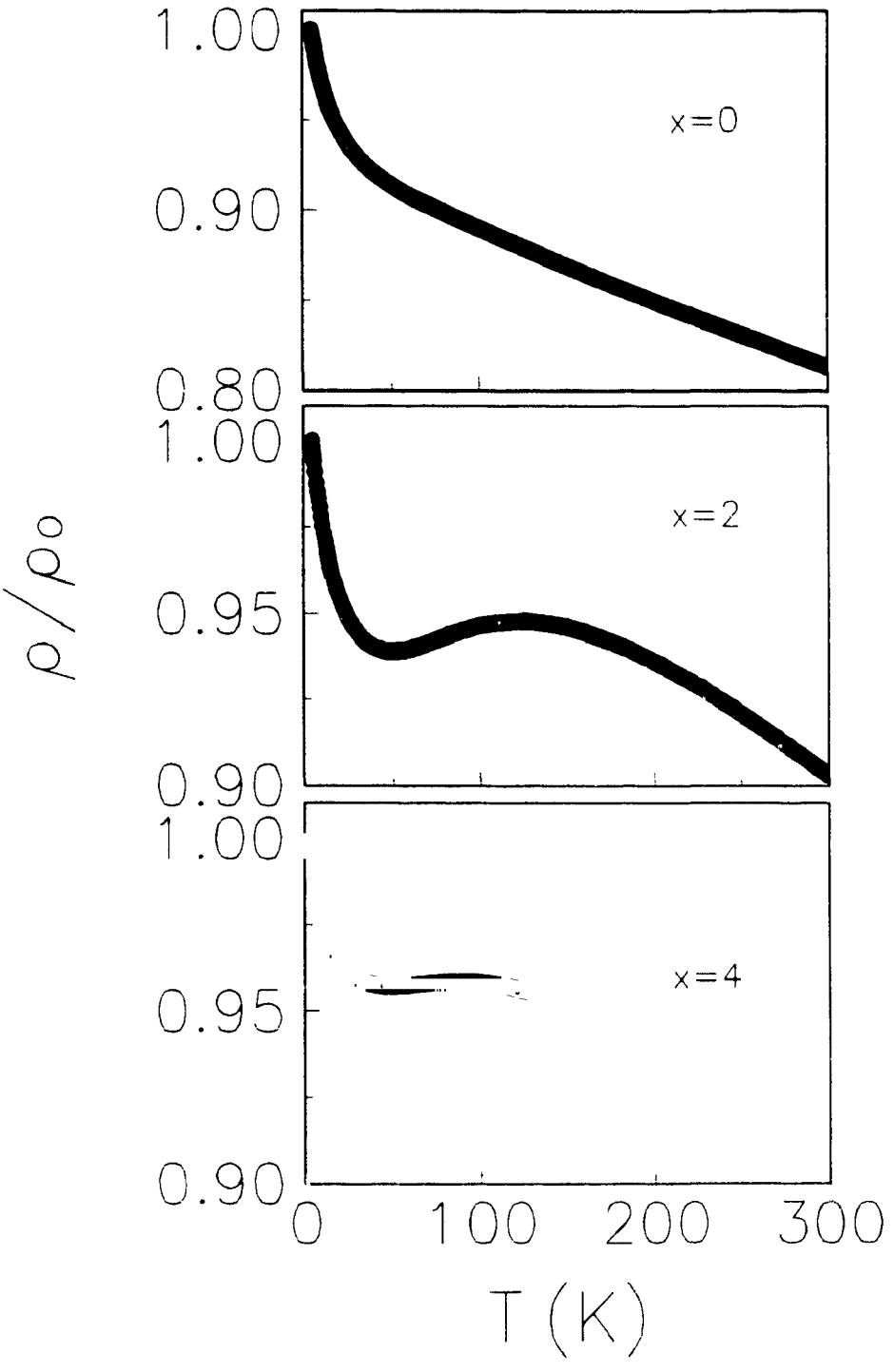

(a)

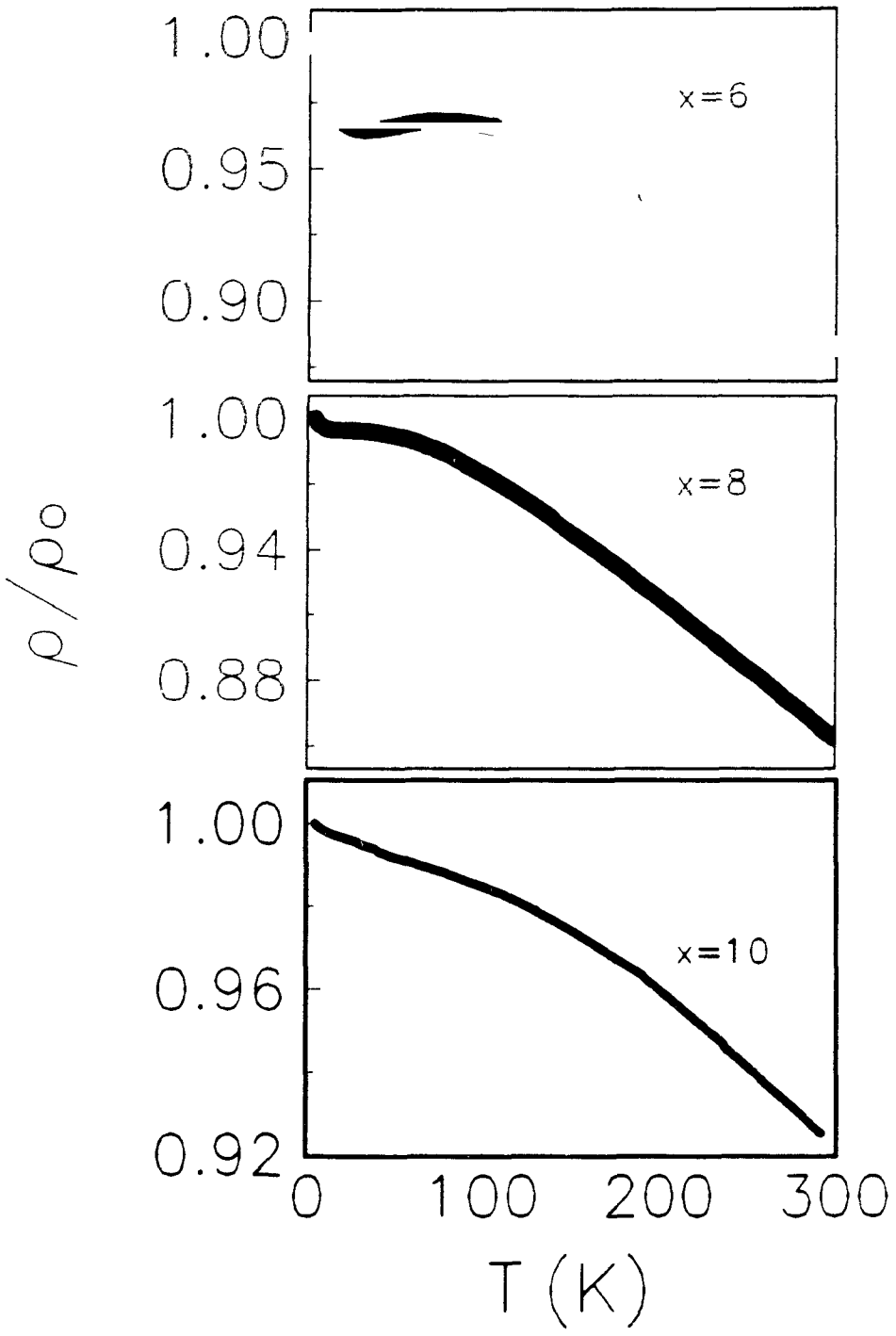

(b)

Figure 4.2. (a) and (b): the temperature dependence of the normalized resistivity of quasicrystalline $Al_{70-x}Pd_{15}Mn_{15}B_x$.

the resistivity in $Al_{70-x}Pd_{15}Mn_{15}B_x$, see Table 4 1, showed no systematic trend with increasing Boron concentration This could probably be due to the different level of the structural defects in each sample which is highly influenced by the quenching process (such as quenching rate, orifice size of the quartz tube, the distance between the quartz tube and copper wheel and argon ejection pressure)

The study of the electron scattering mechanism in non-periodic systems provides a difficult challenge This is particularly true for the interpretation of the transport properties of disordered alloys containing transition metals It is difficult to discuss the transport properties of these alloys in the context of a single theoretical model for all temperature ranges For this reason, we divided the temperature intervals as follows: (a) Low temperature range $T < 30\ K$, (b) Intermediate range: $T_{min} < T < T_{max}$, (c) High temperature range $T > T_{max}$ For $x = 0$, 8 and 10 samples the temperature intervals are $T < 30\ K$ and $T > 30\ K$

So far, the low-temperature resistivity and magnetoresistivity of the high-ρ QC alloys appear to be satisfactorily explained by the WL and EEI theories. As will be discussed in Chapter 5, only the WL contribution to the magnetoresistivity will be considered since the EEI contribution is much smaller in magnitude and can be neglected. The WL contribution to $\rho(T)$ is given by Equation 4.4 Figure 4.3 shows the trend of the theoretical curves for different values of $\tau_i(T)/\tau_{so}$ (τ_i is taken to be proportional to T^{-2}) as obtained from Equation 4 4 For weak and moderate spin-orbit scattering, i.e., $\tau_i/\tau_{so} \leq 1$, due to the destruction of WL by the inelastic scattering of electrons, the resistivity shows a nearly linear decrease with increasing temperature Due to anti-localization effects of spin-

orbit scattering, for strong spin-orbit scattering, i e , $\tau_i/\tau_{so} >> 1$, the low temperature resistivity increases with increasing temperature The temperature dependence of the zero-field resistivity below 30 K is shown in Figure 4 4 The experimental data, shown in Figure 4 4, do not follow the trend of the theoretical curves shown in Figure 4 3 Thus, a direct comparison of $\rho(T)$ data with WL theory do not allow for the determination of the scattering times, i e , inelastic scattering time $\tau_i(T)$, and the temperature independent spin-orbit and spin-flip relaxation times, τ_{so} and $\tau_{s,}$, respectively In all samples the resistivity measured experimentally at low temperature showed a sharp decrease with increasing

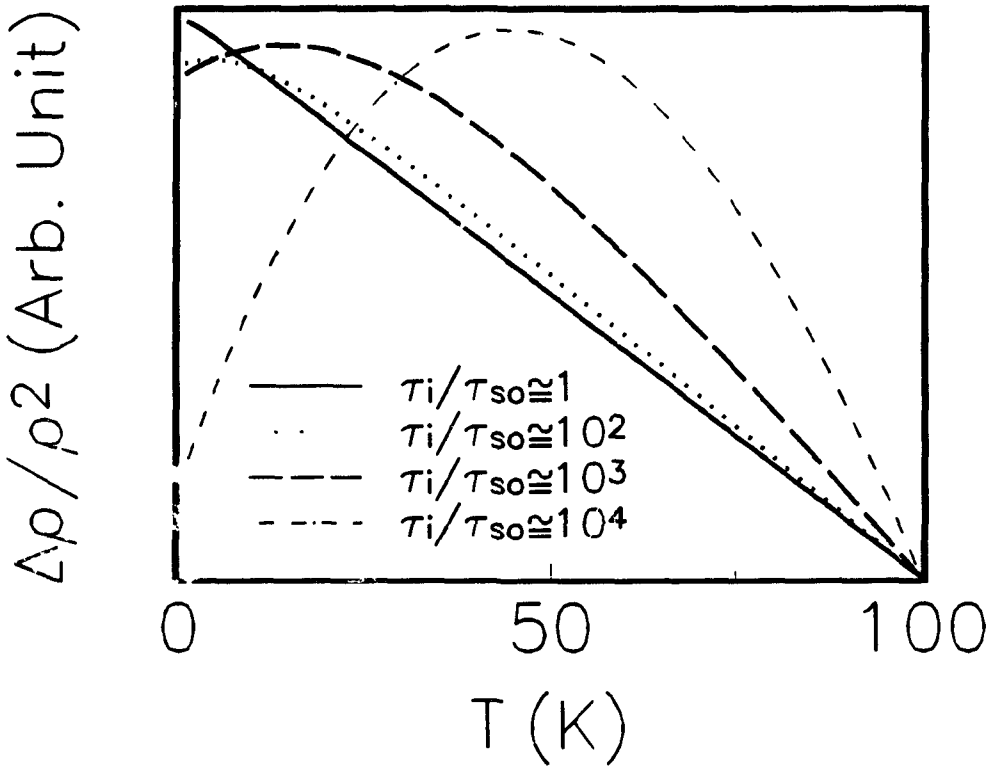

Figure 4 3 The WL contribution to the resistivity, $\Delta\rho/\rho^2$, as function of temperature calculated from Equation 4 4

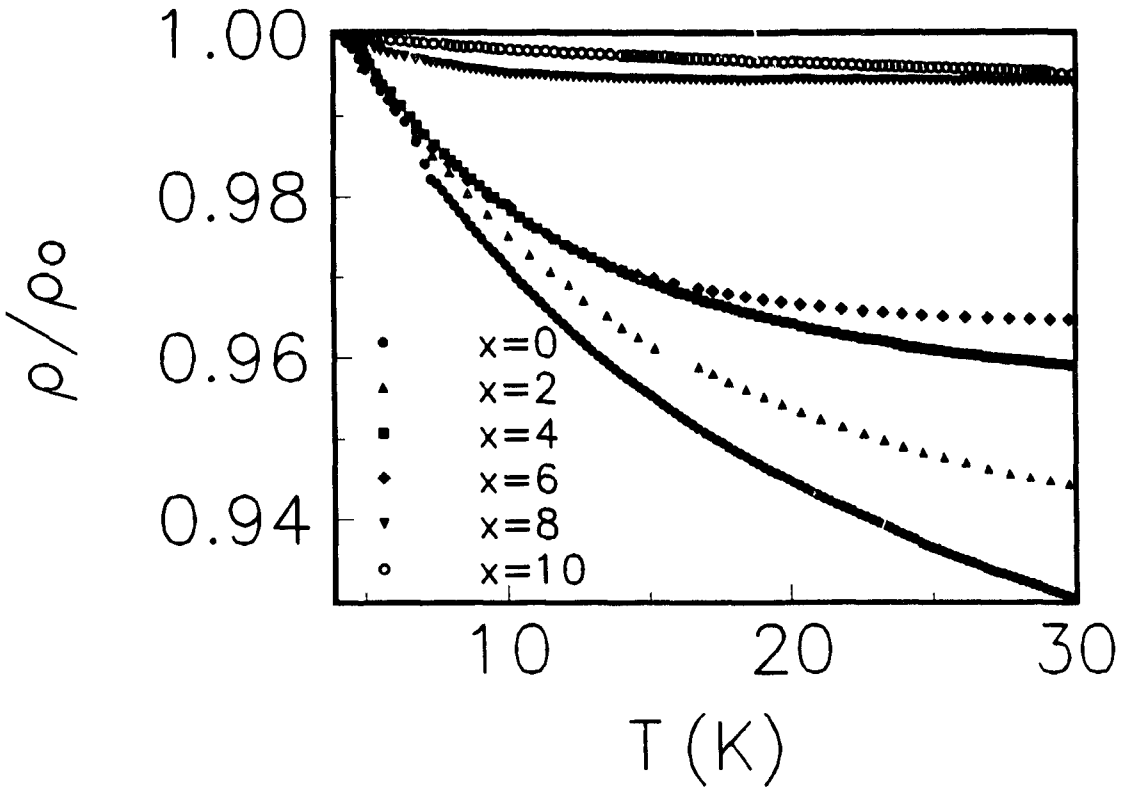

Figure 4 4 The normalized resistivity of $Al_{70-x}Pd_{15}Mn_{15}B_x$ below 30 *K*.

temperature. In order to interpret $\rho(T)$ in this temperature range it is necessary to take into account at least two effects

(1) The low temperature behavior of $\rho(T)$ in AlPdMn Qc alloys is attributed to magnetic scattering effects [27, 95]. The drop in $\rho(T)$ is observed to shift to lower temperature as the Mn concentration decreases and finally disappears in low-Mn alloys [27]. It is also concluded that this is due to the Mn magnetic scattering effect, i.e. a Kondo effect which is characterized by $ln(T)$ dependence [95]. The magnetoresistance of $Al_{70-x}Pd_{15}Mn_{15}B_x$, as discussed in Chapter 5, showed the coexistence of negative classical magnetoresistance due to spin-disorder scattering and magnetoresistance due to WL Therefore, the present

magnetoresistance result supports the assumption that magnetic scattering is at least one contributor to the low temperature behavior of $\rho(T)$ in $Al_{70-x}Pd_{15}Mn_{15}B_x$.

(2) A noteworthy observation in this temperature range is the decrease in the *TCR* with increasing Boron concentration; see Figure 4.4 This can be explained by the WL contribution to $\rho(T)$ In the moderate spin-orbit scattering systems ($x \leq 4$) the WL contribution to $\rho(T)$ decreases nearly linearly with increasing temperature. This WL decrease together with the sharp drop due to the magnetic scattering effect will result in an enhanced *TCR*. However, for strong spin-orbit scattering systems ($x > 4$) the WL contribution to $\rho(T)$ at low temperature increases with increasing temperature This component together with the decrease from magnetic scattering effects results in a decrease of the *TCR*

Two dominant effects appear to contribute to $\rho(T)$ at low temperature. WL and the magnetic scattering effect. The contribution of both effects is affected by the Boron concentration. The WL effect changes from localization to antilocaliztion, i.e. from decrease to an increase in $\rho(T)$ with increasing temperature, with increasing x It is expected that the magnetic scattering effect will increase as the magnetization increases In moderate spin-orbit scattering systems these two effects enhance $\rho(T)$ as exhibited in the high *TCR* value In strong spin-orbit scattering systems however the two effects compete resulting in a decrease of the *TCR*. Therefore, the resistivity behavior at low temperature in $Al_{70-x}Pd_{15}Mn_{15}B_x$ can be related to be primarily to magnetic scattering effects.

The above assertion may be illustrated as follows: The overall contribution to the low temperature resistivity can be written as

$$\rho(T) \approx \Delta\rho_{WL}(\tau_i(T), \tau_{so}, \tau_s, D) + \rho_{Kondo} \tag{4.6}$$

where $\Delta\rho_{WL}$ is the WL contribution and ρ_{Kondo} is a contribution due to a Kondo type magnetic scattering characterized by $ln(T)$ behavior. Using the scattering times values obtained from the magnetoresistance analysis and Equation 4.4, the WL component may be subtracted from the resistivity data. The remaining data, as shown in Figure 4.5, exhibits a $ln(T)$ dependence for all the samples. This demonstrates clearly that the sharp decrease in $\rho(T)$ at low temperature is indeed due to magnetic scattering effects.

The intermediate and high temperature resistivity can be written as

$$\rho(T) \approx \rho_S(T) + \rho_m(T) \tag{4.7}$$

where $\rho_s(T)$ and $\rho_m(T)$ are the structural and magnetic contributions to the total resistivity, respectively. For the intermediate temperature region, $T_{min} < T < T_{max}$, both the electron-magnon scattering, which gives rise to a quadratic temperature dependence [81] and the scattering of conduction electrons due to the structure factor, which also varies as T^2, are expected to give a significant contribution to $\rho(T)$. In the high temperature region, $T > T_{max}$, the structural contribution changes to linear temperature dependence while the electron-magnon scattering remains proportional to T^2 [81]. Therefore, assuming that the total resistivity can be expressed as the sum of these two contribution, the temperature variation of the resistivity can be written as

$$\frac{\rho(T)}{\rho(4.2K)} \approx a_1 + a_2 T^2, \qquad T_{min} < T < T_{max} \tag{4.8}$$

and

$$\frac{\rho(T)}{\rho(4.2K)} \approx b_1 + b_2 T + b_3 T^2, \qquad T > T_{max} \tag{4.9}$$

Least squares fits to the normalized resistivity data using Equations 4 8 and 4 9 give the values for the coefficients a_1, a_2, b_1, b_2 and b_3 listed in Table 4 2 $\rho(T)$ data which do not exhibit a maximum at low temperature are fitted to Equation 4 9 for the range $T > 30\ K$ The linear coefficients observed here are of the order of $10^{-5}\ K^{-1}$ and the quadratic coefficients of the order of $10^{-7}\ K^{-2}$ The fact that the magnitude of the linear coefficients given in Table 4 2 is greater than the quadratic reveals that $\rho_s(T)$ dominates over $\rho_m(T)$ in these temperature ranges Even though in the intermediate temperature range both $\rho_s(T)$ and $\rho_m(T)$ follow a T^2 power law, the contribution of $\rho_s(T)$ is expected to dominate The sign of the linear coefficients, as expected from the Mooij correlation, are negative except for $x = 2$ and 4 This is probably due to the WL effect which has been neglected at higher temperature Although there is an increasing trend to use WL theory up to room temperature [96], this is not appropriate for the $Al_{70-x}Pd_{15}Mn_{15}B_x$ alloys because of the magnetic ordering

Table 4 2 Least square fits parameter values based on Equations 4 8 and 4 9 for $Al_{70-x}Pd_{15}Mn_{15}B_x$ ΔT is the temperature range for intermediate and/or high temperature fits

x (*at* %)	a_1	a_2 ($10^{-7}\ K^{-2}$)	b_1	b_2 ($10^{-5}\ K^{-1}$)	b_3 ($10^{-7}\ K^{-2}$)	ΔT (K)
0	-	-	0 9401(2)	-53 8(3)	3 98(9)	30 - 300
2	0 9356(1)	12(2)	0 9489(5)	11 3 ±0 5	-9 0(1)	67-90 130-300
4	0 95616(1)	3 51(3)	0 9637(2)	3 8(2)	-8 39(6)	50-80 100-300
6	0 96346(4)	11 3(2)	0 9820(4)	-5 1(5)	-9 6(1)	36-61 90-300
8	-	-	1 0067(3)	-24 8(4)	-9 2(1)	30-300
10	-	-	0 99553(6)	-3 70(8)	-7 10(3)	30-300

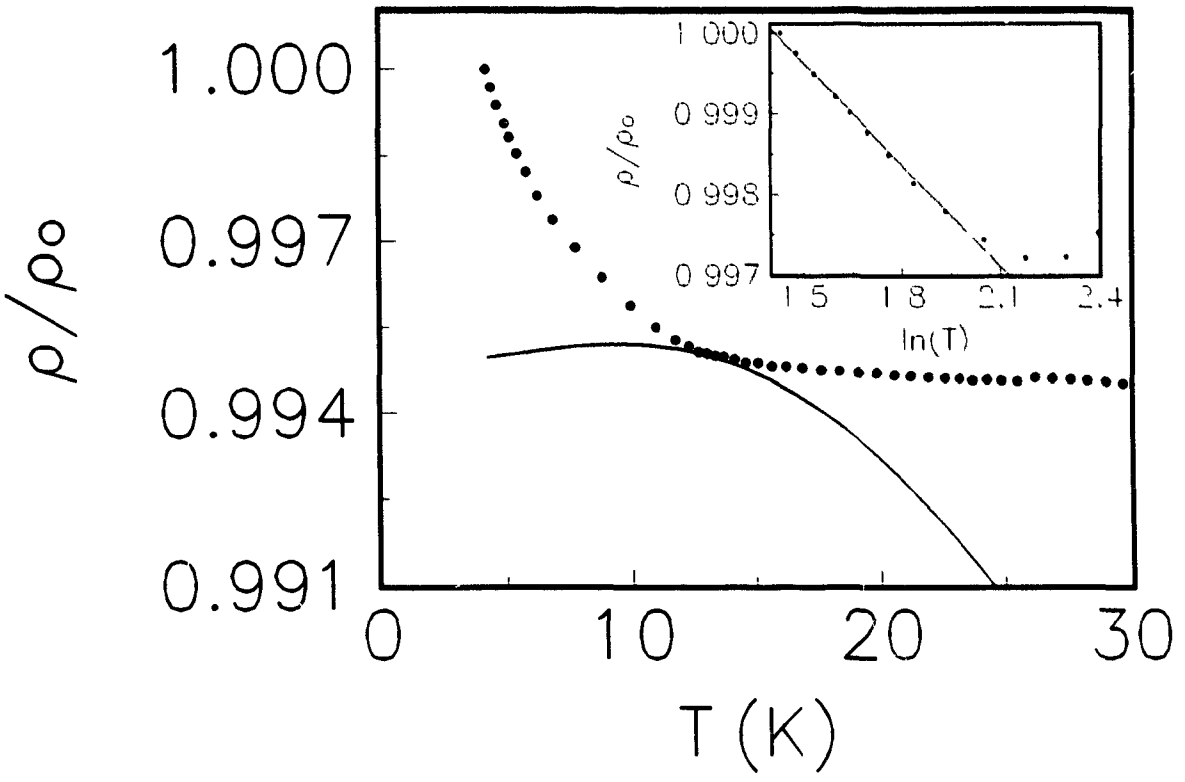

Figure 4 5 Temperature dependence of the resistivity of $Al_{62}Pd_{15}Mn_{15}B_8$ below 30 *K* The full curve shows the WL contribution to the resistivity as calculated using the scattering time values obtained from the magnetoresistance analysis (scaled for comparison) The inset shows the temperature dependence of the resistivity on a $ln(T)$ scale after the WL contribution is subtracted

The measured resistivity for $Al_{70-x}Pd_{15}Mn_{15}B_x$ shows very high values (1900 - 6200 $\mu\Omega cm$ at 4 2 *K*) These very high values reveal peculiar band structure effects, such as the presence of a pseudogap near the Fermi level The temperature dependence of $\rho(T)$ exhibits substantial changes as a function of Boron concentration The electron scattering mechanisms in nonperiodic systems can be separated into the Boltzmann transport and transport characterized by weak localization The transport properties of disordered alloys are sensitive to both magnetism and electronic structure At low temperature, WL and magnetic scattering effects describe the temperature dependence of the resistivity of Al_{70}.

$_x$Pd$_{15}$Mn$_{15}$B$_x$. At low temperature, $T < 30$ K, the resistivity showed a rapid decrease with increasing temperature and the magnitude of the *TCR* decreased with increasing Boron concentration. Two dominant effects appear to contribute to $\rho(T)$ in this temperature range; WL and magnetic scattering. The resistivity behavior at low temperature is primarily due to magnetic scattering effects. The decrease in the *TCR* is due to the transitions which Al$_{70-x}$Pd$_{15}$Mn$_{15}$B$_x$ alloys undergo from moderate spin-orbit scattering systems ($x \leq 4$) to strong spin-orbit scattering systems ($x > 4$) At higher temperatures $\rho(T)$ is adequately described by the temperature dependence of the structural and magnetic contributions to the resistivity as described by the Boltzmann-type transport.

5. Magnetoresistance of $Al_{70-x}Pd_{15}Mn_{15}B_x$

Low temperature magnetoresistance is one of the most powerful experimental probes for the study of the electronic processes in conductors. The magnetoresistance of $Al_{70-x}Pd_{15}Mn_{15}B_x$ consists of a superposition of the WL contribution and a negative classical spin disorder scattering at local magnetic moments. Low temperature magnetoresistance is also one of the most useful probes of quantum corrections to the resistivity, which can distinguish between the various contributions and provide detailed information about the electron scattering processes [82, 97]. WL offers a new method to measure characteristic times of the conduction electrons such as inelastic lifetime, spin-orbit coupling time, and magnetic scattering time. The most important models relevant to an understanding of the magnetoresistance of $Al_{70-x}Pd_{15}Mn_{15}B_x$ are described in Section 5.1. In each case the emphasis is placed on the physics of the models and on the specific predictions. A discussion of the magnetic field dependent experimental data is given in the following sections.

5.1. Theoretical Background: Contributions to the Magnetoresistance

5.1.1. Classical Considerations

In magnetic materials magnetic impurities contribute to the magnetoresistance in disordered conductors in two ways. Spin-flip scattering of conduction electrons by such impurities destroys the phase coherent back-scattering responsible for weak localization,

and so reduces the quantum correction magnetoresistance as discussed in section 5.1.2. The second contribution comes from the field and temperature dependence of the single site magnetic scattering. The single site magnetic scattering has two sources of magnetoresistance; magnetization changes due to domain wall motion and spin rotation and the magnetization changes which occur in strong fields. These cause complex behavior. This classical magnetoresistance is proportional to $-B^2$ at low fields and saturates at high fields [98, 99]

5.1.2. Weak Localization

Section 4.1.4 showed that multiple scattering can enhance the probability of backscattering and result in an increase in electrical resistivity From the following discussion in the present section a most important feature emerges; any process that destroys the phase-coherence of the two-electron partial waves will reduce this additional resistivity. Important examples of such processes are; inelastic scattering, applied magnetic field, spin-orbit coupling, magnetic scattering. These are considered.

Inelastic Scattering -- At low temperature it is necessary to distinguish between two different lifetimes for the conduction electrons, the elastic lifetime τ_o and the inelastic lifetime τ_i. Here τ_o is the lifetime of the electron in an eigenstate of momentum, whereas τ_i is the lifetime in an eigenstate of energy. At 4 K, the latter can exceed the former by several orders of magnitude. As a consequence, a conduction electron in state k can be

scattered by impurities without losing its phase coherence. If the temperature increases phonon scattering comes into play, this induces inelastic scattering which tends to cause phase-incoherent scattering and so reduces the enhancement. This makes the resistivity decrease with rising temperature.

Magnetic field -- In a magnetic field the phase coherence of the two partial waves is weakened or destroyed. When the two partial waves surround an area containing a magnetic flux Φ then the phase of each wavefunction is changed by $e\Phi/\hbar$. The relative phase change of the two counter-propagating waves is thus changed by $2e\Phi/\hbar$. The influence of an increasing magnetic field is, therefore, to gradually dephase the two partial waves and so reduce their mutual enhancement. This diminishes the resistance of the metal and gives rise to a comparatively rare phenomenon, a negative magnetoresistance.

Spin-Orbit Coupling -- The spin of an electron gives an additional degree of freedom which in certain circumstances is very important, for example when there is strong spin-orbit coupling in the ion which scatters the electron. In the presence of spin-orbit coupling the spin is no longer a good quantum number and the spin may be considered as undergoing a change of direction during the scattering process.

Quantum interference can double the probability of an electron returning to its starting point compared to its classical value. It is, however, possible for this probability to be reduced below its classical value by spin-orbit scattering. Thus, paradoxically, the

resistivity of an alloy can, under the right conditions, be made either smaller or greater than the Boltzmann value by appropriate scatterers.

If the two partial waves, described in Section 4.1.4, have the same spin and there is no spin-orbit scattering, then when they recombine after counter-propagation around a closed path they recombine to enhance the classical probability. If the two partial waves have opposite spin and recombine in phase after counter propagation, they recombine to reduce the classical probability Weak localization changes to weak anti-localization in the presence of spin-orbit scattering due to the interference of rotated spins [82] It is a consequence of quantum theory which has been proven by a rather sophisticated neutron experiment that spin 1/2 particles have to be rotated by 4π to transfer the spin function into itself A rotation by 2π reverses the sign of the spin state Without the spin rotation the interference of the two partial waves is constructive (in the absence of an external field). In the presence of spin-orbit scattering the interference becomes destructive if the relative rotation of two partial waves is 2π.

Magnetic Scattering -- Magnetic ions introduce an interaction with conduction electrons. The magnetic ions scatter the two complementary waves differently and destroy their coherence after the magnetic scattering time τ_s The physical reason for the destructive influence of magnetic impurities is quite interesting. The motion of the two complementary waves is illustrated in Figure 4.1 The partial wave which propagates along the first path is scattered by magnetic impurities along its way and exchanges spin with the localized magnetic impurities During this propagation the spin of the electron is rotated during each

"spin-flip process" by a small angle in space (the total spin function which is the sum of the potential scattering and the spin-flip scattering is only slightly tilted during such a process). The complementary electron wave which passes the impurities in the opposite direction meets the magnetic impurities in the same original orientation Only such processes which generate the same "spin-flip" at the magnetic impurities can contribute to the interference For these processes the partial electron wave experiences the same spin rotation as the former complementary wave However, this rotation occurs in the opposite sequence. Since the three-dimensional rotations do not commute (this is a non-Abelian group) the two final spin states are not the same and the interference is progressively destroyed

A number of authors have computed expressions for the contributions to the magnetoresistance due to weak localization The most general expression for the magnetoresistance, $\Delta\rho(B)$, due to Fukuyama and Hoshino [88] which includes the effects of spin-orbit scattering, Zeeman splitting and magnetic impurities is given by

$$\frac{\Delta\rho}{\rho} = \rho A\sqrt{\frac{eB}{\mathrm{h}}}\left(\frac{1}{2\sqrt{1-\gamma}}\left\{f_3\left(\frac{B}{B_-}\right)-f_3\left(\frac{B}{B_+}\right)\right\}-f_3\left(\frac{B}{B_2}\right)-\sqrt{\frac{4B_{so}}{3B}}\left[\frac{\left(\sqrt{t_+}-\sqrt{t_-}\right)}{\sqrt{1-\gamma}}+\sqrt{t}-\sqrt{t+1}\right]\right) \tag{5.1}$$

where

$$A = \frac{e^2}{2\pi^2\mathrm{h}}$$

$$\gamma = \left(\frac{3g^*\mu_B B}{8eD\left(B_{so}-B_s\right)}\right)^2$$

$$B_\phi = B_i + 2B_s$$

$$B_2 = B_i + \frac{2}{3}B_s + \frac{4}{3}B_{so}$$

$$t = \frac{3B_\phi}{4\left(B_{so} - B_s\right)}$$

$$B_\pm = B_\phi + \frac{2}{3}\left(B_{so} - B_s\right)\left(1 \pm \sqrt{1-\gamma}\right) + 2B_s$$

$$t_\pm = t + \frac{1}{2}\left(1 \pm \sqrt{1-\gamma}\right)$$

and D is the diffusion coefficient. The characteristic fields are related to characteristic electron scattering times through relations of the type

$$B_x = \frac{\hbar}{4eD\tau_x} \tag{5.2}$$

where $x = i$, so, and s refer to the inelastic, spin-orbit, and magnetic spin-flip scattering times, respectively. The function $f_3(x)$ is the Kawabata function given by [100];

$$f_3(x) = \sum_{n=0}^{\infty}\left[2\left(n+1+\frac{1}{x}\right)^{1/2} - 2\left(n+\frac{1}{x}\right)^{1/2} - \left(n+\frac{1}{2}+\frac{1}{x}\right)^{-1/2}\right] \tag{5.3}$$

5.1.3. Electron-Electron Interaction Effects

For the magnetoresistance from interaction effects it is necessary to distinguish the two contributions. One is from the spin splitting effect (particle-hole channel) [83] which gives a contribution

$$\frac{\Delta\rho}{\rho} = \rho\frac{e^2}{4\pi^2\hbar}\tilde{F}_\sigma\sqrt{\frac{k_BT}{2\hbar D}}g_3\left(\frac{g\mu_BB}{k_BT}\right)$$

where

$$g_3(h) = \begin{cases} \sqrt{h} - 1.294 & \text{if } h >> 1 \\ 0.056h^2 & \text{if } h << 1 \end{cases}$$

The other is from electron-electron interaction (EEI) effects in the particle-particle channel [101] which gives a contribution

$$\frac{\Delta\rho}{\rho} = \rho g(T,B)\frac{e^2}{2\pi^2 \mathrm{h}}\sqrt{\frac{eB}{\mathrm{h}}}\phi_3\left(\frac{2DeB}{\pi k_B T}\right)$$

where

$$\phi_3(h) = \begin{cases} 1.900 - 2.294/\sqrt{h} & \text{if h} >> 1 \\ 0.329h^{3/2} & \text{if h} << 1 \end{cases}$$

5.2. Result and Discussion

The magnetoresistance due to weak localization, $\Delta\rho_{WL}$, as given by Equation 5.1, is negative in the case of weak spin-orbit scattering systems, i.e. $\tau_i < \tau_{so}$. In the case of strong spin-orbit scattering systems the magnetoresistance is positive and $\tau_i > \tau_{so}$. The main features of the magnetoresistance due to WL arising from Equation 5.1 is shown in Figure 5.1

The overall contribution to the low temperature magnetoresistance, $\Delta\rho(B)=\rho(B)-\rho(0)$, can be written as

$$\Delta\rho(B) = \Delta\rho_{WL} + \Delta\rho_{EEI} + \Delta\rho_{CL} \qquad (5.4)$$

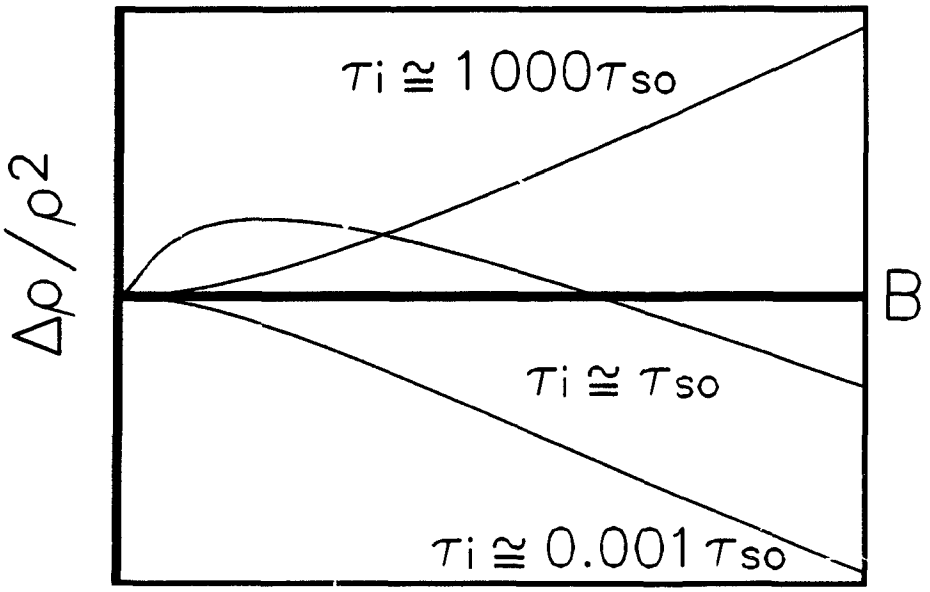

Figure 5.1. Magnetoresistance arising from weak localization as calculated from Equation 5.1 for different τ_i/τ_{so} ratios.

where $\Delta\rho_{WL}$ is due to weak localization, $\Delta\rho_{EEI}$ due to electron-electron interaction effects (which are a combination of two terms: the particle-hole channel term given by Lee and Ramakrishnan [83] and particle-particle channel term given by Altshuler et al [84]), and $\Delta\rho_{CL}$ due to classical magnetoresistance effects.

Quantum corrections are also predicted in other transport properties of disordered materials such as the Hall coefficient and the thermoelectric power [83], and this may also be useful in the study of the low temperature resistance. Altsuler et al. [102] showed that EEI causes a clear change of the Hall constant with decreasing temperature. The magnitude of this anomaly is predicted to be twice that of the resistivity [102] and this has been confirmed experimentally [103]. The present Hall coefficient measurement in Al_{70}-

$_xPd_{15}Mn_{15}B_x$ showed no anomalous temperature dependence as predicted by theory (see Chapter 6). This shows that the contribution from EEI to the magnetoresistance in the samples studied here is negligible, at least in the range of temperatures and magnetic fields of studied.

Apart from this experimental evidence, the contribution of EEI to the magnetoresistance is questionable since fields of a few tesla have been used for the study of the magnetoresistance and $Al_{70-x}Pd_{15}Mn_{15}B_x$ is a magnetic system with strong spin scattering. WL and EEI phenomena arise from quantum interference effects on the electron wave function when elastic scattering is extremely intense compared to all other scattering mechanisms. Their dependence on magnetic field, spin scattering, and inelastic scattering offer many interesting and complex features of the resistivity at low temperature. Typically WL is readily observed and usually dominates in these systems, whereas EEI effects require large magnetic fields and low levels of spin-spin and spin-orbit scattering in order to be detected. The EEI contributions are generally small when $\mu_B/k_BT < 1$. Moreover, this already small contribution to the magnetoresistance is strongly temperature dependent and decreases rapidly with increasing temperature. The EEI terms are very sensitive to spin scattering. In a magnetic-impurity-free system, the particle-particle channel contribution is expected to remain the same [84] while the particle-hole term contribution is expected to completely vanish in the limit of very strong spin-spin scattering [83, 84]. In the presence of high spin-spin scattering, on the other hand, both terms vanish in the same way as the WL contribution.

In general, the size of the quantum interference contribution to the magnetoresistance in 3D samples is quite small and, therefore, experiments on such samples are very susceptible to interference from other effects. In particular, magnetic impurities have a two-fold effect on the magnetoresistance, a direct contribution due to the field dependence of the spin-flip scattering, and an indirect contribution from spin-flip dephasing of the electron wave function. The magnetoresistance measured here confirms this and includes two parts; the WL contribution which dominates at low temperatures (T < 30 K) and is strongly temperature dependent and a negative classical spin disorder scattering from local magnetic moments. This negative contribution is associated with the classical spin-disorder scattering of the conduction electrons by the Mn localized moment

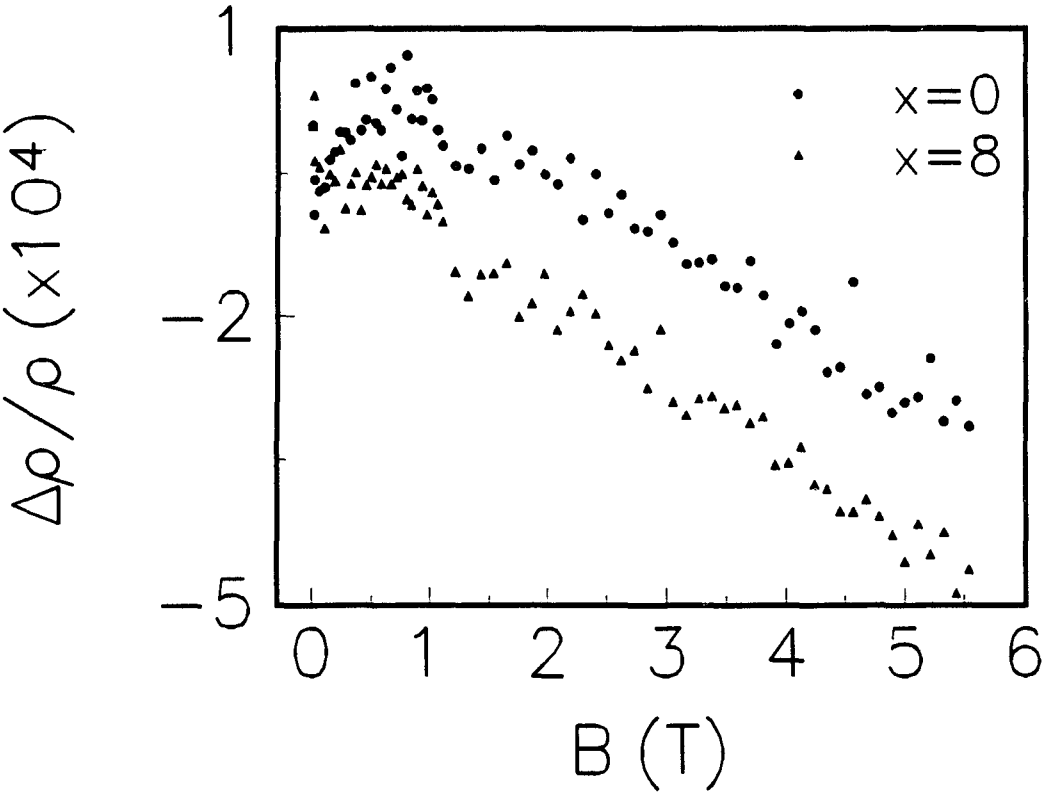

Figure 5 2 Negative magnetoresitance due to classical spin disorder scattering from local magnetic moments for $Al_{70}Pd_{15}Mn_{15}$ and $Al_2Pd_{15}Mn_{15}B_8$ at 56 K.

giving $\Delta\rho/\rho \sim -M^2$, where M is the magnetization The presence of this contribution is observed at higher temperature as shown in Figure 5 2 This contribution is a small fraction of the total magnetoresistance and is nearly temperature independent Therefore, the observed magnetoresistance is analyzed on the basis of the theoretical model of WL, i.e.,

$$\Delta\rho(B) \approx \Delta\rho_{WL} = \Delta\rho_{WL}\left(\tau_i(T), \tau_{so}, \tau_s, \rho, D, g^*, B\right) \tag{5 5}$$

The magnetoresistance data of $Al_{70-x}Pd_{15}Mn_{15}B_x$ QC alloys (x = 0, 2, 4, 6, 8, 10) are shown in Figures 5 3 to 5 8 at different temperatures between 4 2 and 28 K and in fields up to 5 5 T The symbols are the experimental data and the solid lines one fits as discussed below Data have been fit to Equation 5 1 using standard nonlinear least squares methods in a MATLAB program for the IBM PC. The slowly converging Kawabata function, described in Equation 5 3, was replaced by the more compact form proposed by Baxter et al [99],

$$f_3(x) = 2\left[\sqrt{2+\frac{1}{x}} - \sqrt{\frac{1}{x}}\right] - \left[\left(\frac{1}{2}+\frac{1}{x}\right)^{-1/2} + \left(\frac{3}{2}+\frac{1}{x}\right)^{-1/2}\right] + \frac{1}{48}\left(2\,03+\frac{1}{x}\right)^{-3/2}$$

The fitting procedure adopted for the samples studied is as follows The WL contribution to the magnetoresistance is usually fitted by using the characteristic temperature-dependent inelastic scattering time $\tau_i(T)$, and the temperature independent scattering times τ_{so} and τ_s, spin-orbit and spin-flip, respectively as free parameters In addition to the characteristic scattering times, the resistivity ρ, the diffusion constant D, and the effective electron Lande factor g^* are needed g^* is usually taken to be 2 but is

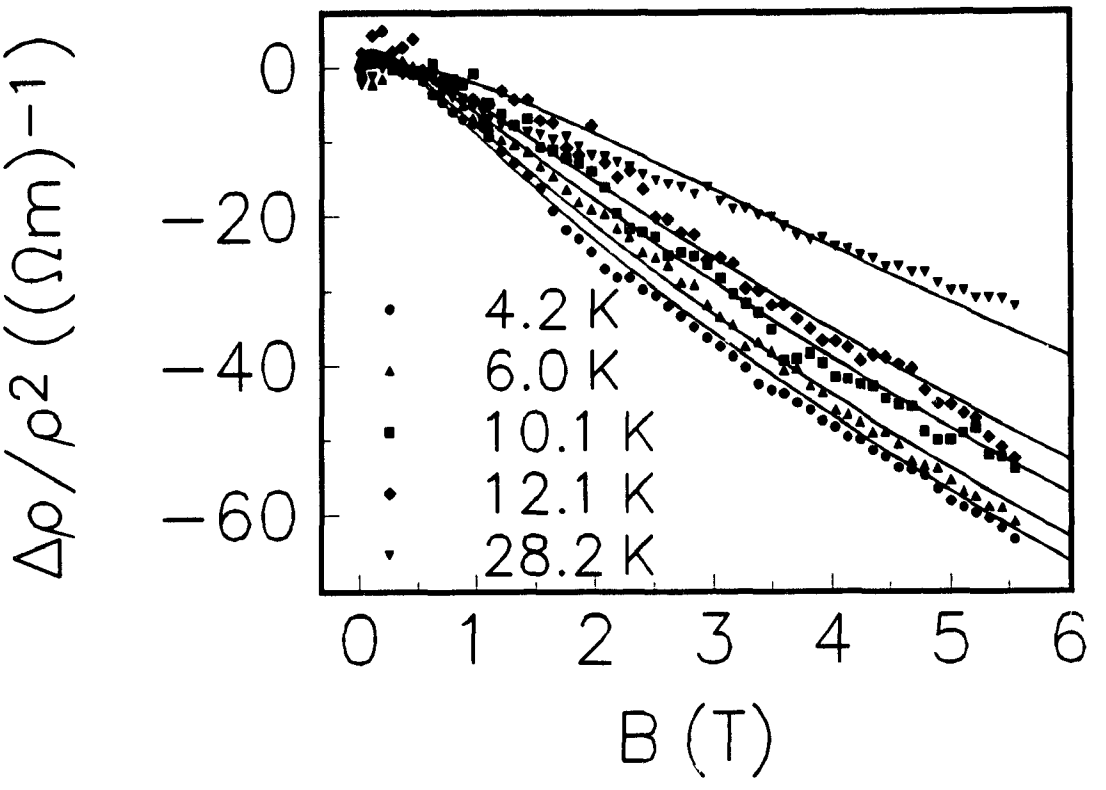

Figure 5.3. Low temperature magnetoresistivity of $Al_{70}Pd_{15}Mn_{15}$ plotted as a function of B at various temperatures. The solid lines are fits to WL theory as described in the text

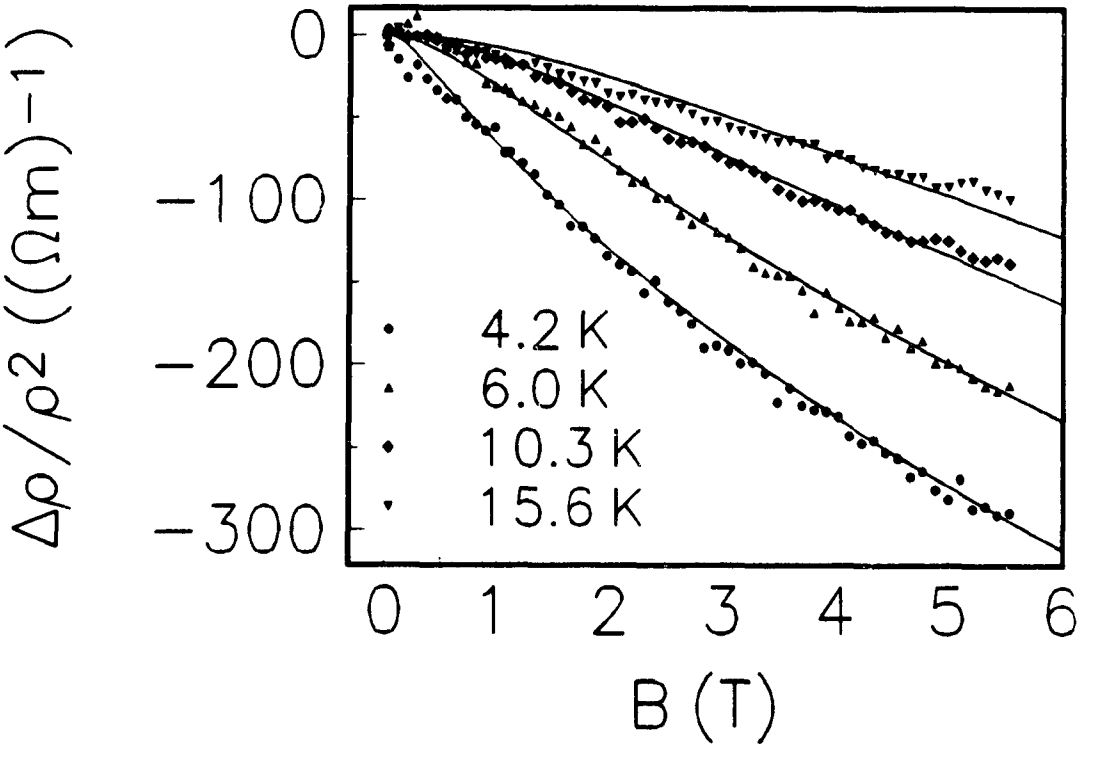

Figure 5.4. Low temperature magnetoresistivity of $Al_{68}Pd_{15}Mn_{15}B_2$ plotted as a function of B and at various temperatures. The solid lines are fits to WL theory as described in the text.

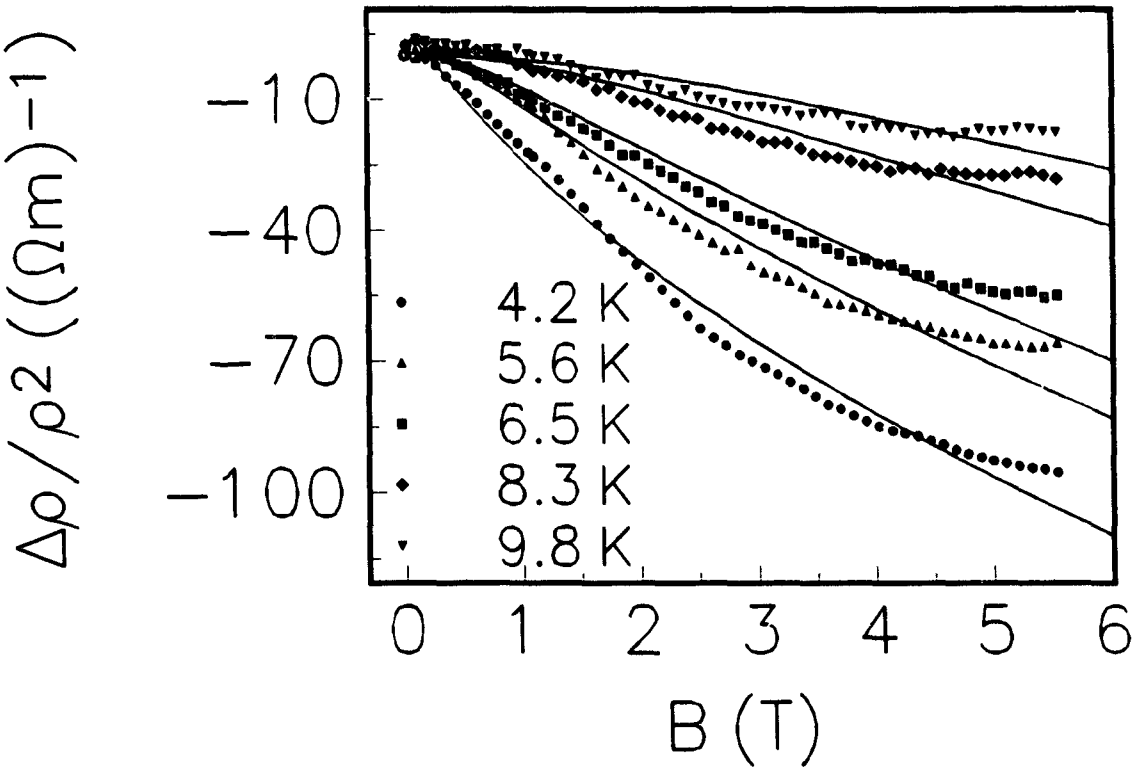

Figure 5 5 Low temperature magnetoresistivity of $Al_{66}Pd_{15}Mn_{15}B_4$ plotted as a function of B at various temperatures The solid lines are fits to WL theory as described in the text.

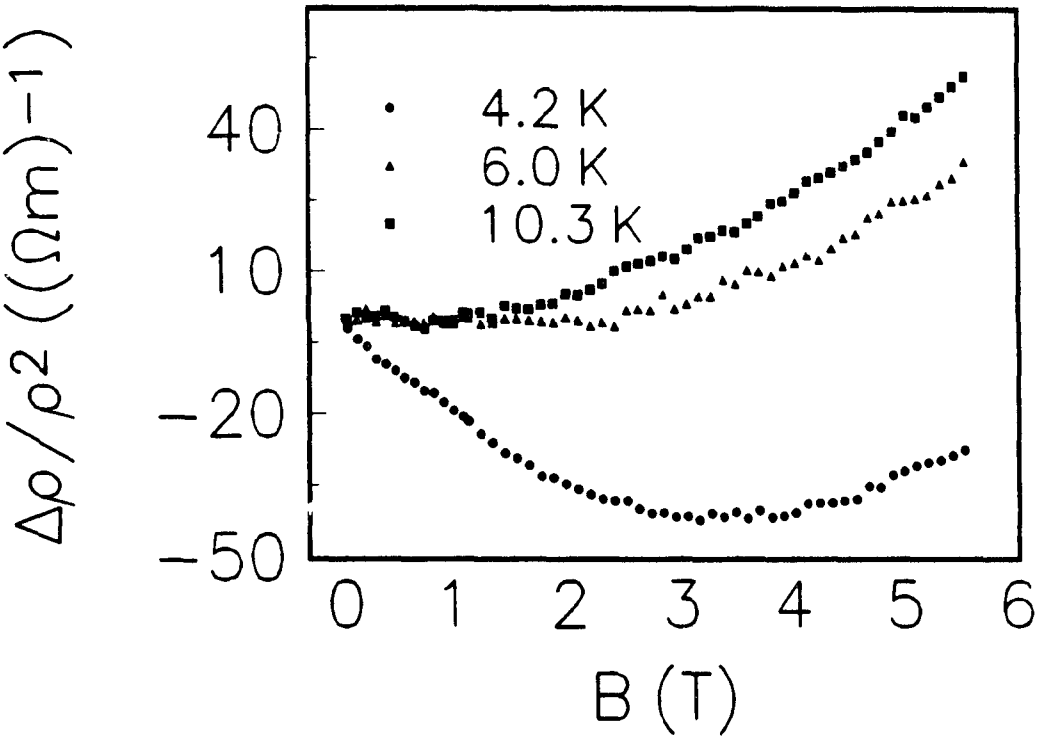

Figures 5 6 Low temperature magnetoresistivity of $Al_{64}Pd_{15}Mn_{15}B_6$ plotted as a function of B at various temperatures The solid lines are fits to WL theory as described in the text

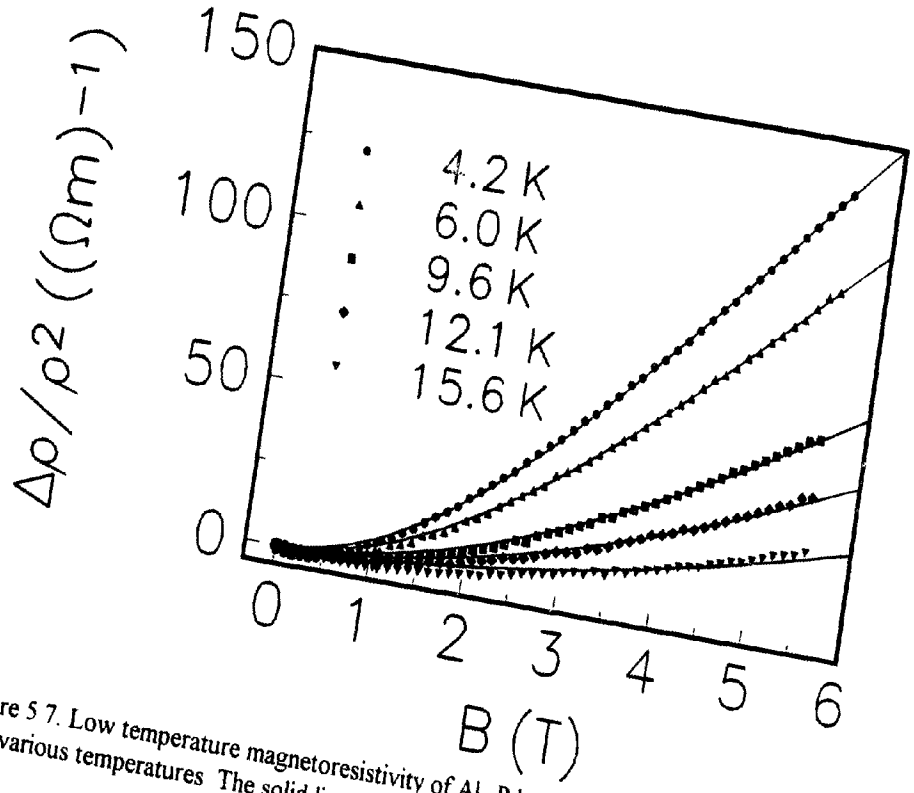

Figure 5.7. Low temperature magnetoresistivity of $Al_{62}Pd_{15}Mn_{15}B_8$ plotted as a function of B at various temperatures. The solid lines are fits to WL theory as described in the text.

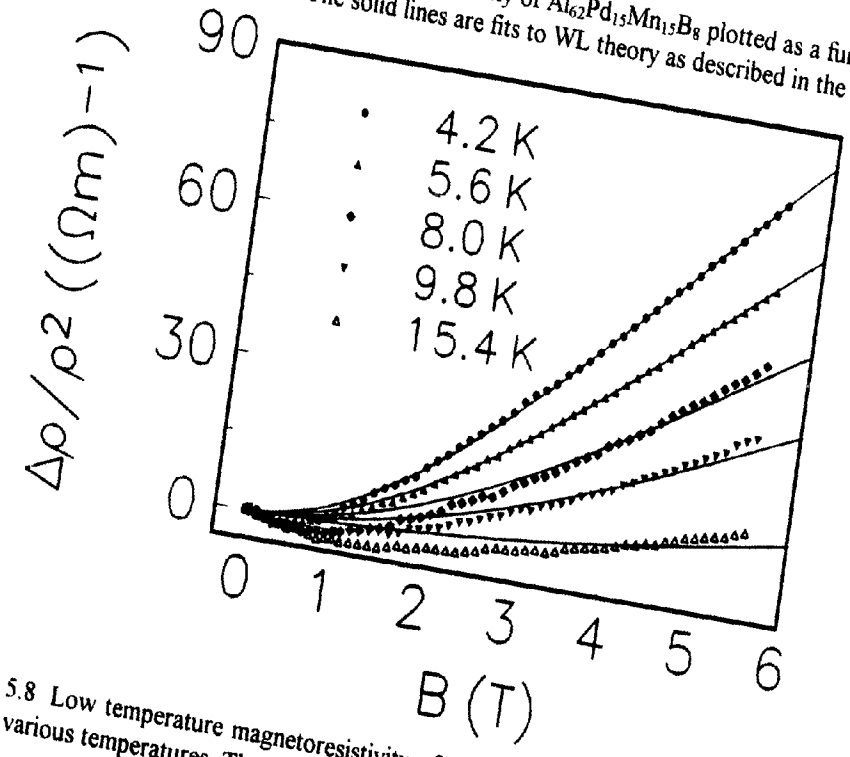

Figure 5.8 Low temperature magnetoresistivity of $Al_{60}Pd_{15}Mn_{15}B_{10}$ plotted as a function of B at various temperatures. The solid lines are fits to WL theory as described in the text

sometimes used as a fitting parameter; for example, Matsuo et al. [104] obtained a fitted value of $g^* = 130$. To avoid such an unlikely value of g^*, it is taken to be 2. ρ and D can be taken from other experimental results or used as a fitting parameters. The diffusion coefficient is taken to be 0.075 $cm^2 \cdot s^{-1}$ [105], from literature values for similar Al-Mn-Pd based quasicrystals. Quantum corrections to the resistivity predict $\Delta\rho / \rho \propto \rho$. Using ρ as a free parameter in the WL expression allows for a determination of the resistivity in a way that is independent of the sample geometry and microcracks that might exist in these brittle ribbons. In so doing, the nontrivial problem of determining the resistivity of small pieces of quasicrystalline ribbon can be avoided. This approach has been used by Sahnoune et al. [106].

The algorithm used for fitting the present data is as follows First, data at 4.2 K were fitted with the characteristics fields B_x (x = i, so, and s) and ρ as free parameters (the characteristic field B_x is related to the scattering time τ_x by Equation 5.2). Second, since B_{so} and B_s must be independent of temperature they are kept constant at the 4.2 K fitted value and, the remaining higher temperature ($4.2 < T < 30$ K) data are fitted to Equation 5 1 using only B_i as a free fitting parameter.

The magnetoresistance of all the samples at a fixed temperature of 4.2 K is plotted in Figure 5.9 The agreement between WL theory and the experimental data is good over the entire range of fields. For the $x \leq 4$ samples, the magnetoresistance is positive in region $B < 0.5$ T, as shown in Figure 5.10a, which is followed by a negative magnetoresistance in the remaining range of field. This feature reflects the moderate spin-orbit scattering case described in Figure 5.1 in which $\tau_i \approx \tau_{so}$. For the x = 8 and 10 samples the opposite trend

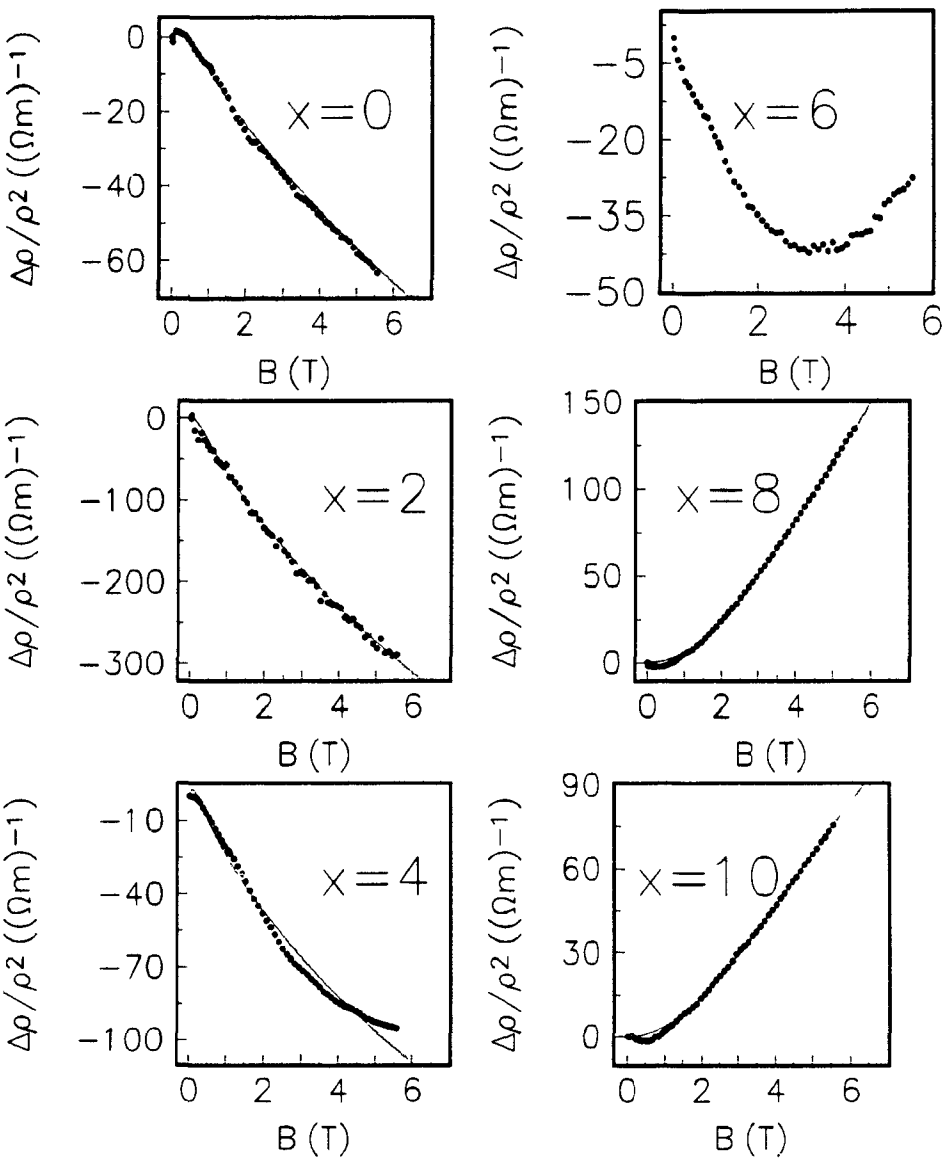

Figure 5.9. The magnetoresistivity measured at 4.2 *K* for $Al_{70-x}Pd_{15}Mn_{15}B_x$. The solid lines are least-squares fits to Equation 5.1. The data show a systematic change from negative to positive values with increasing Boron concentration

is followed, i e , the magnetoresistance is negative in the region $B \sim 0\ 5\ T$, as shown in Figure 5 10b, which is followed by a positive region The positive magnetoresistance reflects the presence of strong spin-orbit scattering, $\tau_i > \tau_{so}$, as described in Figure 5.1. The negative region of this strong spin-orbit scattering system (x = 8 and 10) reflects the coexistence of a negative magnetoresistance component due to classical spin-disorder scattering of the conduction electrons by the Mn localized moment The generalized WL function described by Equation 5 1 in the limit of low field for the strong spin-orbit scattering case increases slowly as it is shown in Figure 5 1 During this limiting case the classical contribution to the magnetoresistance exceeds the dominant WL contribution This shift towards negative value of the magnetoresistance is a clear evidence for the coexistence of classical and quantum contributions

As the temperature increases, the magnitude of the magnetoresistance decreases (the magnetoresistance becomes less positive or negative as the temperature increases) for each family of curves due to the destruction of phase coherence by inelastic scattering events, see Figures 5 3 to 5 8 The quality of the fit remains reasonably good at higher temperature for all samples except the x = 10 sample in which a significant difference is seen between the theoretical curve and the experimental data In this sample, the data points are below the fitted curve at low field ($B < 3\ 5\ T$) As the temperature increases the WL contribution weakens and the nearly temperature independent classical spin-disorder scattering starts to be noticeable by being comparable to the WL contribution in the low field region This is additional evidence for the presence of a negative magnetoresistance

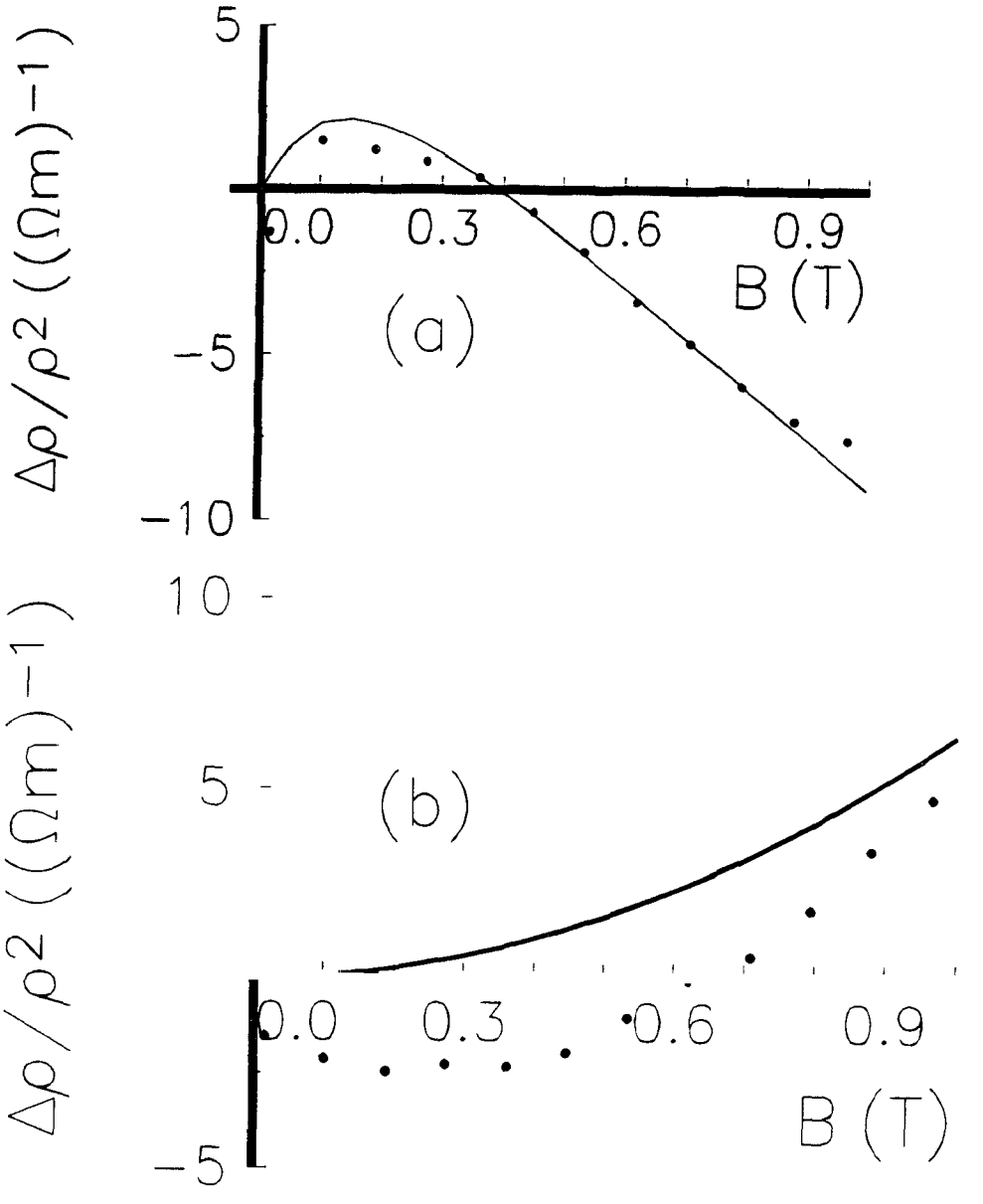

Figure 5.10. Low field (enlargement of Figure 5.9) magnetoresistivity measured at 4.2 *K* for: (a) $Al_{70}Pd_{15}Mn_{15}$, where small maximum can be seen at about 1.5 *T*, and (b) $Al_{62}Pd_{15}Mn_{15}B_8$, where the fitted curve is above the experimental data. The solid lines are least-squares fits to Equation 5.1.

component due to the classical spin-disorder scattering of the conduction electrons by the Mn localized moments The quality of the fit for x=4 sample is relatively poor and a sensible fit for x = 6 sample was not achieved In addition to the difficulty in fitting the data for the x = 6 sample the trend seen for the magnetoresistance with increasing temperature is different The magnitude of the magnetoresistance decreases for each family of curves due to the destruction of phase coherence by inelastic scattering events with increasing temperature, however, the alloy with x = 6 *at.%* boron exhibits complex behaviour of $\Delta\rho/\rho$ as a function of applied field The magnetoresistance at 4 2 K shows a minimum at about *3 T* and is negative With increasing temperature the magnetoresistance becomes positive and the magnitude increases and then decreases Subsequently the function given in equation 5 1 does not provide a suitable description of the experimental data for the x= 6 alloy

Equation 5 1 gives a good fit to the data for the alloys shown in Figures 5.3 to 5 8. The presence of strong spin-orbit scattering in these alloys is evidenced by the relative values obtained from the fits to the scattering times, $\tau_i > \tau_{so}$ The fit for alloys with moderate spin-orbit scattering, i e alloys with 0, 2 and 4 *at* % boron, indicates that the relative scattering times are $\tau_i \approx \tau_{so}$ The value of the fitted parameters are given in Table 5 1 The values of the resistivity obtained from the fits are compatible with measurements made at 4 2 K as shown in Table 5 1

Table 5 1 Fitted parameters values for $Al_{70-x}Pd_{15}Mn_{15}B_x$

Alloy (x)	$1/\tau_i$ (10^9 s^{-1})	$1/\tau_{so}$ (10^{11} s^{-1})	$1/\tau_s$ (10^{11} s^{-1})	β (10^{-10} s)	ρ (Fitted) (μΩcm) (±2%)	ρ(Exp) (μΩcm) (±12%)	p
0	2 7(8)	0 0170(3)	0 00210(6)	16 8	1000	6200	1.1(1)
2	1 4(4)	0 0105(2)	0 0100(3)	14 5	1257	1900	1.4(3)
4	0 5(1)	0 0094(2)	0 00164(5)	53 5	824	3800	2 3(6)
6						3500	
8	0 5(2)	7 9(2)	3 03(9)	5 3	5076	3700	2 3(2)
10	0 9(3)	5 6(1)	3 5(1)	4 8	3037	2400	2 4(1)

The magnetoresistance due to WL involves a combination of effects due to applied magnetic field, inelastic scattering, spin scattering and spin-orbit processes, and thus provides a useful tool for studying the relative importance of these effects The inelastic scattering time is expected to exhibit a power-law dependence on temperature, $\tau_i(T)=\beta T^{-p}$ The temperature dependence of the inelastic scattering time τ_i deduced from the magnetoresistance analysis is shown in Figure 5 11 The fitted values of both p and β are also shown in Table 5 1 According to Chakravarty and Schmid [107], the exponent p can take any value between 2 and 4 depending on the different phonon modes involved in the scattering process In the case of inelastic electron-electron scattering for disordered metals p=1 5 [108] or even p=1 0 very near the critical metal-insulator transition [109]. Experiments have yielded different results for p in the range 0 5 to 4 [110]. Thus, for

values of p= 1.1 to 2 4 as given in Table 5 1, the dephasing in $x \geq 4$ alloys appears to be due to inelastic electron-phonon scattering and in $x \leq 2$ alloys to electron-electron scattering This distinct difference in p seems to indicate that WL theory does not offer a complete description of the behavior of all $Al_{70-x}Pd_{15}Mn_{15}B_x$

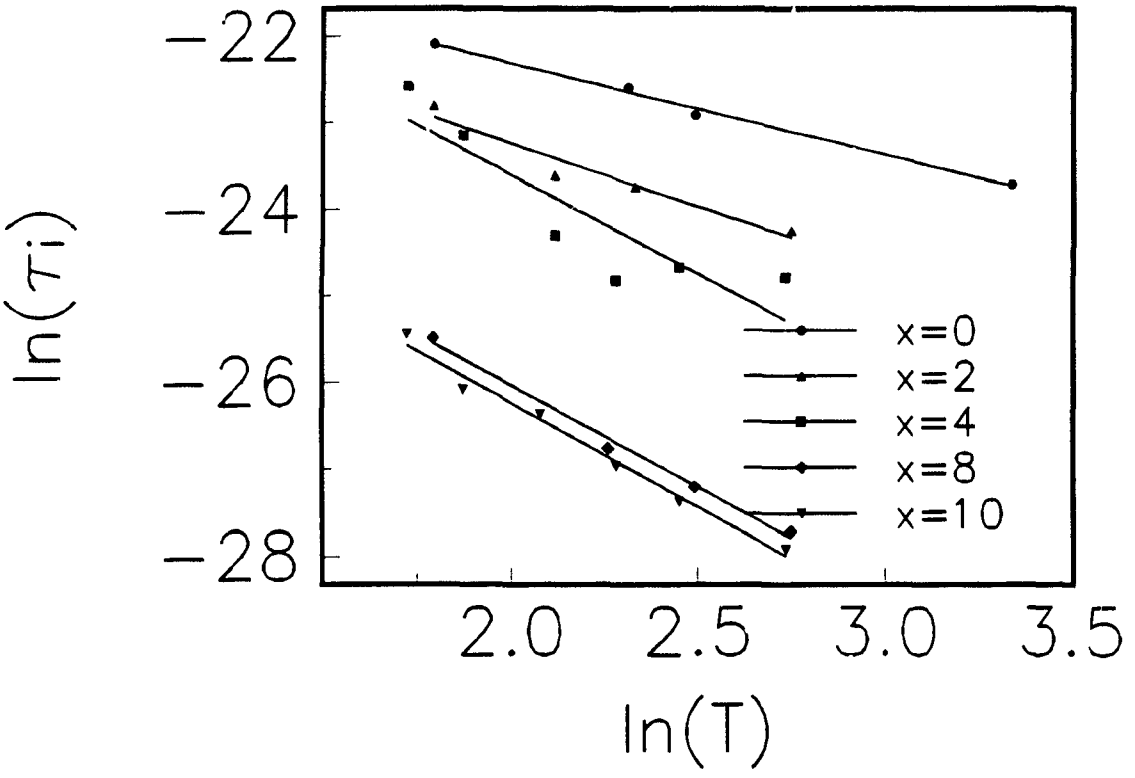

Figure 5 11 Temperature dependence of the inelastic scattering time τ_i fo· $Al_{70-x}Pd_{15}Mn_{15}B_x$ The solid lines denote the slope

The order of magnitude of τ_i obtained here for $Al_{70-x}Pd_{15}Mn_{15}B_x$ is comparable to that obtained from magnetoresistance data for various other quasicrystalline alloys [111, 112] The change in the magnitude of the dephasing rate, $1/\tau_i$, as a function of Boron concentration is shown in Figure 5 12 Even though the dephasing rate appears to decrease with increasing Boron concentration the variation is not well defined

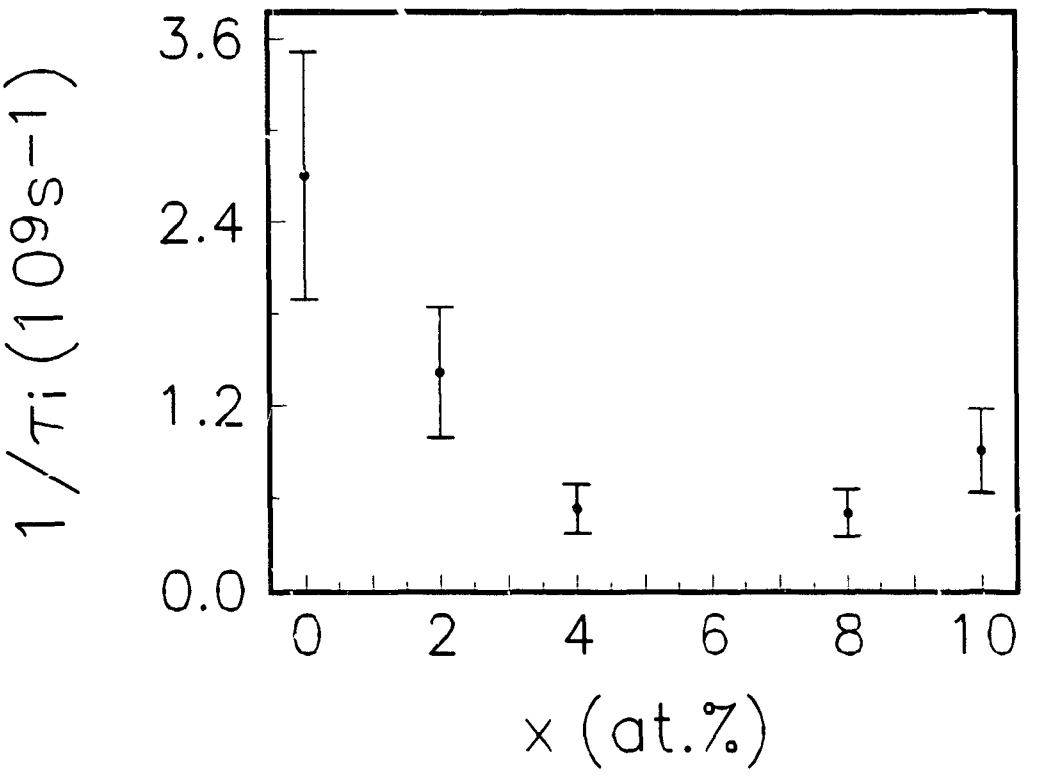

Figure 5 12 Dephasing rate, $1/\tau_i$, as a function of Boron concentration in $Al_{70-x}Pd_{15}Mn_{15}B_x$

The values of the spin-orbit scattering rate, $1/\tau_{so}$, determined from the magnetoresistance analysis are listed in Table 5 1 and the spin-orbit scattering rate is plotted in Figure 5 13 For the $Al_{70-x}Pd_{15}Mn_{15}B_x$ alloy series, $1/\tau_{so}$ shows a strong dependence on Boron concentration increasing significantly by more than a factor of 400. τ_{so} is the spin-flip relaxation time due to the spin-orbit interaction and depends mainly on the spin-orbit coupling of *d* states at the Fermi level The influence of Boron can be explained by assuming that most of the spin-orbit scattering occurs at Mn sites and Boron atoms are located in site with high Mn coordination hybridize with the Mn *d* band The

Boron thereby increases the *d*-band density of states at the Fermi level enhancing the effective spin-orbit contribution to the magnetoresistance [113, 114].

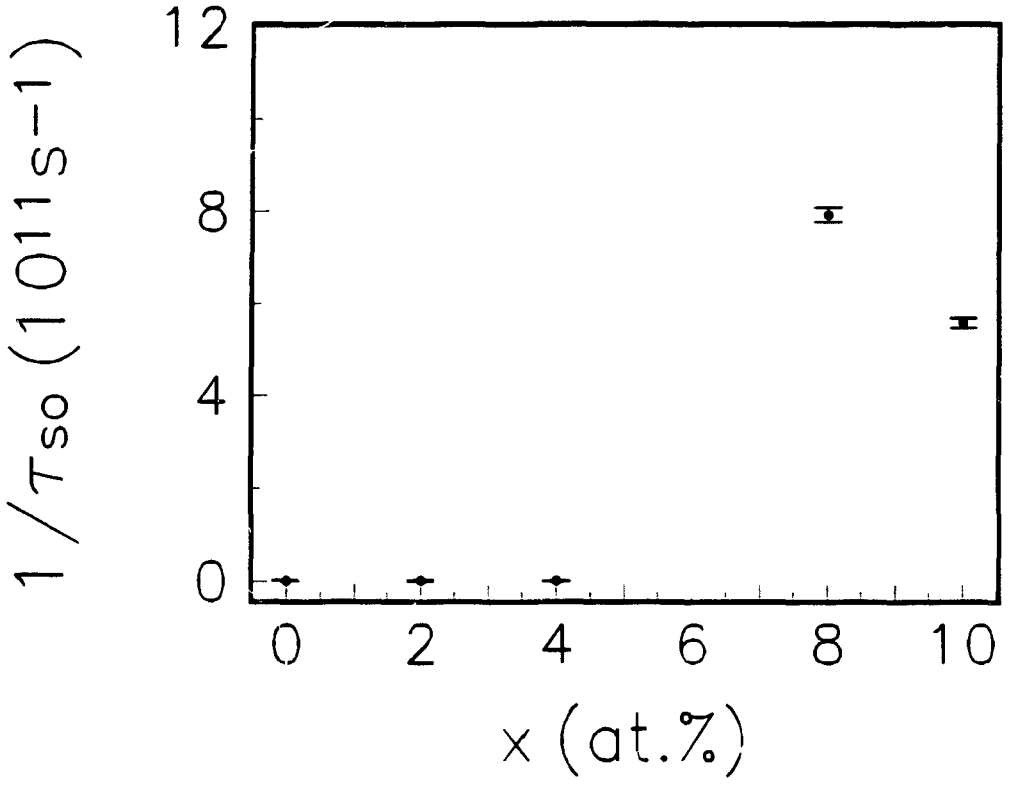

Figure 5 13. The spin-orbit scattering rate $1/\tau_{so}$ as a function of Boron concentration in $Al_{70-x}Pd_{15}Mn_{15}B_x$.

The spin scattering rate $1/\tau_s$ as a function of Boron concentration is shown in Figure 5.14 and $1/\tau_s$ is given in Table 5.1. The value of the spin scattering probability increases by more than a factor of 1600 as x changes from 0 to 10. Spin-dependent scattering by Mn magnetic ions is expected to contribute to phase breaking and to depress the WL [82] In other systems [115], in which the magnetic interaction is negligible, the spin scattering dephasing rate showed a linear variation with magnetic impurity content. The increase in spin scattering rate in the present case shows the increase in the number of

magnetic sites and the non-linear variation observed shows the influence of the magnetic interaction between the Mn magnetic ions. The spin scattering rate estimated from the magnetoresistance data was as high as $3.4 \times 10^{11}\ s^{-1}$, and suppress almost completely the magnetoresistance arising from (anti)localization. In contradiction, a positive magnetoresistance due to strong spin-orbit scattering is observed. Mn magnetic ions introduces an interaction with a conduction electron.

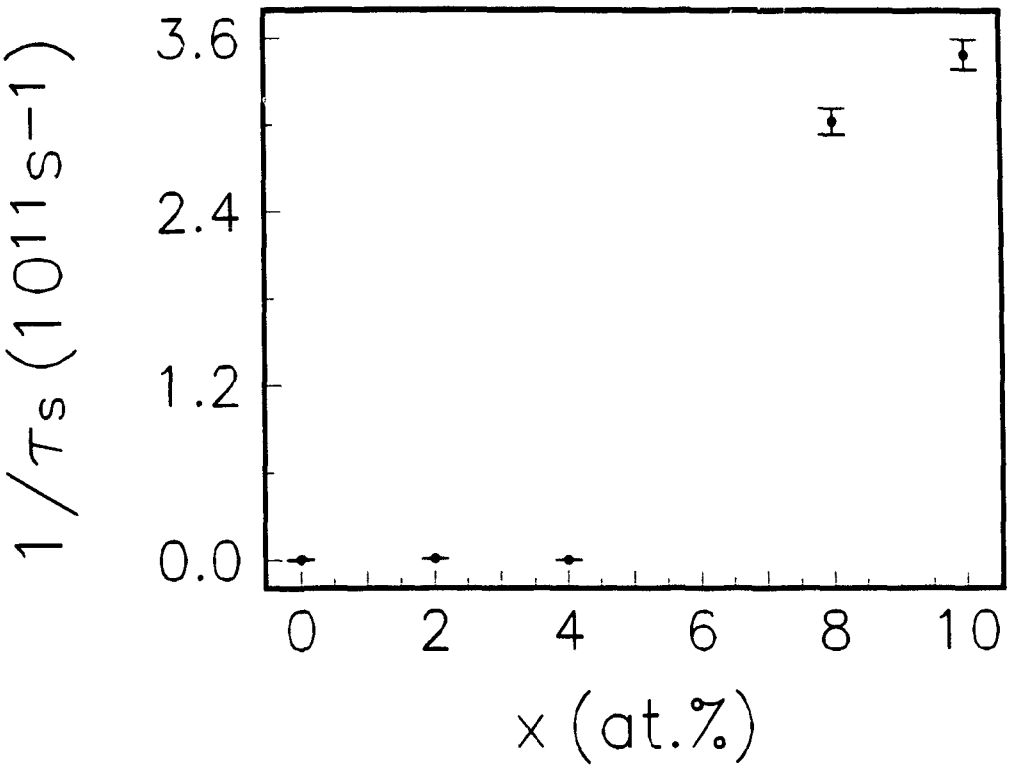

Figure 5.14. The spin scattering rate $1/\tau_s$ as a function of Boron concentration in $Al_{70-x}Pd_{15}Mn_{15}B_x$.

In summary, magnetoresistance data for $Al_{70-x}Pd_{15}Mn_{15}B_x$ quasicrystalline alloys has been analyzed on the basis of WL theory and information on the compositional and temperature dependence of τ_i, τ_{so}, τ_s and ρ has been obtained. The first notable conclusion

from this investigation is that WL theory gives a good description of the field and temperature dependence of the magnetoresistance of the data in this alloy system in spite of the magnetic ordering The exponent associated with temperature dependent inelastic scattering time $\tau_i(T)=\beta T^p$ changes from $p = 1\ 1$ dependence to $p = 2\ 4$ This temperature dependence change seems to be the result of dephasing dominated by inelastic electron-phonon scattering The value of τ_i at $4\ 2\ K$ appears to be Boron concentration independent The spin-orbit scattering rate showed a significant increase with increasing Boron concentration and appears to be due to Boron locating in Mn-rich environments and hybridizing with the Mn *d* band This increases the d-band density of states at the Fermi level and enhances the effective spin-orbit contribution to the magnetoresistance The spin scattering rate estimated from the magnetoresistance also showed a significant increase with increasing Boron concentration which could be due to both an increase in the concentration of magnetic Mn sites and to magnetic ordering

As the Boron concentration is varied, $Al_{70-x}Pd_{15}Mn_{15}B_x$ undergoes a magnetic transformation from paramagnetic to weakly ferromagnetic long-range order The dramatic result of the present work is that the interaction between Mn moments seems to have no significant effect on WL The magnetoresistance (of the strong spin-orbit scattering) is slightly negative in the very low field region For strong spin-orbit scattering alloys at low field the fitted curve was always above the experimental curve This deviation is due to the coexistence of classical magnetoresistance due to spin-disorder scattering and quantum effects

6. Hall Effect in $Al_{70-x}Pd_{15}Mn_{15}B_x$

In 1879 E.H. Hall observed for the first time (what we now know as the Hall effect) that when a magnetic field is applied at right angles to the direction of current flow in a conductor, an electric field is set up in a direction perpendicular to both the current and magnetic field directions. The study of the Hall effect has contributed much to the understanding of the electronic nature of matter and provides details of the scattering mechanism and character of conduction electrons that are inaccessible to other probes. The origin of the Hall effect in QC's is not yet fully understood. However, the theory of the Hall effect in QC's is similar to that of amorphous alloys and the most successful models of amorphous metals which are relevant for the current data analysis are discussed in the first section of this chapter. In the section 6.2 the behavior of the Hall coefficient data of $Al_{70-x}Pd_{15}Mn_{15}B_x$ ($x = 0 \ldots 10$) is investigated in light of the existing theories.

6.1. The Hall Effect in Disordered Magnetic Metals

The application of an electric current density, J_x, along the x-axis of a thin slab specimen extending in the x-y plane, and of a magnetic induction, B_z, perpendicular to the plane, generates a transverse electric field, E_y, in the y-direction given by;

$$E_y = R_H J_x B_z \tag{6.1}$$

where R_H is called the Hall coefficient The physical implication of this expression is generally understood as follows, the Lorentz force under such conditions acts to deflect electrons in the y-direction and to accumulate them against one side of the specimen As the electrons are deflected to the sides of the sample initially a transient transverse electric current is established Since the electrons are mutually repulsive in steady state the transverse electric field produced by their concentration gradient exactly opposes their further deflection Consequently, once the transients have diminished to zero, an electric E_y is then built up to oppose the Lorentz force and current flows only in the x-direction, as if there were no magnetic field

The Hall coefficient, which may be a function of the magnetic field, is in general defined as

$$R_H(B) = \frac{1}{J}\left[\frac{\partial E_H}{\partial B}\right] \tag{6 2}$$

where J is the current density, E_H is the Hall field and $\partial E_H/\partial B$ is the local gradient of E_H vs B at which the Hall coefficient is defined [116] For simple metals with a spherical Fermi surface (free electron approximation) the Hall effect simplifies to the most commonly used expression in connection with experimental data

$$R_H = \frac{1}{en^*} \tag{6 3}$$

where n^* is the "effective number of electrons per unit volume", determined by $n^*=k_F S/12\pi^3$ and S is the Fermi surface and e is the electron charge

The Hall effect in metals showing appreciable magnetization exhibits some unusual features Two effects are observed when a magnetic field is applied to a magnetic sample,

the ordinary Hall effect (OHE) and the extraordinary or spontaneous Hall effect (SHE). The Hall voltage in magnetic materials depends mainly on the magnetization rather than on the external field Also, it arises from electron scattering rather than from the free motion of electrons. There are two mechanisms responsible for this "anomalous" Hall effect; skew scattering and side jump. We examine the magnitudes, the signs, and the temperature dependence of the OHE and SHE in magnetic disordered materials in this section.

6.1.1. The Field Dependence of the Hall Coefficient

The observed Hall effect for a magnetic metal (a ferromagnet, for example) shows a unique behavior, such as that illustrated schematically in Figure 6 1 This includes an initially rapid, linear rise of the Hall voltage with increasing B followed, in general, by a second linear portion having a relatively smaller gradient. It is obvious that the Hall effect in such a case does not arise solely from the simple application of the Lorentz force on the electrons, and it has, therefore, become known as an anomalous Hall effect. It is now known that such an anomalous effect is not restricted to ferromagnetic materials, but can appear in any material where there are large, localized magnetic moments, such as in strongly paramagnetic and in antiferromagnetic metals [116].

The Hall resistivity in magnetic alloys is usually given by [116]

$$\rho_H = R_o B + 4\pi R_s M_s \tag{6.4}$$

where B is applied magnetic field and M_s the saturation magnetization. The first term on the right-hand side of Equation 6.4 accounts for the ordinary Hall effect arising from the influence of the Lorentz force on the electrons and is present in nonmagnetic materials as well. The ordinary Hall effect is characterized by the constant R_o, the ordinary Hall coefficient. The second term, characteristic of magnetic materials, depends on the magnetization and R_s is known as the extraordinary or spontaneous Hall coefficient.

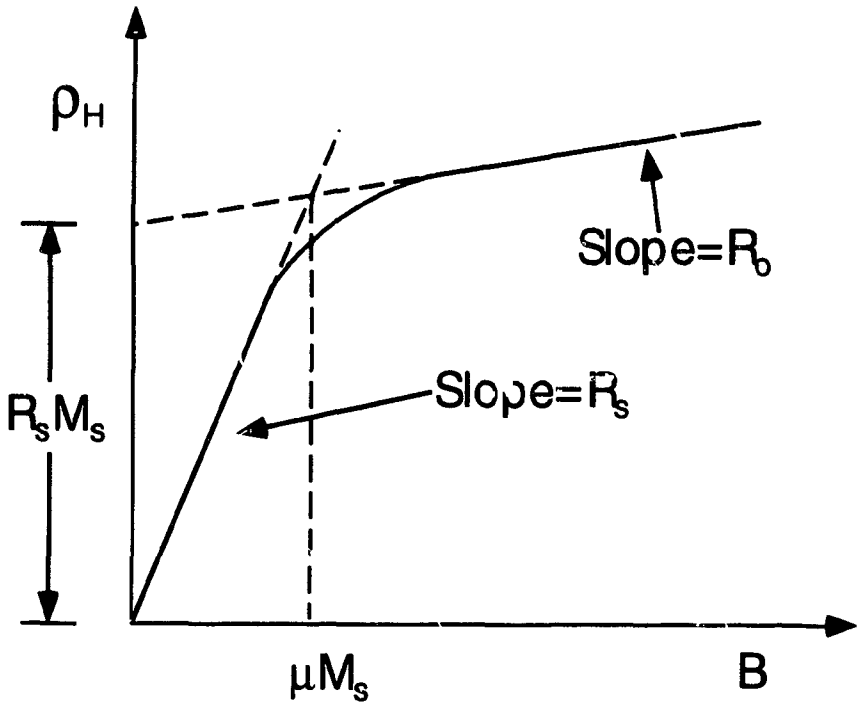

Figure 6.1 Schematic behavior of the Hall resistivity ρ_H as a function of magnetic field of magnetic metals and graphical determination of the two Hall coefficients R_o and R_s.

The ordinary Hall effect (OHE) is a consequence of Lorentz force acting on the current carriers and is dependent on the field B. Amorphous alloys, because of their disordered structure, are expected to have a spherical Fermi surface and, therefore, to be

nearly free-electron like. The interpretation of OHE of these metals should then be straight forward.

The spontaneous Hall coefficient depends on the magnetization, that is, on the electron spin, and since the spins influence the transport process, this effect also depends on the scattering potentials created by impurities, phonons, magnons, etc The ferromagnetic Hall coefficient R_s is associated with that part of the transverse voltage which depends on the magnetization of a magnetic metal Considerable theoretical work has been conducted in this area and indicates that some aspect of the spin-orbit coupling interaction is responsible for the effect. The spontaneous Hall effect (SHE) arises from spin-orbit interactions and other coupling [117] Two types of scattering are distinguished in SHE:

(a) Skew scattering which is characterized by a constant spontaneous Hall angle

$$\theta_s = \rho_H / \rho$$

at which the scattered carriers are deflected from their original trajectories (Figure 6.2). Thus for skew scattering

$$\rho_H \propto \rho$$

In the presence of the spin-orbit interaction electrons with spin polarizations parallel and antiparallel to the magnetization are deflected in opposite directions at the right angles to the electric current. If the two spin populations are unequal then a net transverse current appears which is canceled by the resulting Hall voltage. This is caused by spin-orbit interaction, and is important at low temperatures. Skew scattering describes the classical asymmetric scattering of charge carriers by impurities.

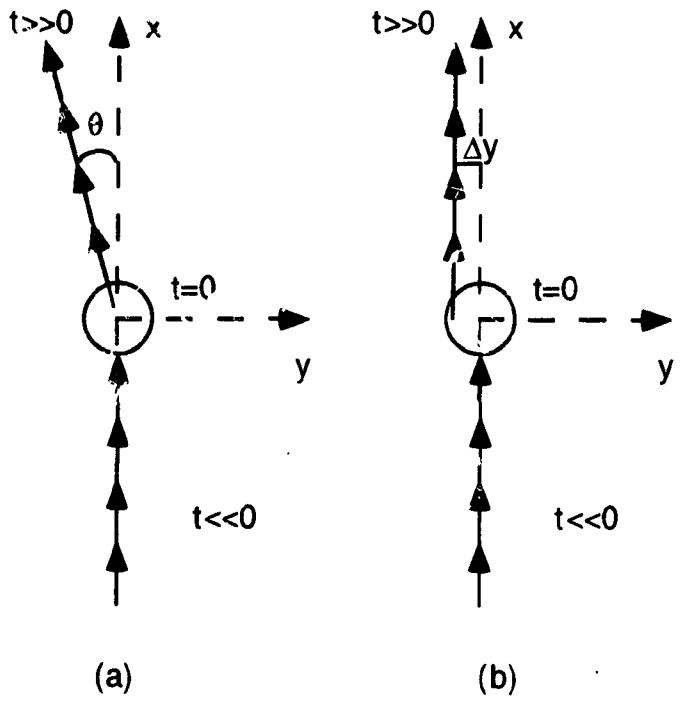

Figure 6.2 Schematic comparison of a) skew scattering characterized by a constant spontaneous Hall angle θ and b) side-jump, characterized by a constant lateral displacement Δy of carrier trajectory.

(b) Aside from the OHE which is due to the Lorentz force and the skew scattering mechanism which makes the scattering probability antisymmetric with respect to interchange of scattering vectors, there exists an additional contribution to the Hall effect known as the side-jump effect. The side-jump effect is due to a change in the expression for the current operator in the presence of spin orbit forces. It arises from the non-commutativity of the position operator of the conduction electron with terms in the Hamiltonian other than the kinetic energy operator. These nonclassical contribution may be expected to become important in cases where the dimensionless quantity $\hbar/\varepsilon_F\tau$ is not very small, ε_F is the Fermi energy and τ the electron relaxation time. This corresponds to

high temperatures for concentrated alloys (small τ) It is generally accepted [116, 118] that in strongly disordered transition metal alloys the main contribution to the extraordinary Hall effect comes from the side-jump mechanism [119] and this leads to the ρ^2 dependence of the extraordinary Hall coefficient R_s The side-jump mechanism is characterized by a finite lateral displacement of the conduction electron trajectory (Figure 6 2)

6.1.2. The Temperature Dependence of the Hall Coefficient

In general, the Hall coefficient is a difficult quantity to calculate since it depends intimately upon details of the electronic transport However, Tsuji [120] has solved the Boltzman equation for a metal with cubic symmetry and has obtained

$$R_H = \frac{12\pi^3}{e} \frac{\int v^2(k)\tau^2(k)(\overline{1/\bar{\rho}})uds}{\left(\int \tau(k)v(k)_i s\right)^2} \qquad (6\ 5)$$

where $v(k)$ and $\tau(k)$ are the group velocity and relaxation time, respectively $\bar{\rho}$ is the radius of curvature of the Fermi surface and the integral is over the Fermi surface It is clear that if the scattering mechanism is isotropic, then τ is eliminated from Equation 6 5 This is significant, since, at low temperatures, the temperature dependence of R_H is usually attributed to the temperature dependence of τ Therefore, if the scattering is isotropic, R_H is expected to be temperature independent based on Equation 6 5, and this is often observed in metallic glasses and most crystalline compounds [121] The apparent absence of a temperature dependence of the Hall coefficient for a number of metallic glasses is usually assumed to be due to the isotropic nature of the scattering in metallic glasses

In the ferromagnetic state R_s is found experimentally to have a strong characteristic temperature dependence It should be zero in a perfect lattice at absolute zero and it is found to increase with temperature up to a maximum which occurs at a temperature close to the Curie temperature In the antiferromagnetic state R_s shows, in general, an even stronger temperature dependence including, frequently, a change in sign in this region R_o, on the other hand, can generally be regarded as temperature independent compared with R_s in all of these regions In the paramagnetic region, both R_o and R_s are found to be independent of temperature

6.1.3. The Effect of s-d Hybridization on the Hall Coefficient

The Hall coefficient of metallic glasses composed of simple metals is negative, whereas the Hall coefficient of many of those containing transition metals is positive. The Hall coefficient has been measured in many amorphous metal alloys and it has been observed to change sign with composition A number of approaches have been taken to explain this effect [122] The most successful explanation so far is that it arises from so called s-d hybridization As discussed in Section 4 1 4, in transition metal alloys there are two somewhat distinct groups of conduction electrons the free-electron-like s-electrons on the one hand and the lower-velocity d like electrons whose band is much narrower in energy Where these bands overlap in energy, hybridization between them can occur and modify the properties of each

Hybridization between the free electrons and the d-band in an amorphous alloy gives rise to an *S* shaped anomaly in the *E(k)* dispersion relation [122, 66] as shown in Figure 6.3. The figure shows a free-electron-like dispersion curve for the s-like electrons passing through a region of broadened d-states whose energies lie between E_1 and E_2. After hybridization the new dispersion curve has a broadened region of anomalous dispersion, i.e. one in which the electron velocity is negative (i.e. the slope of the *E-k* curve). Hence the Hall coefficient is positive. This modified "*s*"-band approach gives a simple and effective explanation of how a positive Hall effect arises The Hall coefficient magnitude, at least as a first approximation, is determined, as before, by the carrier density [123] (Equation 6 3).

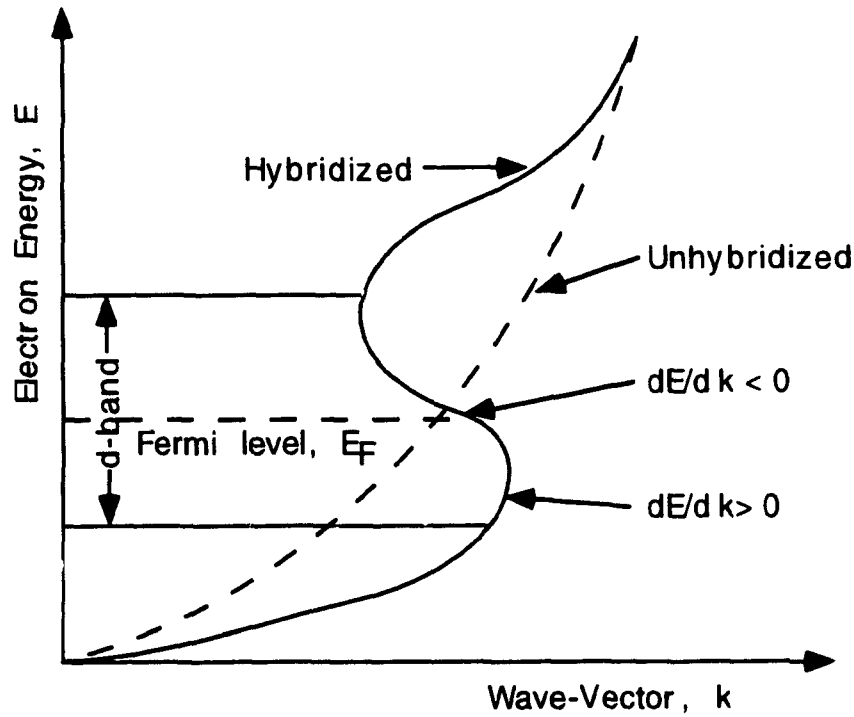

Figure 6.3. The effect of *s-d* hybridization on the dispersion curve (energy against wave-vector) of the *s*-like electrons. The dashed curve is the unhybridized free-electron-like curve In the energy region between E_1 and E_2, where the *d*-states lie, the hybridization induces a negative group velocity (essentially the slope of the dispersion curve) and can account for a positive Hall coefficient.

6.1.4. Electron-Electron Interaction Effects

Altshuler et al [102] have predicted that the fractional change in R_H with temperature produced by the electron-electron interaction effect is just twice that of the fractional change in resistivity,

$$\frac{\Delta R_H(T)}{R_H(0)} = 2\frac{\Delta\rho(T)}{\rho(0)} = -2\left(\frac{4}{3} - 2F\right)\left(\frac{1.3e^2}{4\pi^2\hbar}\right)\left(\frac{kT}{2\hbar D}\right)^{1/2} \tag{6.6}$$

where F is an integral over scattering angle of the screened Coulomb interaction and D is the diffusion constant. The general prediction of the theory is that, for high-resistance disordered alloys $R_H(T)$ should decrease as $\sqrt{T}$ for positive $R_H(0)$ and increase as $\sqrt{T}$ for negative $R_H(0)$ (i.e. become more positive). Fukuyama [124] has shown that weak localization makes no contribution to the temperature dependence of R_H. These predictions have been confirmed experimentally [125, 126]. The $R_H(T)$ results are therefore of crucial importance in establishing the importance of interaction effects in disordered systems.

6.2. Result and Discussion

The field dependence of the Hall resistivity $\rho_H(B)$ at 4.2 K for $Al_{70-x}Pd_{15}Mn_{15}B_x$ is shown in Figure 6.4. It is evident that ρ_H is non-linear in the field with an anomalous magnetic contribution to the Hall effect. There is a clear saturation in the $\rho_H(B)$ curve with

increasing Boron concentration. This confirms the magnetic nature of the samples, i.e ρ_H ~M_s. For this reason the field dependence of ρ_H follows the empirical expression for ferromagnetic materials given by Equation 6.4. Guided by this empirical expression the

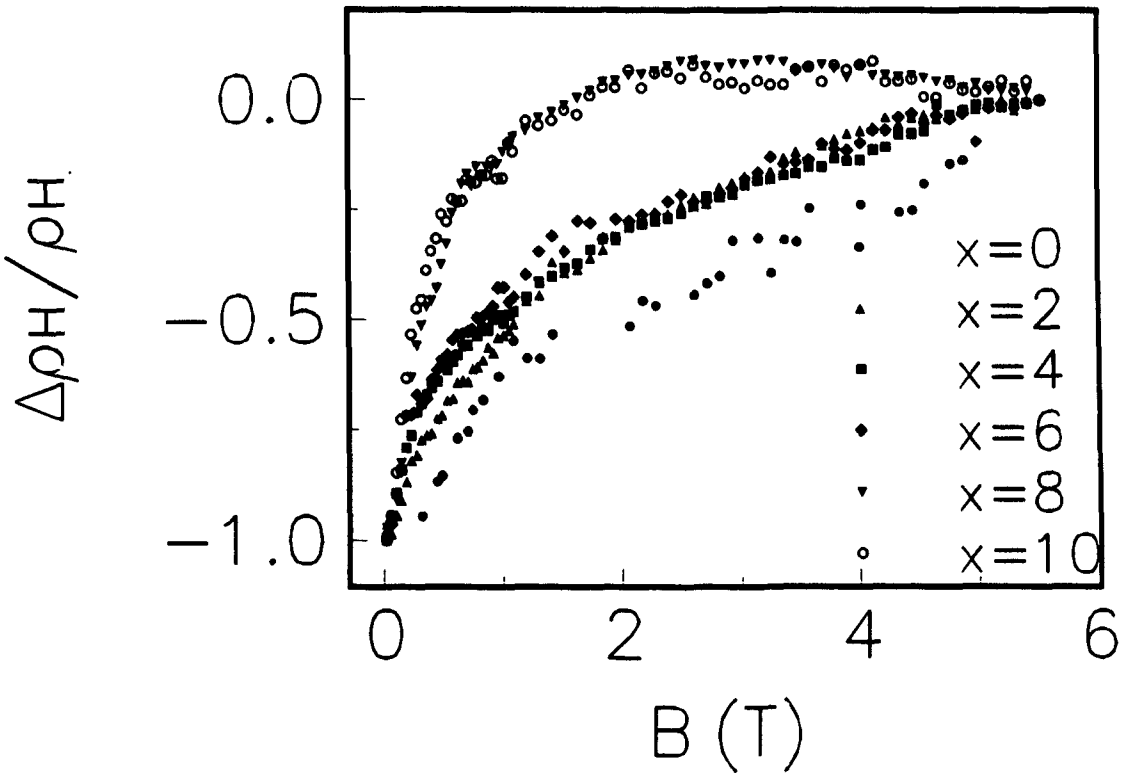

Figure 6.4 Hall resistivity versus field for $Al_{70-x}Pd_{15}Mn_{15}B_x$ at 4.2 K.

following data reduction for the $\rho_H(B)$ curve is achieved. For a thin rectangular sample the initial slope, i.e. well below saturation, gives

$$R_H = \left(\frac{\partial \rho_H}{\partial B}\right)_{B\to 0} \cong R_s$$

The slope at high fields, saturation slope, can be used to derive the ordinary Hall coefficient

$$R_H = \left(\frac{\partial \rho_H}{\partial B}\right)_{B \to \infty} \cong R_o$$

An example of this approach is shown in Figure 6.5. The point of intersection of the two straight line segments gives $B = \mu_o M_s$. The values of the ordinary and extraordinary (spontaneous) Hall coefficients and spontaneous magnetization are listed in Table 6.1. $\rho_H(B)$ is found to be temperature independent in all the alloys as illustrated in Figure 6.6. Even though R_o is practically temperature independent, strangely enough, R_s is virtually temperature independent.

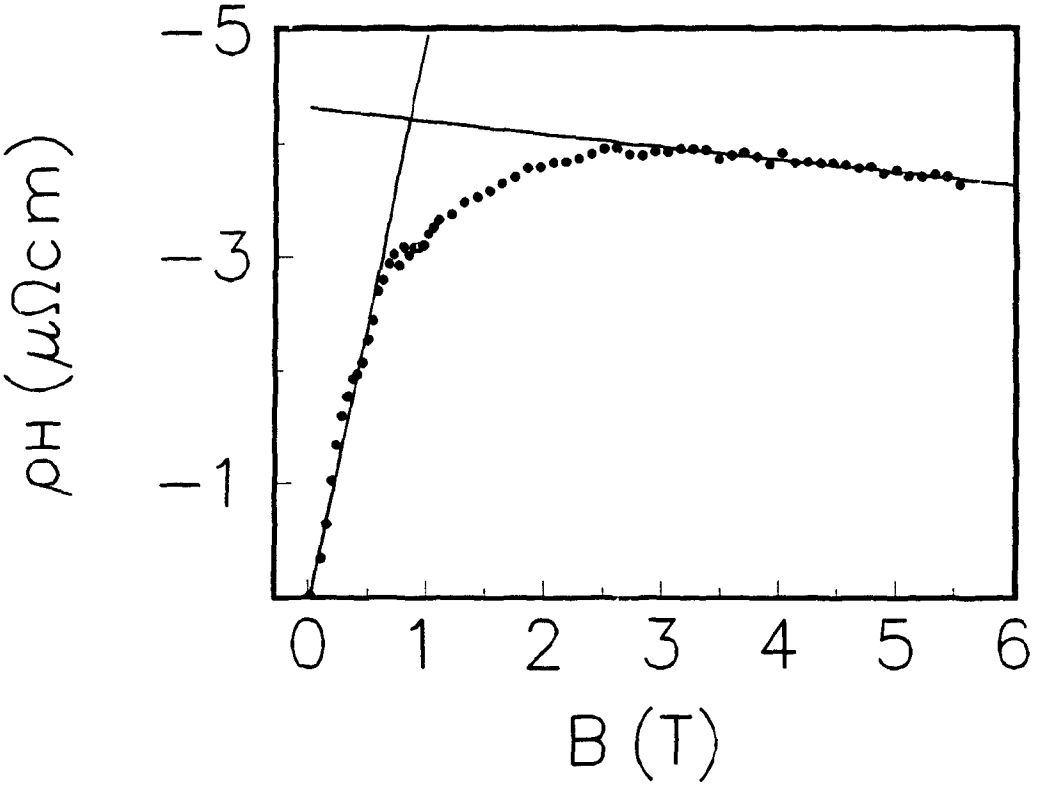

Figure 6.5 Hall resistivity as function of field for $Al_{62}Pd_{15}Mn_{15}B_8$ at 4.2 K (showing the data reduction). The point of intersection of the two fitted linear regions correspond to $B=\mu_o M_s$.

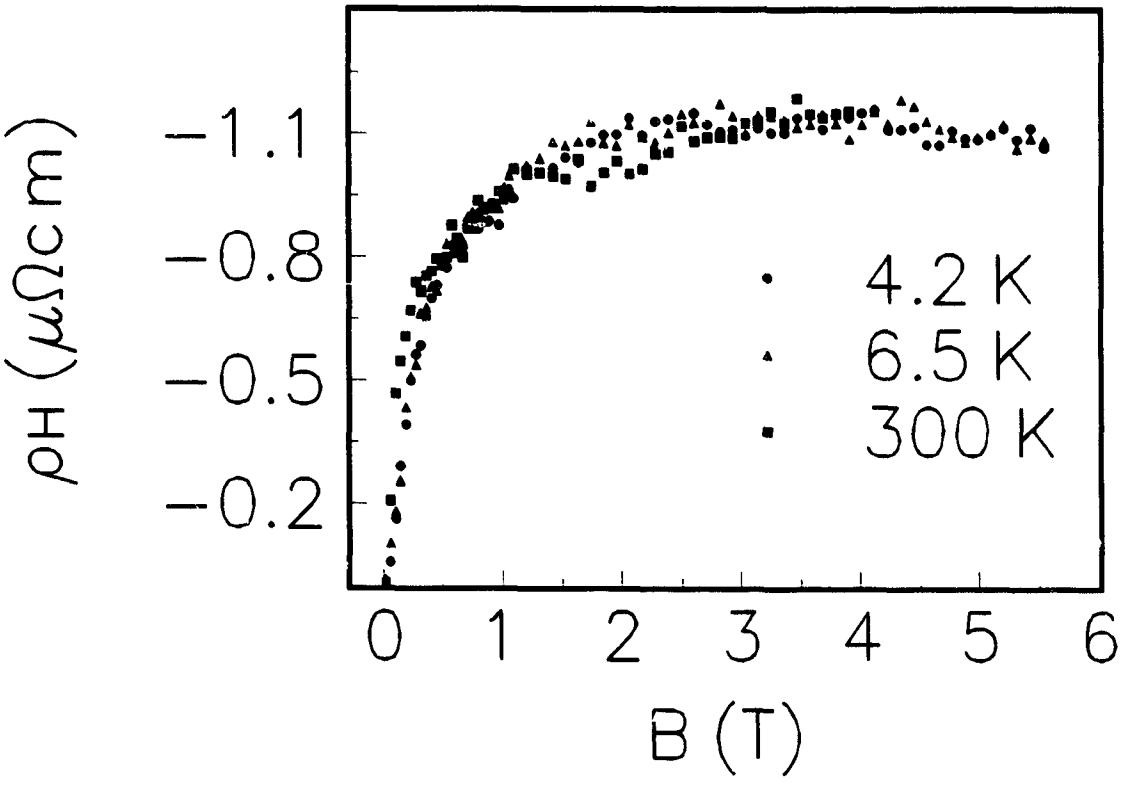

Figure 6 6 Hall resistivity as function of field for $Al_{60}Pd_{15}Mn_{15}B_{10}$ at various temperature $\rho_H(B)$ is virtually independent of temperature

Table 6 1 Hall effect data for $Al_{70-x}Pd_{15}Mn_{15}B_x$ at 4 2 *K*

x (at. %)	R_s *(μΩcm/T)*	R_o *(μΩcm/T)*	$\mu_o M_s$ *(T)*
0	-0 5(2)	-0 13(4)	1 2(3)
2	-0 73(4)	-0 082(5)	1 16(6)
4	-1 4(1)	-0 17(8)	0 78(6)
6	-2 7(1)	-0 04(2)	1 1(5)
8	-5 0(3)	0 112(8)	0 9(1)
10	-1 5(1)	0 015(7)	0 7(5)

Even though the high field slope is in principle equal to R_o, in practice such an approach is dangerous For example, if there is a non-zero high field susceptibility, the high field slope will be enhanced Thus, high field slope can be regarded only as an upper

limit to the ordinary Hall coefficient[127], and an attempt to discuss the free carrier concentration will be risky However, from the sign of R_o we can deduce the type of carriers Figure 6 7 shows the concentration dependence of R_o for $Al_{70-x}Pd_{15}Mn_{15}B_x$ alloys at 4 2 K R_o stays within the same order of magnitude and its contribution to R_H is negligible with respect to R_s One of the interesting findings is that R_o passes from negative to positive with increasing Boron concentration as shown in Figure 6 7 This change from negative to positive values of R_o can be explained by considering the effect of s-d hybridization as discussed in section 6 1 3. The s-d hybridization mechanism has been widely accepted as being responsible for the positive values of R_o commonly observed in amorphous transition metal alloys This effect gives rise to regions of negative group velocity ($v_o=\partial E/\partial k$) in k-space leading to positive Hall coefficients This results from the shifting of the Fermi level The substitution of *B* for *Al* causes the Fermi level to increase Since both elements belong to Group III of the periodic level, the change results from a reduction of unit cell volume due to different atomic radii

One of the characteristic features of disordered transition metal alloys is a large extraordinary Hall effect Generally, this anomalous Hall effect results from anisotropic scattering and this in turn comes from an interplay of internal polarization, scattering centers and spin-orbit coupling The most applicable anisotropic scattering mechanisms are the quasiclassical skew scattering (that leads to the ρ dependence) and the quantum mechanical side jump (that leads to the ρ^2 dependence) [116, 118] Therefore R_s may be written as

$$R_s(T) = a\rho(T) + b\rho^2(T) \qquad (6\ 6)$$

In amorphous alloys, because of the large number of scattering centers, the quadratic term is believed to dominate. In the present alloys R_s is constant in temperature while $\rho(T)$ changes by 8 to 23 % between 4.2 and 300 K (Table 4.1). This suggests that neither $R_s \sim \rho^2$ nor $R_s \sim \rho$ correlations are valid. Even though the $R_s \sim \rho^2$ correlation is confirmed in some amorphous alloys the experimental confirmation of this dependence is somewhat difficult in amorphous alloys because their resistivity, that is already large, changes only slightly with temperature. The same holds for R_s as well. Therefore, a very accurate determination of R_s is required in order to deduce the correlation between R_s and ρ. There are also systems in which this correlations does not hold [128] and for this reason it has been suggested that the scattering situations for ρ and ρ_H must be different. This seems to be true for the present alloys as well.

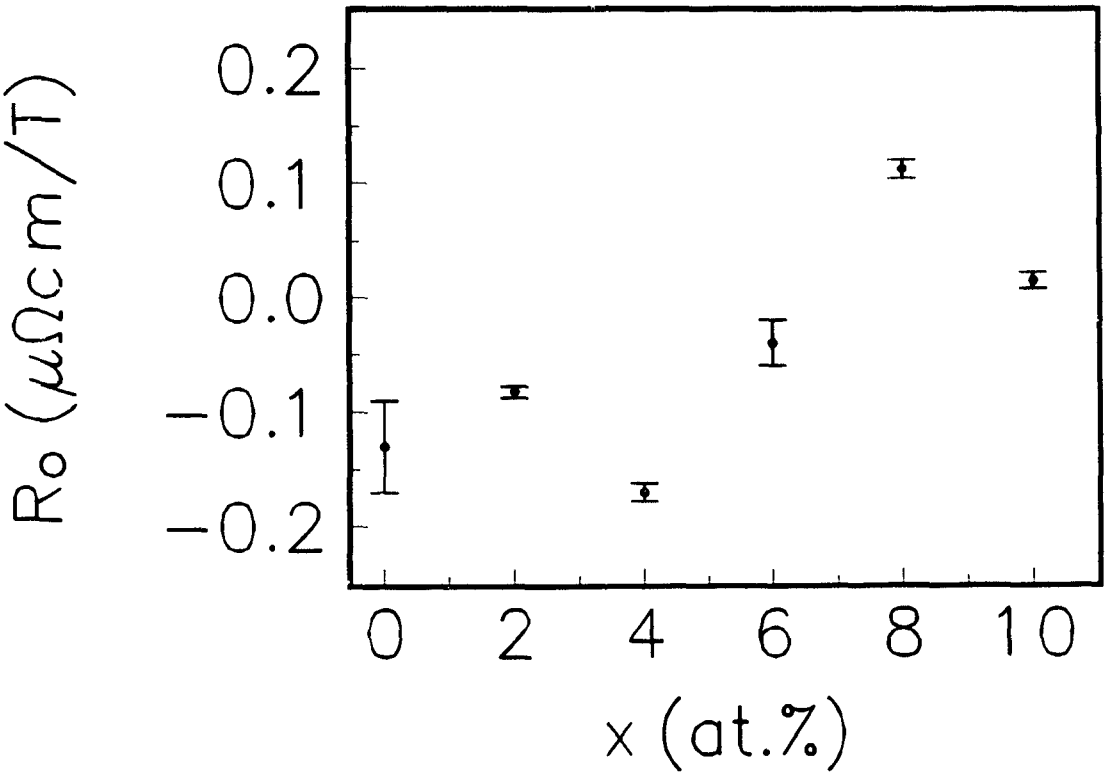

Figure 6.7 The ordinary Hall coefficient versus Boron concentration for $Al_{70-x}Pd_{15}Mn_{15}B_x$ at 4.2 K.

The concentration dependence of R_s for $Al_{70-x}Pd_{15}Mn_{15}B_x$ at 4.2 K is shown in Figure 6.8. R_s is negative for all alloys and shows a systematic change with Boron addition. R_s can take either sign in ferromagnetic alloys since the charge carriers may be of either spin direction, possibly giving rise to competing spin-orbit forces for the two sub-bands. As mentioned above, R_s results from the spin-orbit interaction between the charge carriers and the ions. In Figure 6.9 R_s is plotted along the spin-orbit scattering rate obtained from magnetoresistance data (Figure 5.13). The magnitude of R_s increases with the scattering rate showing that the spin-orbit interaction is indeed the important contributor to the Hall resistivity. The two most widely used anisotropic scattering mechanisms, skew scattering and the side jump, whose origin is spin-orbit interaction, are not valid and the mechanism by which the spin-orbit interaction influences the Hall resistivity is not obvious.

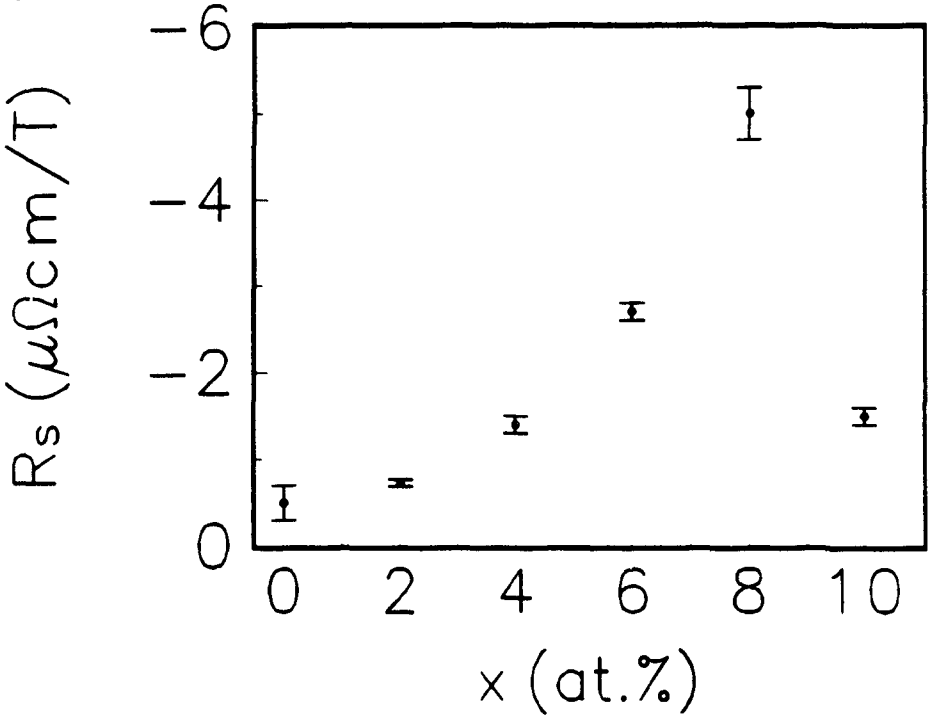

Figure 6.8 The spontaneous Hall coefficient versus Boron concentration for $Al_{70-x}Pd_{15}Mn_{15}B_x$ at 4.2 K.

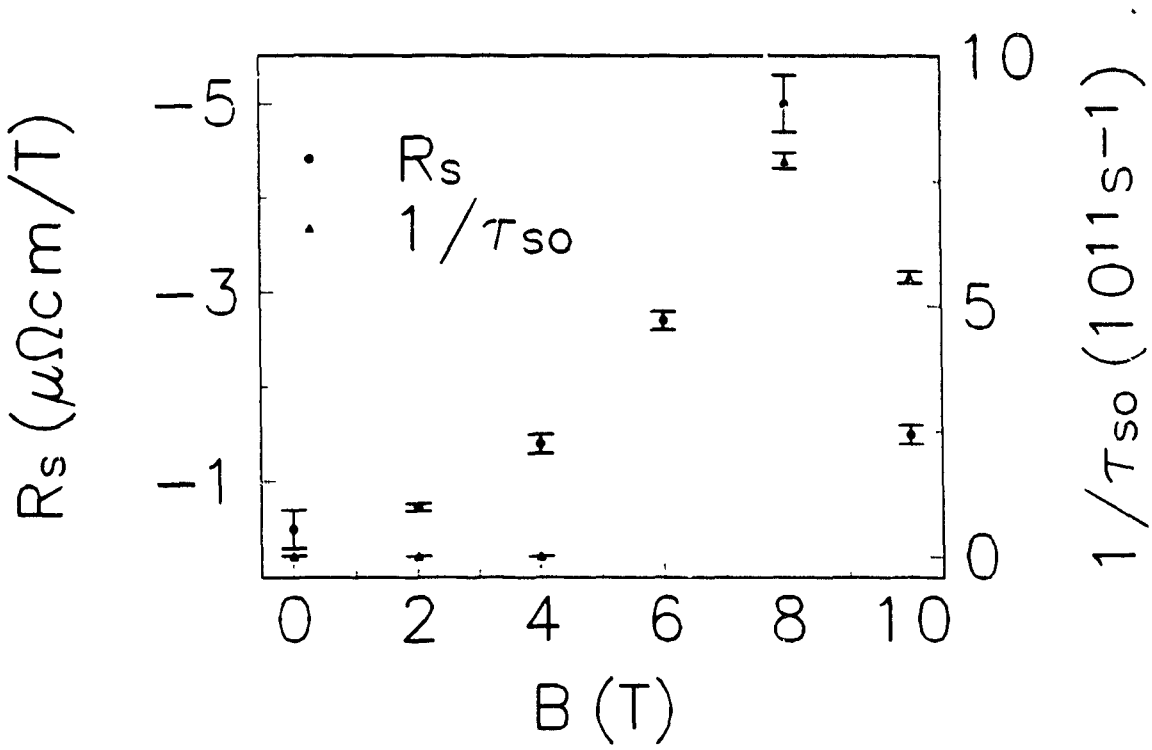

Figure 6.9 The spontaneous Hall coefficient and the spin-orbit scattering rate of $Al_{70-x}Pd_{15}Mn_{15}B_x$ as a function of Boron concentration at 4.2 *K*.

The results presented in this chapter, show that the Hall resistivity ρ_H is the result of two contributions; the normal term R_oB, due to the Lorentz force and anomalous term $\mu_o M_s R_s$ due to the spin-orbit interaction. R_o is independent of temperature in all the alloys and it passes from negative to positive with increasing Boron concentration. This can be explained by the effects of s-d hybridization. R_s is also found to be temperature independent in spite of the suggestion of current theories of the spontaneous Hall effect that there is a close correlation between $R_s(T)$ and $\rho(T)$ This suggest that the scattering mechanisms for the two cases are different. The compositional dependence of R_s is similar to that of the spin-orbit scattering rate and this suggests that the spin-orbit interaction is

responsible for the anomalous Hall effect. However, while it is evident that the spin-orbit interaction is responsible, the mechanism by which this interaction influences the Hall effect behaviour is not obvious.

7. Conclusions

In this thesis the first systematic study of the electron transport properties of ferromagnetically ordered icosahedral quasicrystalline alloys is presented Magnetic susceptibility, electrical resistivity, magnetoresistivity and Hall effect were performed on $Al_{70-x}Pd_{15}Mn_{15}B_x$ (x = 0, 2, 4, 6, 8, 10) icosahedral quasicrystalline alloys to obtain a coherent picture of the electronic properties as related to the quasicrystalline symmetry and the unusual ferromagnetic ordering.

Temperature dependent magnetic susceptibility measurement show that the alloys exhibit re-entrant magnetic behaviour at low temperature The measured zero field electrical resistivity showed very high values (1900 - 6200 $\mu\Omega cm$ at 4 2 K) and these very high values reveal peculiar band structure effects, such as the presence of a pseudogap near the Fermi level. Even though in thermally stable i-AlPdMn QC's it is observed that the more diamagnetic the sample is the higher the resistivity, the present observations showed no appreciable change with increasing magnetization Therefore, it seems that high resistivity is a common feature of QC's in spite of magnetic ordering The temperature dependence of $\rho(T)$ exhibits substantial changes as a function of Boron concentration At low temperature, $T < 30$ K, the resistivity showed a rapid decrease with increasing temperature and the magnitude of the TCR decreased with increasing Boron concentration Two effects appear to contribute to $\rho(T)$ in this temperature range, WL and magnetic scattering, where the magnetic effect is shown to be dominant At higher

temperatures $\rho(T)$ is dominated by the structural and magnetic contributions to the resistivity

The magnetoresistance result has established the coexistence of classical magnetoresistance due to spin-disorder scattering and quantum effects The quantum effect is found to be dominant at low temperature while the classical magnetoresistance is dominant at high temperature. In spite of the magnetic ordering in $Al_{70-x}Pd_{15}Mn_{15}B_x$ quasicrystalline alloys, this work has demonstrated that WL theory gives a good description of the field and temperature dependence of the magnetoresistance data The scattering times obtained from this analysis are consistent with similar results on other systems This temperature dependence of the inelastic scattering time is observed to be the result of dephasing dominated by inelastic electron-phonon scattering. The spin-orbit scattering rate showed a significant increase with increasing Boron concentration and appears to be due to Boron locating in Mn-rich environments and hybridizing with the Mn *d*-band This increases the *d*-band density of states at the Fermi level and enhances the effective spin-orbit contribution to the magnetoresistance The spin scattering rate estimated from the magnetoresistance also showed a significant increase with increasing Boron concentration which could be due to both an increase in the concentration of magnetic Mn sites and to magnetic ordering

The Hall resistivity ρ_H is the result of two contributions, the normal term R_oB, due to the Lorentz force and anomalous term $\mu_o M_s R_s$ due to the spin-orbit interaction R_o is independent of temperature in all the alloys and changes from negative to positive with increasing Boron concentration The change in sign of this Hall coefficient is attributed to

an effect of *sp-d* hybridization. R_s is also found to be temperature independent in spite of the suggestion of current spontaneous Hall effect theories that there is a close correlation between $R_s(T)$ and $\rho(T)$ R_s has a marked compositional dependence and this compositional dependence of R_s is similar to that of the spin-orbit scattering rate obtained from the magnetoresistance indicating that the spin-orbit interaction is responsible for the anomalous Hall effect

Although substantial contribution has been made towards the understanding of the electronic properties of magnetically ordered QC's in this work, it is clear that the discovery of a stable magnetically ordered QC will help future detailed investigations and improve the understanding the electronic properties magnetic QC's

References

1 D Shechtman, I Blech, D Gratias, and J W Cahn, Phys Rev Lett **53**, 1951, 1984

2 N Wang, H Chen and K H Kuo, Phys Rev Lett **58**, 706, 1987

3 L Bendersky, Phys Rev Lett **55**, 1561, 1985

4 J W Chen, D Gratias and B Mozer, J Phys , Paris, **49**, 1225, 1988

5 Y. Calvayrac, A Quivy, M Bessiere, S Lefebvre, M Cornier-Quiquandon and D Gratias, J Phys France **51**, 417-31, 1990

6 C Janot, *Quasicrystals : A Primer*, Oxford University Press, New York, 1992

7 V Elser, Phys Rev **B32**, 4892, 1985

8 D Levine and P J Steinhardt, Phys Rev Lett **53**, 2477, 1984,
D Levine and P J Steinhardt, Phys Rev **B34**, 596, 1986, J E S Socolar and P J Steinhardt, Phys Rev **B34**, 617, 1986 1

9 R Penrose, Bull Inst Math Appl **10**, 266, 1974, M Gardner, Sci Am **236**, 110, 1977

10 A L Mackay, Physica **114A**, 609, 1982

11 S J. Poon, Adv Phys **41**, 303, 1992

12 F. Hippert and D Gratias, *Lectures on Quasicrystals*, (Les Editions de Physique, France, 1994) and references therein

13 D W Lawther, PhD Thesis (Dalhousie University, unpubiished, 1993)

14 C Berger, in *Lectures on Quasicrystals*, eds F Hippert and D Gratias, (Les Editions de Physique, France, 1994) p 463

15 T. Klein, C Berger, D Mayou, and F Cyrot-Lackmann, Phys Rev Lett **66**, 2907, 1991

16 D Mayou, C Berger, , F Cyrot-Lackmann, T Klein, and P Lanco, Phys Rev Lett **70**, 3915, 1993

17 B D Biggs, S J Poon and N R Munirathnam, Phys Rev Lett **65**, 2700, 1990

18 E Belin, in *Physics and Chemistry of Finite Systems*, eds S N Khanna and B K Rao (NATO ASI Series C, Vol **374**, Kluwer Acadamic Publishers, Dordrecht, 1992) p. 829)

19 A P Tsai, Y Yokoyama, A Inoue and T Masumoto, in *Physics and Chemistry of Finite Systems*, eds S N Khanna and B K Rao (NATO ASI Series C, Vol **374**, Kluwer Acadamic Publishers, Dordrecht, 1992) p 177

20 D Mayou, in *Lectures on Quasicrystals*, eds F Hippert and D Gratias, (Les Editions de Physique, France, 1994) p 417

21. M Kohmoto and H Hiramoto, Mod Phys B**7**, 183, 1993

22 H Matubara, S Ogawa, T Kinoshita, K Kishi, S Takeuchi, K Kimura and S. Suga, Jpn J Phys **30**, L389, 1991

23 M Mori. S Matuo, T Ishimasa, T Matsuura, K Kamiya, H Inokuchi and T Matsukawa, J Phys Condens Matter **3**, 767, 1991

24 E Belin, Z Dankhazi, A Sadoc, Y Calvayrac, T Klein and J M Dubois, J Phys. Condens Matter **4**, 4459, 1992

25. R C O'Handley, R A Dunlap and M E McHenry, in *Handbook of Magnetic Materials*, ed K H J Bushow (North Holland, Amsterdam, 1991) Vol **6**, Chap 5, and references therein

26 W Warren, H S Chen and G P Espinosa, Phys Rev B**34**, 4902, 1986

27 P Lanco, T Klein, C Berger, F Cyrot-Lackmann, G Fourcaudot and A Sulpice, Europhys Lett **18**, 227, 1992

28 M A Chernikov, A Bernasconi, C Beeli, A. Schilling and H.R Ott, Phys. Rev B **48**, 3058, 1993

29 Y Yokoyama, A Inoue and T Masumoto Mater Trans JIM **33**, 1012, 1992.

30 T Shinohara, Y Yokoyama, M Sato, A Inoue and T Masumoto J Phys Condens Matter **5**, 3673, 1993

31 L Koszegi, M Foldeaki and R A Dunlap, Rev Sci Instrum. **62**, 793, 1991.

32 J G Zhao, L Y Yang, Q Fu and H Q Guo, Suppl Trans JIM **29**, 497, 1988

33 A.P Tsai, A. Inoue, T Masumoto and N Kataoka Japan J Appl Phys **27**, L2252, 1988

34 R A. Dunlap, M E McHenry, V Srinivas, D Bahadur and R C O'Handley, Phys Rev B **39**, 1942, 1989

35 V Srinivas and R A Dunlap Mater Sci Engg A **125**, 115, 1989

36 M E McHenry, V Srinivas, D Bahadur, R C O'Handley, D J Lloyd and R A Dunlap Phys Rev B **39**, 3611, 1989

37 M Eibschutz, H S Chen and J J Hauser Phys Rev Lett **56**, 169, 1986

38 R Bellisent, F Hippert, P Monod and F Vigneron Phys Rev B **36**, 5540, 1987

39 V Srinivas, M E McHenry and R A Dunlap Phys Rev B **40**, 9590, 1989

40 C Berger, J C Lasjaunias, J L Tholence, D Pavuna and P Germi Phys Rev B **37**, 6525, 1988

41 M Eibschutz, M E Lines, H S Chen, J V Waszczak, G P Espinosa and A S Cooper Phys Rev B **41**, 4606, 1990

42 V L Moruzzi, P M Marcus and P C Pattnaik Phys Rev B **37**, 8003, 1988

43 C Berger and J J Prejean Phys Rev Lett **64**, 1769, 1990

44 M Eibschutz, M E Lines, H S Chen, J V Waszczak, G Papaefthymiou and R B Frankel Phys Rev Lett **59**, 2443, 1987

45 D Bahadur and K Singh J Magn Magn Mater **119**, 76, 1993

46 D Bahadur, P H Gaskell and D I Irneson Phys Lett A **120**, 417, 1987

47 J Hauser, H S Chen, G P Espinosa, and J V Waszczak Phys Rev B **34**, 4674, 1986

48 R A Dunlap, M E McHenry, V Srinivas, D Bahadur and R C O'Handley Phys Rev B **39**, 4808, 1989

49 M E McHenry, D D Vvedensky, M E Eberhart, and R C O'Handley Phys Rev B **37**, 10887, 1988

50 D Bagayoko, N Brener, D Kanhere, and J Callaway Phys Rev B **36**, 9263, 1987

51 V de Coulon, F A Reuse, and S N Khanna Phys Rev B **48**, 814, 1993

52 Y Imry and S K Ma Phys Rev Lett **35**, 1399, 1975

53 D J Sellmyer and S Nafis J Appl Phys **57**, 3584, 1985

54 R.A Alben, J I Budnick and G S Cargill III, in *Metalic Glasses*, J J Gilman and H J Leamy eds (ASM, Metals Park, 1978) p 304

55 J M D Coey, J Chappert, J P Rebouillat, and T S Wang Phys Rev Lett **36**, 1061, 1976

56 J M D Coey J Appl Phys **49**, 1646, 1978

57 D Bahadur, C M Srivastava, M H Yewondwossen and R A Dunlap J Phys Condens Matter, submited, 1995

58 Y Hattori, K Fukamichi, H Chikama, H Aruga-Katori and T Goto, J Phys Condens Matter, in press, 1995

59 F A. Campbell and S Senoussi, Phil Mag B **65**, 1267, 1992

60 K H Fischer and J A Hertz *Spin Glasses*, Cambridge University Press, Cambridge, p322-326, 1991

61 J Nogues and K V Rao, J Magn Mag Mater **135**, L11, 1994

62 K H Fischer, Phys Status Solidi (b) **130**, 13, 1985

63 J R L de Almeida and D J Thouless, J Phys A **11**, 983, 1978

64 M Gabey and G Toulouse, Phys Rev B **26**, 5285, 1982

65 M A Howson and B L Gallagher, Phys Reports **170**, 265, (1988)

66 J S Dugdale, Contemp Phys **28**, 547, (1987)

67 K V Rao, in *Amorphous Metallic Alloys*, F E Luborsky ed (Butterworths, London, 1983), p 403

68 U Mizutani, Phys Stat Sol (b) **176,** 9, 1993

69 J H Mooij, Phys Status Solidi (a) **17**, 521, 1973

70 H J Gutherodt and H U Kunzi, in *Metallic Glasses*, O Parks, ed (American Society of Metals, New York, 1978), p 247

71 J M Ziman, Philos Mag **6**, 1013, 1961

72 R Evans, D A Greenwood and P Lioyd, Phys Lett A **35**, 57, 1971

73 S R Nagel, Phys Rev B **16,** 1694, 1977

74 P J Cote and L V Meisel, Phys Rev Lett **39,** 102, 1977

75 K Frobose and J Jackle, J Phys F **7,** 2331, 1977

76 J Hafner and A Philipp, J Phys F **14,** 1685, 1984

77 L V Meisel and P J Cote, Phys Rev B **31**, 4872, 1985

78 J Hafner, J Non-crystall Solids **69,** 325, 1985

79 G Bergmann and Marquadrt, Phys Rev B **17**, 1355, 1978

80 R Richter, M Wolf, and F Goedsche, Phys Status Sol (b) **95**, 473, 1979

81 S N Kaul, W Kettler, and M Rosenberg, Phys Rev B **33**, 4987, 1986

82 G Bergmann, Phys Rep **107**, 1, 1984

83 P Lee and T V Ramakrishnan, Rev Mod Phys **57,** 287, 1985

84 B L Altshuler and A G Aronov, *Electron Electron Interactions in Disordered Solid,* A Efros and M Pollak eds(North-Holland, Amsterdam) 1985, p 1

85 E Abrahams, P W Anderson, D C Licciardello, and T V Ramakrishanan, Phys Rev Lett **42,** 673, 1979

86 P W Anderson, Phys Rev **109**, 1492, 1958

87 A J Leggett, Rev Mod Phys **59**, 1, 1987

88 H Fukuyama and K Hoshino , J Phys Soc Japan **50**, 2131, 1981

89 J C Phillips and K M Robe, Phys Rev Lett **66**, 923, 1991

90 S E Burkov, T Timusk and N W Aschcroft, J Phys Condens Matter **4** , 9447, 1992

91 T Fujiwara, S Yamamoto and G Trambly de Laissaridiere, Phys Rev Lett **20**, 4116, 1993

92 K Kimura and S Takeuchi, *Quasicrystals: The State of the Art*, D. P DiVincenzo and P Steinhardt eds (World Scientific, Singapore, 1991) p 313

93 M Kohmoto and H Hiramoto, Mod Phys Lett B 7, 183, 1993

94 F S Pierece, S J Poon and B D Biggs, Phys Rev Lett **70**, 3919, 1993

95 H Akiyama, T Hashimoto, T Shibuya, K Edagawa and S Takeuchi, J Phys Soc Jpn **62**, 639, 1993

96 S Matsuo, H Nakano, T Ishimasa and M Mori, Solid State Commum **92**, 811, 1994

97 K K Chai, G Bergmann and R M Mueller, Phys Rev Lett **58**, 1964, 1987.

98 M T Beal-Monod and R A Weiner, Phys Rev **170**, 552, 1968

99 D V Baxter, R Richter, M L Trudeau, R W Cochrane, and J O Strom-Olson, J Physique **50,** 1673, 1989

100 A Kawabata, Solid State Commun **34**, 431 (1980)

101 B L Altshuler, A G Aronov, A G Larkin and D E Khmelnitzki, Sov Phys JETP **54,** 411, 1981

102 B L Altshuler, D Khmelnitzkii, A I Larkin and P A Lee, Phys Rev B **22**, 5142, 1980

103 J S Drewery and R H Friend, J Phys F **17**, 1739, 1987

104 S Matsuo, H Nakano, K Saito, M Mori, and T Ishimasa, Solid State Commum **86**, 707, 1993

105 M A Chernikov, A Bernasconi, C Beel and H R Ott, Europhys Lett , **21,** 767 (1993)

106 A Sahnoune, J O Strom-Olsen, and A Zaluska, Phys Rev B **46**, 10629, 1992

107 S Chakravarty and A Schmid, Phys Rep **140**, 195, 1986

108 A Schmid, Z Phys **271**, 251, 1974

109 D Belitz and K I Wysokinski, Phys Rev B **36**, 9333, 1987

110 O Rapp in *Disordered Systems and New Materials*, M Borisov, N Kirov and A Vavrek eds (World Scientific, Singapore, 1987) p 687

111 M Ahlgren, M Rodmar, Th Klein and O Rapp, Phys Rev B **51**, 1995

112 A Sahnoune, J O Strom-Olsen and A Zaluska, Phys Rev B **46**, 10629, 1992

113 M H Yewondwossen, S P Ritcey, Z J Yang and R A Dunlap, J Appl Phys , **76** 6499, 1994

114 D Bahadur, C M Srivastava, M H Yewondwossen and R A Dunlap, Phys Rev B, submitted, 1995

115 B Barbara, V S Amaral, J Filippi, A G M Jansen, J B Sousa and J M Moreira, J Appl Phys **70,** 5813, 1991

116 C M Hurd, *The Hall Effect in Metals and Alloys* (Plenum Press, New York-London, 1972)

117 A Fert and A Friederich, Phys Rev B **13**, 397, 1976

118 T R McGuire, R J Gambino and R C O'Handley, in *The Hall Effect and its Applications*, C L Chen and C R Westgate, eds (New York, Plenum), (1980), p 137

119 L Berger, Phys Rev B **2**, 4559, 1970

120 M Tsuji, J Phys Soc Jpn **13**, 979, 1958

121 R Bachman, F J Disalvo, Jr , T H Geballe, R L Greene, R E Howard, C N King, H C Kirch, K N Lee, R E Schwall, H W Thomas, and R B Zubeck, Rev Sci Instrum **43**, 205, 1972

122 M A Howson and B L Gallagher, Physics Reports **170**, 265, 1988

123 M A Howson and G J Morgan, Phil Mag B **51**, 439, 1985

124 H Fukuyama, in *Electron Electron Interactions in Disordered Solids*, A Efros and M Pollak, eds (North-Holland, Amsterdam) 1985, p155

125 G Bergmann, Solid State Commun **49**, 775, 1984

126 B L Gallagher, D, Greig and M A Howson, J Phys F Met Phys **14**, L225, 1984

127. R. Malmhall, S M. Bhagat, K.V. Rao, and G. Backstrom, Phys. Stat. Sol. (a) **53**, 641, (1979).

128. D. Muller, J.W. Shunemann and K. Barner, J. Magn Mater. **110**, 161, 1992